Synthesis, thermal stability and electrochemical behavior of lithium boron nitride intercalation compounds

Jungryang Kim

Contents

List of Tables

List of Figures

Chapter 1

Introduction

1.1 Lithium-ion battery

1.1.1 Lithium battery and lithium ion battery

Fossil fuels, which are the main energy resources in our life, are faced with several problems such as the depletion (non-renewable resources), environmental destruction (emissions of CO_2 gas), unstable supplies from oil-producing countries and so on. Thereby, the development of alternative energies which are renewable and eco-friendly energies such as solar, wind, tidal, and geothermal energy are urgently needed. In order to store energy from these resources, electrochemical systems are required. Among several electrochemical systems, batteries are the most convenient to store and deliver energy with portability.

Batteries are broadly divided into two kinds: primary cell and secondary cell. The former can be used once and cannot be recharged, namely its electrochemical reaction is irreversible. In other words, primary cells are known as a disposable battery and include mercury, lithium, manganese and alkaline batteries which each respective material is an anode. Mainly, these primary cells are used for watches and calculators. On the other hands, the secondary cells can be reused by charging/discharging electrochemically and are also known as a rechargeable battery and storage battery. These secondary cells are typically used in various portable devices, which are cell phones, smart phones, laptop computers, tablets and digital cameras, etc. The well-known secondary cell is the lithium ion battery (Li-ion battery, LIB). Its principle is that Li ions are moved between anode and cathode and electricity is produced (Fig. 1.1). Many authors have reviewed lithium (primary) and lithium-ion batteries'

histories, principles, challenges and future [1–8].

In the 1970s, the primary lithium batteries have been commercialized. The most commonly used type of lithium batteries are composed of metallic lithium as anode and manganese dioxide (MnO_2) [9] or fluorinated carbon (CF_x) [10] as cathode with a salt of lithium dissolved in an organic solvent. The advantages of lithium metal for electrochemical properties are:

▷ Firstly, it is the lightest metal (molecular weight : 6.94 g/mol) under standard conditions, thus it can reach high electrochemical capacity about 3860 mA/g,

▷ Secondly, it has the lowest standard reduction potential (E^0 : -3.04 V versus SHE (Standard hydrogen electrode)).

Due to these superior properties, Li metal have been tried for the application to the secondary cells as an anode material with various cathodes, which are capable of reversible lithium intercalation such as TiS_2 [11, 12], MoS_2 [13] and Li_xMnO_2 [14]. Unfortunately, it is not possible to use metallic Li as an anode for secondary batteries because dendritic lithium is often formed on the surface of lithium metal during the charge/discharge reaction, and it could lead to internal short circuits and finally caused an explosion [15]. In order to overcome this problem, lithium-ion batteries have been developed using layered-structural materials, in which lithium ions can be intercalated/deintercalated. Fig. 1.1 shows schematic diagram of typical lithium ion battery consisting of graphite (anode)/separator/$LiCoO_2$ (cathode) in electrolyte solutions [7]. This system was first commercialized by SONY Corporation [16] and the following reactions occur in anode and cathode, respectively in the charge/discharge.

▷ Anode:

$$xLiC_6 \rightleftharpoons xLi^+ + xe^- + xC_6 \tag{1.1}$$

▷ Cathode:

$$Li_{1-x}CoO_2 + xLi^+ + xe^- \rightleftharpoons LiCoO_2 \tag{1.2}$$

Li ions are deintercalated form LiC_6 and moved into $LiCoO_2$ by discharging, and opposite reaction occurs by charging as seen in Fig. 1.1. For the electrolytes for LIBs, nonaqueous liquids are usually used because lithium highly reacts to water. These nonaqueous liquid electrolytes consist of binary solvent mixtures, which are organic

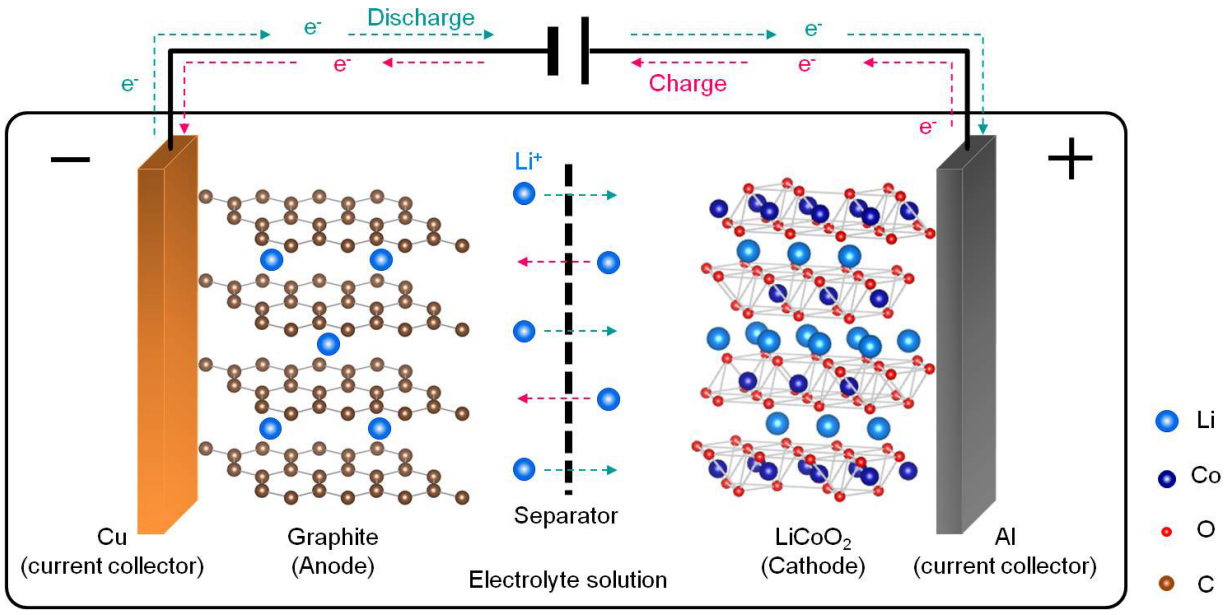

Fig. 1.1. Diagram of typical lithium ion battery consisting of graphite (anode) / separator / $LiCoO_2$ (cathode) in electrolyte solutions.

solvents such as PC (propylene carbonate) and EC-DMC or EC-DME [ethylene carbonate (EC), dimethyl carbonate (DMC), 1,2-dimethoxyethane (DME)], and lithium salt solvents, such as $LiPF_6$, $LiClO_4$ and $LiBF_4$, thus these electrolytes allow movement of ionic lithium [17, 18]. Over these electrolyte solutions, the EC-DMC and $LiPF_6$ mixture is the most used for Li-ion batteries due to its high ionic conductivity, highest anodic stability of EC-DMC and high solubility of $LiPF_6$ in all alkyl carbonate solvents [6, 19].

Fig. 1.2 shows potential (vs. Li/Li^+) versus capacity of cathodes and anodes. Many cathode materials for LiBs with various structures, such as layered structure $LiMO_2$ (M = Co, Ni) and spinel structure LiM_2O_4 (M = Ti, V, Mn), olivine structure $LiMPO_4$ (M = Fe), have been studied and so on [8, 20, 21]. Their electrochemical potentials are about $2.5 \sim 4.5$ V versus Li/Li^+ and capacities are about $100 \sim 250$ mAh/g (except for Cr_3O_8) as seen Fig. 1.2. Over these cathodes, $LiCoO_2$, which is one of the layered lithium transition metal oxides, is mainly used since the 1980s to the end of 1990s due to its high stability and rate capability, and its limited potential is 4.2 V versus Li/Li^+ with 140 mAh/g capacity. Then, spinel and olivine materials have been tried and studied for improvement to reach more sophisticated battery abilities e.g. higher safeties, higher capacities and also lower production costs, which was required by the development of industry. Especially $LiFePO_4$ was actively researched from the end of the 1990s and nowadays it is commonly used due to its excellent safety features and higher capacity 170 mAh/g though relatively low potential about 3.5 V versus Li/Li^+.

Meanwhile, lithium intercalation to graphite, which was already synthesized through heat treatment and reported by Hérold in 1955 [22], have been tried in order to use it for anode material of LIBs. Mohri et al. have discovered that carbonaceous material exhibits highly reversible lithium intercalation/deintercalation process with low voltage in 1989 [23]. As mentioned above, after this discovery, SONY Corporation commercialized $C/LiCoO_2$ system. Also, ongoing research efforts for the larger capacities and slightly higher potential versus Li/Li^+ (due to safety problems) than carbonaceous materials, have been carried out and various materials were tried for research purposes such as Li–M (M = Si, Al, Sn, Sb, Pb) alloys [24], Li transition-metal nitrides [$Li_{3-x}M_xN$ (M = Co, Ni or Cu)] [25], amorphous tin composite oxide (ATCO) [26, 27], intermetallic alloys (Cu_6Sn_5, InSb and Cu_2Sb) [28] and so on. However, they could not be commercialized due to their poor cyclability caused by forming their lithiated products at the initial cycle.

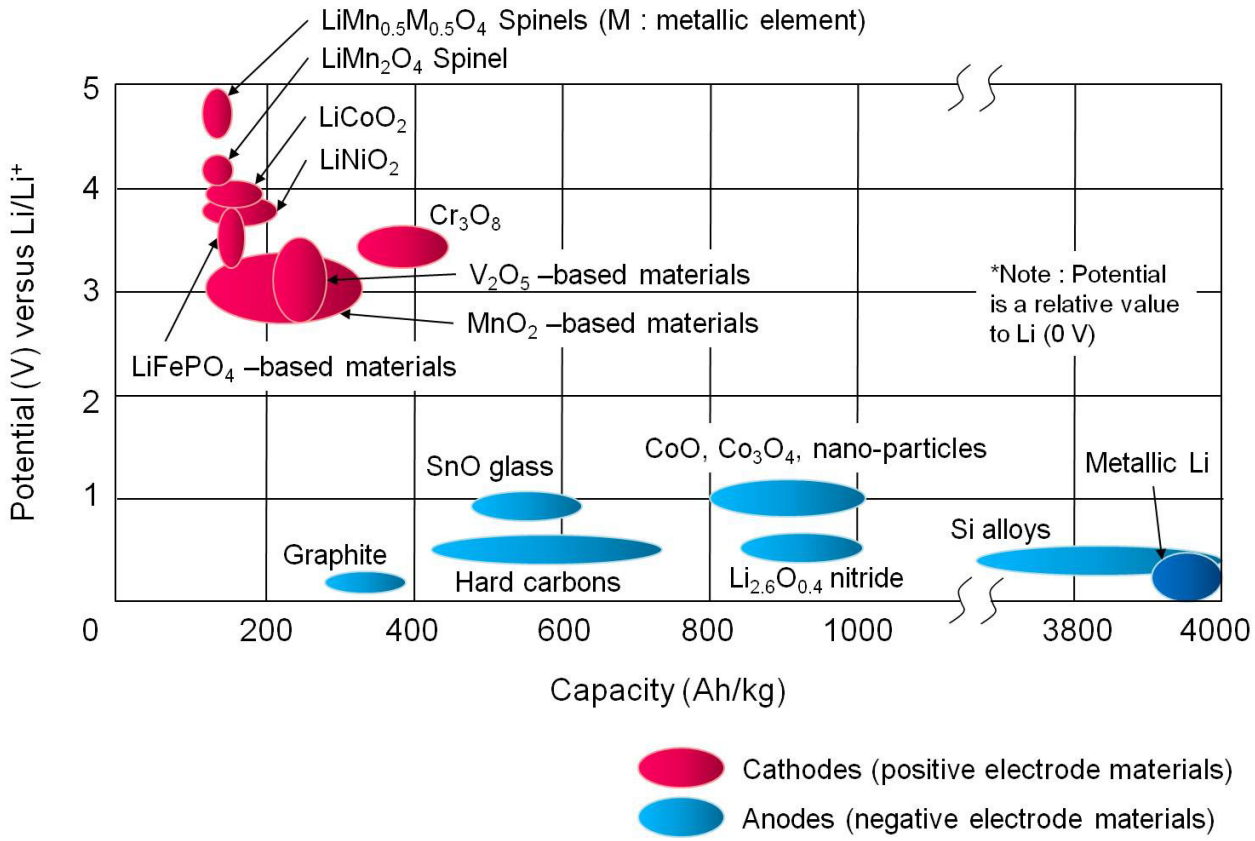

Fig. 1.2. Potential (vs. Li/Li^+) versus capacity of cathodes and anodes. Redrawn from [8].

1.1.2 Graphite as anode materials

The most investigated and studied graphite for anode of LIBs, exhibits theoretical capacity of 372 mAh/g for LiC_6 in full-charge and chemical potential of under 0.3 V versus Li/Li^+. The advantages of graphite as anode materials lay in the fact that small structural decomposition occurs during the charge/discharge process, i.e. dimensional stability, thus good cyclability and thanks to its low cost and availability as a resource on earth.

The unique characteristics of electrochemical intercalation of Li ions into graphite is the staging phenomenon, which is ordering property of layers. The layers of inserted Li ions are periodically stacking with graphite layers. These periods of stacking states are called in terms of stage "n" index, which is the number of graphite layers (graphene planes) between two adjacent intercalant layers. Thus, the intercalated graphite by Li (it is called by lithium intercalation compounds, Li-GICs) is classified by this n index, i.e. 1^{st}, 2^{nd}, 3^{rd} and 4^{th} stage. This staging phenomenon, have been investigated and clearly obtained through X-ray diffraction analysis [29] or *in-situ* ^{7}Li nuclear magnetic resonance (NMR) observation [30, 31] with electrochemical intercalation. During the charge reaction, the stoichiometry of Li-GICs has been changed to gas-like stage 1' and dilute $LiC_{9\,n}$ type (such as 4^{th} stage LiC_{36}, 3^{rd} stage LiC_{27} and 2^{nd} stage LiC_{18}), then dense LiC_{6n} type (such as 2^{nd} stage LiC_{12} and 1^{st} stage LiC_6). Fig. 1.3 shows the formation stage during which electrochemical intercalation of lithium into graphite occurs. The left and right figures show schematic galvanostatic curve and schematic voltammetric curve, respectively. This figures are modified and redrawn from reference of [1, 32, 33].

1.2 Graphite intercalation compounds (GICs)

As explained in Section 1.1.2, lithium ions can be inserted into interlayers of graphite. The interlayer of the layered materials like graphite are bonded by relatively week van der Waals (vdW) forces, thus, ions, atoms or molecules, which are called by intercalants, can be inserted into atomic layers of host materials without variation in-pane structure. This phenomenon is called "intercalation".

In 1841, Schaffautl firstly reported this intercalation phenomenon graphite using sulfate ions (H_2SO_4/SO_3) [34]. Many years later, Fredenhagen and Cadenbach reported the intercalation reaction of graphite with potassium, rubidium and cesium in

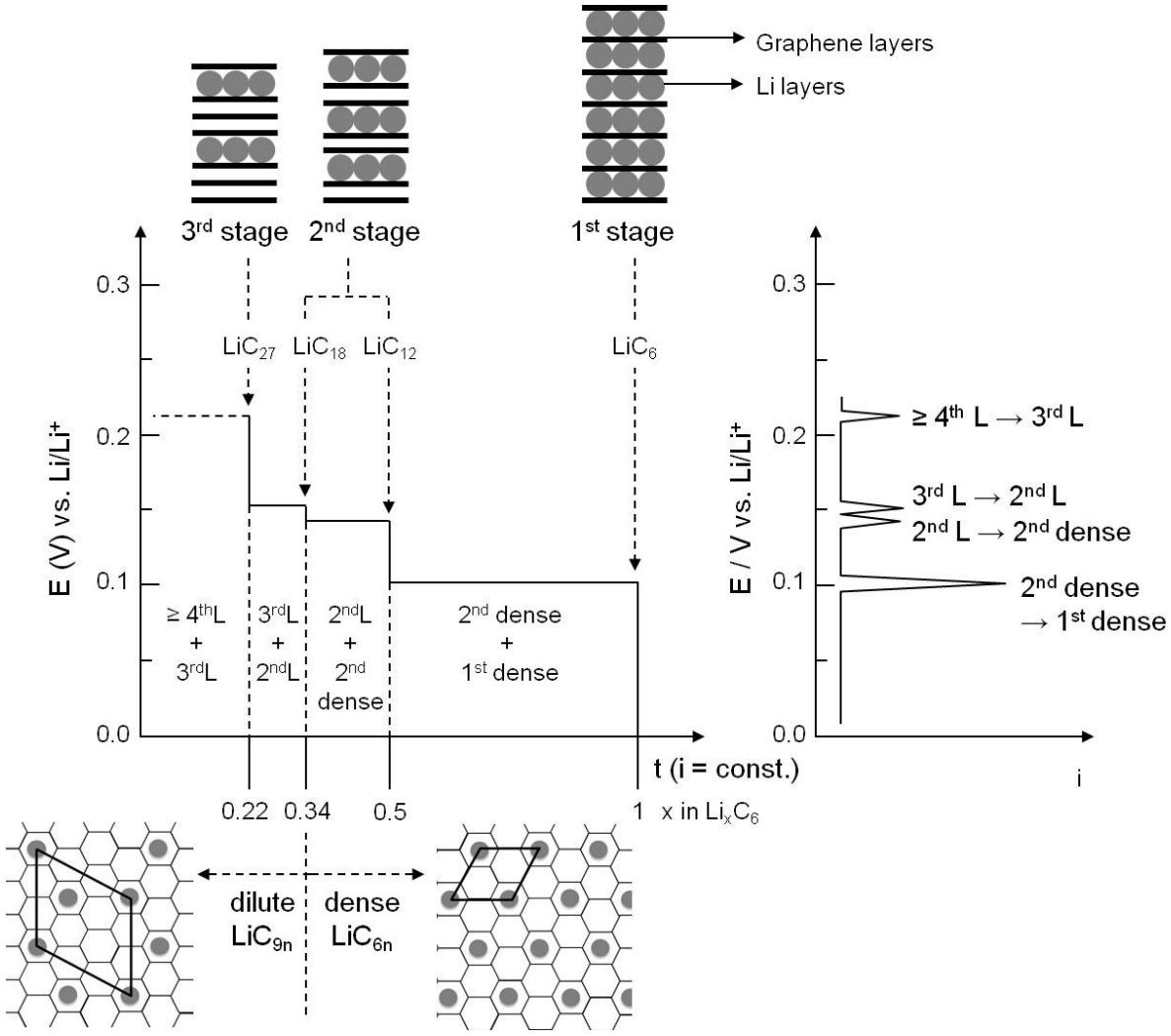

Fig. 1.3. Stage formation during electrochemical intercalation of lithium into graphite. Left: schematic galvanostatic curve. Right: schematic voltammetric curve. Modified and redrawn from [1, 32, 33].

1926 [35]. First structural study (stage index) using x-ray diffraction (XRD) started in 1931 by Hofmann and Frenzel [36] and systematic studies on graphite intercalation compounds (GICs) have been reported constantly and various authors summarized histories and studies of GICs [33, 37–41].

The staging phenomenon, which is special properties of GICs and already explained in subsection 1.1.2, has been studied in two kinds of models for staging as seen in Fig. 1.4 [42,43]. Rüdorff and his co-worker have firstly reported a simple stacking model (Rüdorff model), which includes no structural distortions of the individual graphene sheets as seen in Fig. 1.4 (a) [44, 45] and then Daumas and Hérold suggested a more detailed model (Daumas–Hérold model), where this is inducing flexible graphene layers by deforming it according to intercalants (Fig. 1.4 (b)) [46]. Regardless of these staking models, the repeat interplanar distance of GICs, I_c become the lattice parameter c determined by $00l$ reflections of XRD and can be calculated as following equation [47, 48]:

$$I_c = d_i + (n-1) \times 0.335\text{nm} \tag{1.3}$$

where, d_i is the distance of inserted layers (in nm) and depends on the kinds of intercalants (e.g. lithium: 0.370 nm and cesium: 0.595 nm), and 0.335 nm is from the distance of graphene layers in graphite.

Studies of GICs are classified under two large groups by superconducting properties and electrochemical intercalation. For the former studies, ternary GICs ($C_{4n}AM_x$; n = stage number; A = K, Rb, Cs; M = Hg, Bi, Tl), potassium, ytterbium and calcium-GIC have been reported [33]. The latter studies are well-known for the anode electrodes of lithium-ion batteries.

1.2.1 Lithium-Graphite intercalation compounds (Li-GICs)

The first synthesis method of lithium graphite intercalation compounds (Li-GICs) is the reaction between lithium vapor and graphite. Hérold made a first attempt to use this method in 1955 [22,49,50] and Juza and Wehle have reported various Li-GICs, which are LiC_6, LiC_{12} and LiC_{18} using vapor lithium [51]. In this case, temperatures below 400 °C have been usually selected to suppress synthesis of Li_2C_2, which is not an intercalation compound [50].

The second reported synthesis method is the solid state reaction of Li and graphite

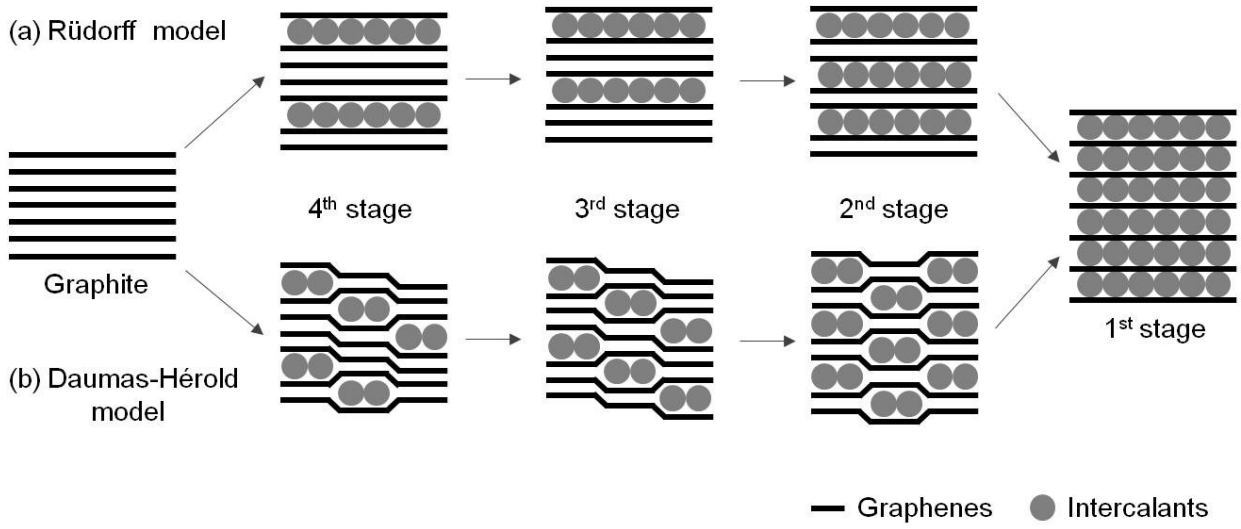

Fig. 1.4. Schematic of staging for GICs redrawn from ref. [42,43]. (a) Rüdorff model (b) Daumas–Hérold model.

powders by inducing compression under pressure (from 15 to 20 kbars). This method have been reported by Guérard and Hérold [52] and 1^{st}, 2^{nd}, 3^{rd} and 4^{th} stages of Li-GICs can be produced by this method with variation of the Li/C ratio. Then, Janot and Guérard have reported a new method, which is ball milling, for the synthesis of superdense Li-GICs [48, 53, 54] and successfully synthesized superdense LiC_3 with 1^{st} stage phase. Meanwhile, another superdense Li-GIC, LiC_2, which is occupied in all hexagonal sites of graphite by lithium ions, have been reported by Bindra et al. in 1998 and synthesized at 300 °C under 50 kbars [55]. Except for LiC_6, the stoichiometry is sensitive to temperature when synthesized under lower pressures, whereas it becomes sensitive to pressure (less sensitive to temperature) under high-pressure preparative methods [50].

Lastly, one of typical synthesis method is electrochemical intercalation. This method is usually used for lithium-ion batteries and it has been explained in section 1.1 which is about electrochemistry. By this synthesis, until LiC_6 can be produced, namely, superdense Li-GICs can not be synthesized.

1.3 Hexagonal boron nitride vs. graphite

Hexagonal boron nitride (h-BN) is an outstanding ceramic material with low coefficient of thermal expansion and high thermal conductivity. In addition, h-BN is known as similar material to graphite and their similarities can be seen as follows:

▷ Very similar unit cell (lattice parameter)
▷ Lubricative materials
▷ Superior impact resistance, corrosion resistance, heat-resisting property and heat conduction quality
▷ Existence of various allotropes

First, their lattice parameters are very similar, respectively a = 0.2505 nm, c = 0.6660 nm [56] and a = 0.245 nm, c = 0.670 nm [57] (Table 1.1). Fig. 1.5 shows the atomic structures of h-BN and graphite, and as seen in this figure, both show layered structure. Their interlayers are bonded by relatively weak vdW forces with the hexagonal two-dimension lattice. Thus, h-BN and graphite are useful for lubricant even at high temperatures due to their superior heat-resisting property. h-BN also has various phase transitions and allotropes like graphite: the former includes cubic (zinc-blende

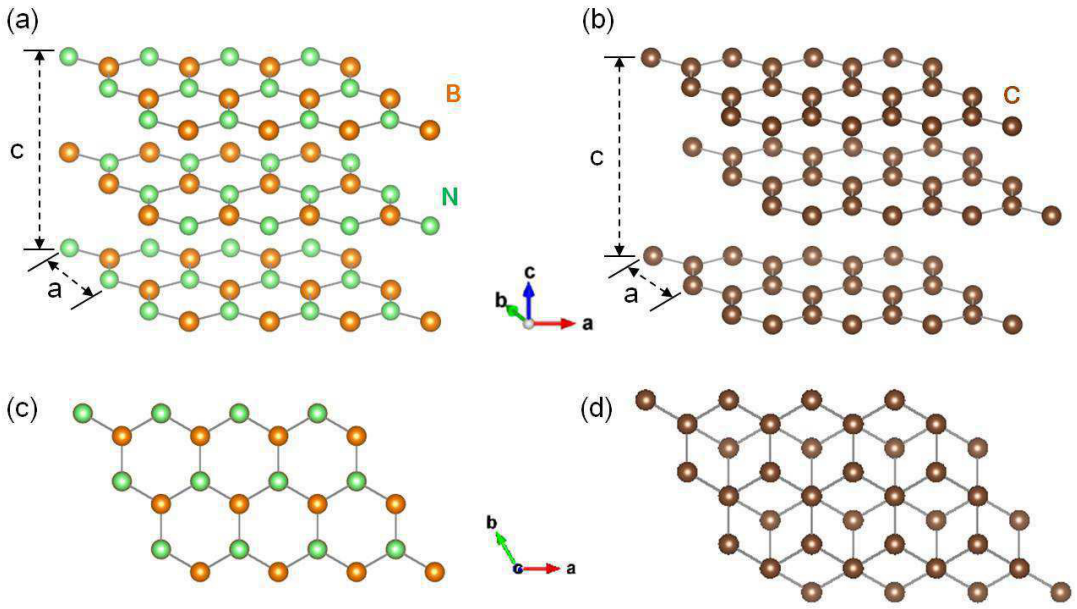

Fig. 1.5. Atomic structures of (a) hexagonal boron nitride and (b) graphite. (c) and (d) show two dimensions lattice of (a) and (b), respectively.

Table 1.1. Properties of hexagonal boron nitride and graphite.

	Hexagonal boron nitride	Graphite
Lattice parameter (nm)	a = 0.2505, c = 0.6660 [56]	a = 0.245, c = 0.670 [57]
Density (g/cm^3)	$2.0 \sim 2.29$ [62, 63]	$2.09 \sim 2.265$ [63]
Color	white	black
Mohs scale	1.65 [63]	$1 \sim 2$ [63]
Stacking state	AA' stacking	AB stacking
Electrical conductivity	an insulator	a conductor

form, diamond), wurzite (hexagonal diamond), rhombohedral and the letter includes nanosheets (graphenes), nanoribbons, nanotubes and fullerene structure, etc. [58–61].

However, despite these facts in common, there are very big differences of stacking state and electrical conductivity as seen in Fig. 1.5 (c) and (d) and Table 1.1. In case of h-BN, boron atom is horizontally bonded with three nitrogen atoms (also, nitrogen atom with three boron atoms) by strong covalent bond. These B–N bonds exhibit high polarization due to electronegativity difference between boron and nitrogen nucleus. Moreover, layers of h-BN are stacking by B–N–B–N $\cdots$, i.e. AA' stacking. Thereby, h-BN is an insulator with wide band gap ($\sim$6 eV [62]). On the other hands, graphite exhibits a homonuclear C–C bond. Over 4 valance electrons of carbon, three electrons are bonded with neighbor electrons of other three carbons, respectively, and the other electron is delocalized, namely called free electron. This free electron is attributed to semi-metal characteristics of graphite, thus graphite is a conductor.

1.4 Hexagonal boron nitride intercalation compounds (BNICs)

Intercalation into h-BN has been started for reason of similar atomic structure with graphite as seen in previous Section, thus many researchers thought h-BN intercalation compounds (BNICs) could be synthesized like GICs. First report of BNICs is presumed to intercalate aluminum chloride ($AlCl_3$) and ferric chloride ($FeCl_3$) studied by Croft [64]. In this report, other materials, which are $SbCl_5$, $SbCl_3$, $AsCl_3$, CuCl, $CuCl_2$, Br_2, ICl, NH_3, BCl_3 and BF_3, were also tried, but their intercalation has failed. At this time, Croft used black color h-BN, but Freeman et al. have reproduced Croft's results using white h-BN with halides($FeCl_3$, CuCI, Hg_2I_2 and $AsCI_3$) [65]. It suggested the evidence of successful intercalation of $FeCl_3$ through Mössbauer spectrum. Meanwhile, alkali-metal (Li, Na and K) intercalation has been also reported and it was contended that Na and K have been successfully intercalated [66].

After that, various studies on intercalation of molecules and atoms into h-BN were progressively reported by many authors. First, for the molecules, Br_2 [67], S–O–F (SO_3F [68], $(SO_3F)_2$ [69], $S_2O_6F_2$ [70]) and Brønsted acids [71] have been reported. Sakamoto et al. have reported intercalation of Cs and Br into h-BN [67], where Br does not intercalate into BN while there is a possibility of intercalation for Cs. Shen et al. reported synthesis of (BN)$\sim 3SO_3F$ that exhibits metallic electrical conductivity

and an increase in interlayer distance [70], and Kovtyukhova et al. reported reversible intercalation of h-BN with Brønsted acids [71].

For the atoms intercalation, alkali metal [66, 72–75] and transition metal [76] have been reported, where the intercalation is more difficult compared with graphite because the interlayer interaction of h-BN is stronger than that of graphite. This is due to partial ionic characteristics of h-BN originating from the charge transfer from N to B. In case of the potassium intercalation reported by Doll et al., the K atoms occupy (2×2) R (0°) superlattice, which is commensurate with the BN lattice [72]. Erhan Budak et al. also tried to attain intercalation of h-BN using transition metals (Cr, Mn, Fe, Co, Ni, Cu, Zn, and Ag) and reported a change in the interlayer spacing due to the intercalation of Cr, Mn, Fe and Ag according to X-ray diffractometry (XRD) [76]. Sumiyoshi et al. also reported successful synthesis of Li-BNICs (BN intercalation compounds) at 1250 °C for 10h, where its interlayer distance was expanded by 12.86% [73].

1.5 Thesis objectives and framework

Hexagonal BN (h-BN) has not been tried for application of Li-ion batteries as anode material although Li intercalation into h-BN has successfully occurred. It might be because h-BN is an insulator and Li intercalation into h-BN is more difficult than into graphite caused by interlayer bonding with heteroatomic boron and nitrogen.

As for producing Li-BNICs, Sumiyoshi et al. have successfully synthesized it through two kinds of methods that involve annealing: first, h-BN bulk and Li metal at 1250 °C for 10 h [73, 74] and second, h-BN and Li_3N mixture at about 950 °C for 10 h [75]. They also have suggested that its structure exhibits "1L model", which indicates the structure without the two-layer stacking periodicity, not "2L model" which indicates two-layer stacking periodicity structure of the pristine h-BN [75].

However still, it is difficult to exactly figure out the Li concentrations in synthesized Li-BNICs, namely its atomic structures. Altintas et al. have reported *Ab initio* quantum chemistry investigation on hypothetical Li-BNICs, which are $Li(BN)_3$ and $Li_4(BN)_6$ (= $Li_2(BN)_3$) using DFT [77]. They calculated lattice structure, cohesive energy, formation enthalpy, charge transfer and electronic structure for these three considered Li-BNICs. The calculated formation enthalpies are found to be positive, thereby, h-BN intercalation needs externally supplied energy to be synthesized. Doh et al. have also reported the structure, total energy, reaction energy and reaction

potential of hypothetic of Li-BNICs ($Li_3(BN)_3$ (=Li(BN)), $Li_2(BN)_3$ and $Li(BN)_3$) in terms of electrochemistry [78]. Negative reaction potentials against lithium deposition for Li-BNICs have been estimated and it means hypothetic of Li-BNICs are not usable for battery materials.

In this thesis, firstly the synthesis of Li-BNICs by inducing ball milling process for easy intercalation, will be investigated; then Li–BN–graphite ternary system will be studied to investigate behavior of Li intercalation in BN–graphite host. Furthermore, in order to investigate the possibility of application for Li-ion batteries, electrochemical Li intercalation into h-BN will be also considered. Finally, hypothetic Li-BNICs will be calculated for investigating a possible structure of Li-BNICs.

The overall framework of this thesis is as follows:
Chapter 2 describes the experimental, analytical and computational methods used in this thesis. Chapter 3 investigates Li-BNICs synthesized by combined ball milling and heat treatment, and its structure using Rietveld method (Li–BN system). Chapter 4 reports Li–BN–graphite system using same synthesis method with Li–BN system and the behavior of Li intercalation into BN and graphite matrix. Investigation for electrochemical Li intercalation into the pristine and milled h-BN is described in Chapter 5. Chapter 6 discusses the possible Li-BNICs using DFT calculation in order to investigated Li concentration. Chapter 7 presents summaries of this thesis and suggests future research.

Reference

[1] M. Winter, J. O. Besenhard, M. E. Spahr, and P. Novak, "Insertion electrode materials for rechargeable lithium batteries," *Advanced materials*, vol. 10, no. 10, pp. 725–763, 1998.

[2] R. Dell, "Batteries: fifty years of materials development," *Solid State Ionics*, vol. 134, no. 1, pp. 139–158, 2000.

[3] C. A. Vincent, "Lithium batteries: a 50-year perspective, 1959–2009," *Solid State Ionics*, vol. 134, no. 1, pp. 159–167, 2000.

[4] B. Scrosati and J. Garche, "Lithium batteries: Status, prospects and future," *Journal of Power Sources*, vol. 195, no. 9, pp. 2419–2430, 2010.

[5] J.-M. Tarascon and M. Armand, "Issues and challenges facing rechargeable lithium batteries," *Nature*, vol. 414, no. 6861, pp. 359–367, 2001.

[6] V. Etacheri, R. Marom, R. Elazari, G. Salitra, and D. Aurbach, "Challenges in the development of advanced Li-ion batteries: a review," *Energy & Environmental Science*, vol. 4, no. 9, pp. 3243–3262, 2011.

[7] J. B. Goodenough and K.-S. Park, "The Li-ion rechargeable battery: a perspective," *Journal of the American Chemical Society*, vol. 135, no. 4, pp. 1167–1176, 2013.

[8] M. D. Bhatt and C. O'Dwyer, "Recent progress in theoretical and computational investigations of Li-ion battery materials and electrolytes," *Physical Chemistry Chemical Physics*, vol. 17, no. 7, pp. 4799–4844, 2015.

[9] H. Ikeda, T. Saito, and H. Tamura, "Manganese dioxide as cathodes for lithium batteries," in *Manganese Dioxide Symp.,[Proc.]*, vol. 1, pp. 384–401, 1975.

[10] D. N. Bennion and S. L. Deshpande, "Lithium-graphite secondary battery.," tech. rep., DTIC Document, 1976.

[11] M. S. Whittingham, "Electrical energy storage and intercalation chemistry," *Science*, vol. 192, no. 4244, pp. 1126–1127, 1976.

[12] K. Abraham, D. Pasquariello, and D. Schwartz, "Practical rechargeable lithium batteries," *Journal of Power Sources*, vol. 26, no. 1-2, pp. 247–255, 1989.

[13] K. Brandt and F. Laman, "Reproducibility and reliability of rechargeable lithium/molybdenum disulfide batteries," *Journal of Power Sources*, vol. 25, no. 4, pp. 265–276, 1989.

[14] P. Dan, E. Mengeritski, Y. Geronov, D. Aurbach, and I. Weisman, "Performances and safety behaviour of rechargeable AA-size Li/Li_xMnO_2 cell," *Journal of power sources*, vol. 54, no. 1, pp. 143–145, 1995.

[15] N. Goldenfeld, "Dynamics of dendritic growth," *Journal of Power Sources*, vol. 26, no. 1-2, pp. 121–128, 1989.

[16] T. Nagaura and K. Tozawa, "Lithium ion rechargeable battery," *Prog. Batteries Solar Cells*, vol. 9, p. 209, 1990.

[17] D. Guyomard and J. Tarascon, "Li metal-free rechargeable $LiMn_2O_4$/carbon cells: Their understanding and optimization," *Journal of The Electrochemical Society*, vol. 139, no. 4, pp. 937–948, 1992.

[18] J. Tarascon, W. McKinnon, F. Coowar, T. Bowmer, G. Amatucci, and D. Guyomard, "Synthesis conditions and oxygen stoichiometry effects on Li insertion into the spinel $LiMn_2O_4$," *Journal of The Electrochemical Society*, vol. 141, no. 6, pp. 1421–1431, 1994.

[19] K. Xu, "Nonaqueous liquid electrolytes for lithium-based rechargeable batteries," *Chemical reviews*, vol. 104, no. 10, pp. 4303–4418, 2004.

[20] M. S. Whittingham, "Lithium batteries and cathode materials," *Chemical reviews*, vol. 104, no. 10, pp. 4271–4302, 2004.

[21] B. L. Ellis, K. T. Lee, and L. F. Nazar, "Positive electrode materials for Li-ion and Li-batteries," *Chemistry of Materials*, vol. 22, no. 3, pp. 691–714, 2010.

[22] A. Hérold, "Recherches sur les composés d'insertion du graphite," *Bulletin de la Société Chimique de France*, no. 7-8, pp. 999–1012, 1955.

[23] M. Mohri, N. Yanagisawa, Y. Tajima, H. Tanaka, T. Mitate, S. Nakajima, M. Yoshida, Y. Yoshimoto, T. Suzuki, and H. Wada, "Rechargeable lithium battery based on pyrolytic carbon as a negative electrode," *Journal of Power Sources*, vol. 26, no. 3, pp. 545–551, 1989.

[24] M. Winter and J. O. Besenhard, "Electrochemical lithiation of tin and tin-based intermetallics and composites," *Electrochimica Acta*, vol. 45, no. 1, pp. 31–50, 1999.

[25] T. Shodai, S. Okada, S.-i. Tobishima, and J.-i. Yamaki, "Study of $Li_{3-x}M_xN$(M: Co, Ni or Cu) system for use as anode material in lithium rechargeable cells," *Solid State Ionics*, vol. 86, pp. 785–789, 1996.

[26] Y. Idota, T. Kubota, A. Matsufuji, Y. Maekawa, and T. Miyasaka, "Tin-based amorphous oxide: a high-capacity lithium-ion-storage material," *Science*, vol. 276, no. 5317, pp. 1395–1397, 1997.

[27] I. A. Courtney and J. Dahn, "Electrochemical and *in situ* X-ray diffraction studies of the reaction of lithium with tin oxide composites," *Journal of The Electrochemical Society*, vol. 144, no. 6, pp. 2045–2052, 1997.

[28] K. D. Kepler, J. T. Vaughey, and M. M. Thackeray, "$Li_xCu_6Sn_5$ (0<x<13): An intermetallic insertion electrode for rechargeable lithium batteries," *Electrochemical and Solid-State Letters*, vol. 2, no. 7, pp. 307–309, 1999.

[29] T. Ohzuku, Y. Iwakoshi, and K. Sawai, "Formation of lithium-graphite intercalation compounds in nonaqueous electrolytes and their application as a negative electrode for a lithium ion (shuttlecock) cell," *Journal of The Electrochemical Society*, vol. 140, no. 9, pp. 2490–2498, 1993.

[30] K. Zaghib, K. Tatsumi, Y. Sawada, S. Higuchi, H. Abe, and T. Ohsaki, "^{7}Li-NMR of well-graphitized vapor-grown carbon fibers and natural graphite negative electrodes of rechargeable lithium-ion batteries," *Journal of The Electrochemical Society*, vol. 146, no. 8, pp. 2784–2793, 1999.

[31] F. Chevallier, F. Poli, B. Montigny, and M. Letellier, "*In situ* ^{7}Li nuclear magnetic resonance observation of the electrochemical intercalation of lithium in graphite: second cycle analysis," *Carbon*, vol. 61, pp. 140–153, 2013.

[32] J. O. Besenhard and H. P. Fritz, "The electrochemistry of black carbons," *Angewandte Chemie International Edition in English*, vol. 22, no. 12, pp. 950–975, 1983.

[33] A. Lerf, "Storylines in intercalation chemistry," *Dalton Transactions*, vol. 43, no. 27, pp. 10276–10291, 2014.

[34] P. Schauffaütl, "Bisulfate inercalation compound of graphite," *Journal für praktische Chemie*, vol. 21, p. 155, 1841.

[35] K. Fredenhagen and G. Cadenbach, "Die bindung von kalium durch kohlenstoff," *Zeitschrift für anorganische und allgemeine Chemie*, vol. 158, no. 1, pp. 249–263, 1926.

[36] U. Hofmann and A. Frenzel, "Über permutoide Reaktionen des Graphits," *Zeitschrift für Elektrochemie und angewandte physikalische Chemie*, vol. 37, no. 8-9, pp. 613–618, 1931.

[37] W. Rüdorff, "Graphite intercalation compounds," *Advances in Inorganic Chemistry and Radiochemistry*, vol. 1, pp. 223–266, 1959.

[38] L. B. Ebert, "Intercalation compounds of graphite," *Annual Review of Materials Science*, vol. 6, no. 1, pp. 181–211, 1976.

[39] H. Selig and L. B. Ebert, "Graphite intercalation compounds," *Advances in Inorganic Chemistry and Radiochemistry*, vol. 23, pp. 281–327, 1980.

[40] M. Inagaki, "Applications of graphite intercalation compounds," *Journal of Materials Research*, vol. 4, no. 06, pp. 1560–1568, 1989.

[41] M. Dresselhaus and G. Dresselhaus, "Intercalation compounds of graphite," *Advances in Physics*, vol. 30, no. 2, pp. 139–326, 1981.

[42] G. R. Williams, A. M. Fogg, J. Sloan, C. Taviot-Gueho, and D. O'Hare, "Staging during anion-exchange intercalation into $[LiAl_2(OH)_6]Cl{\cdot}yH_2O$: structural and mechanistic insights," *Dalton Transactions*, no. 32, pp. 3499–3506, 2007.

[43] C. Sole, N. E. Drewett, and L. J. Hardwick, "*In situ* raman study of lithium-ion intercalation into microcrystalline graphite," *Faraday discussions*, vol. 172, pp. 223–237, 2014.

[44] W. Rüdorff and U. Hofmann, "Über graphitsalze," *Zeitschrift für anorganische und allgemeine Chemie*, vol. 238, no. 1, pp. 1–50, 1938.

[45] W. Rüdorff and H. Schulz, "Über die einlagerung von ferrichlorid in das gitter von graphit," *Zeitschrift für anorganische und allgemeine Chemie*, vol. 245, no. 2, pp. 121–156, 1940.

[46] N. Daumas and A. Herold, "Relations between phase concept and reaction mechanics in graphite insertion compounds," *Comptes Rendus Hebdomadaires Des Seances De L Academie Des Sciences Serie C*, vol. 268, no. 5, p. 373, 1969.

[47] R. Setton, P. Bernier, and S. Lefrant, *Carbon molecules and materials*. CRC Press, 2002.

[48] R. Janot and D. Guerard, "Ball-milling in liquid media: Applications to the preparation of anodic materials for lithium-ion batteries," *Progress in Materials Science*, vol. 50, no. 1, pp. 1–92, 2005.

[49] H. Okamoto, "The C-Li (carbon-lithium) system," *Journal of Phase Equilibria*, vol. 10, no. 1, pp. 69–72, 1989.

[50] J. Sangster, "C-Li (Carbon-Lithium) system," *Journal of Phase Equilibria and Diffusion*, vol. 28, no. 6, pp. 561–570, 2007.

[51] R. Juza and V. Wehle, "Lithium-graphit-einlagerungsverbindungen," *Naturwissenschaften*, vol. 52, no. 20, pp. 560–560, 1965.

[52] D. Guerard and A. Herold, "Intercalation of lithium into graphite and other carbons," *Carbon*, vol. 13, no. 4, pp. 337–345, 1975.

[53] R. Janot, J. Conard, and D. Gurard, "Ball milling: a new route for the synthesis of superdense lithium GICs," *Carbon*, vol. 39, no. 12, pp. 1931–1934, 2001.

[54] D. Guérard and R. Janot, "Structure of the superdense LiC_3 compound prepared by ball-milling," *Journal of Physics and Chemistry of Solids*, vol. 65, no. 2, pp. 147–152, 2004.

[55] C. Bindra, V. A. Nalimova, D. E. Sklovsky, Z. Benes, and J. E. Fischer, "Super dense LiC_2 as a high capacity Li intercalation anode," *Journal of the Electrochemical Society*, vol. 145, no. 7, pp. 2377–2380, 1998.

[56] V. Solozhenko and T. Peun, "Compression and thermal expansion of hexagonal graphite-like boron nitride up to 7GPa and 1800 K," *Journal of Physics and Chemistry of Solids*, vol. 58, no. 9, pp. 1321–1323, 1997.

[57] R. Nicklow, N. Wakabayashi, and H. Smith, "Lattice dynamics of pyrolytic graphite," *Physical Review B*, vol. 5, no. 12, p. 4951, 1972.

[58] B. T. Kelly, "Physics of graphite," *Applied Science, London*, vol. 13, no. 7, p. 477, 1981.

[59] A. Kurdyumov, V. Solozhenko, and W. Zelyavski, "Lattice parameters of boron nitride polymorphous modifications as a function of their crystal-structure perfection," *Journal of applied crystallography*, vol. 28, no. 5, pp. 540–545, 1995.

[60] M. S. Dresselhaus, G. Dresselhaus, and P. C. Eklund, *Science of fullerenes and carbon nanotubes: their properties and applications*. Academic press, 1996.

[61] A. Pakdel, Y. Bando, and D. Golberg, "Nano boron nitride flatland," *Chemical Society Reviews*, vol. 43, no. 3, pp. 934–959, 2014.

[62] M. E. Levinshtein, S. L. Rumyantsev, and M. S. Shur, *Properties of Advanced Semiconductor Materials: GaN, AIN, InN, BN, SiC, SiGe*. John Wiley & Sons, 2001.

[63] M. Petrescu, "Boron nitride theoretical hardness compared to carbon polymorphs," *Diamond and related materials*, vol. 13, no. 10, pp. 1848–1853, 2004.

[64] R. Croft, "New molecular compounds of the layer lattice type. IV. new molecular compounds of boron nitride," *Australian Journal of Chemistry*, vol. 9, no. 2, pp. 206–211, 1956.

[65] A. Freeman and J. Larkindale, "Preparation, mössbauer spectra, and structure of intercalation compounds of boron nitride with metal halides," *Journal of the Chemical Society A: Inorganic, Physical, Theoretical*, pp. 1307–1308, 1969.

[66] A. Freeman and J. Larkindale, "Evidence for the formation of boron nitride-alkali metal intercalation compounds," *Inorganic and Nuclear Chemistry Letters*, vol. 5, no. 11, pp. 937–939, 1969.

[67] M. Sakamoto, J. Speck, and M. Dresselhaus, "Cesium and bromine doping into hexagonal boron nitride," *Journal of Materials Research*, vol. 1, no. 05, pp. 685–692, 1986.

[68] N. Bartlett, R. Biagioni, B. McQuillan, A. Robertson, and A. Thompson, "Novel salts of graphite and a boron nitride salt," *Journal of the Chemical Society, Chemical Communications*, no. 5, pp. 200–201, 1978.

[69] J. Hooley, "Intercalation by $(SO_3F)_2$ in various forms of graphite and boron nitride," *Carbon*, vol. 21, no. 3, pp. 181–188, 1983.

[70] C. Shen, S. G. Mayorga, R. Biagioni, C. Piskoti, M. Ishigami, A. Zettl, and N. Bartlett, "Intercalation of hexagonal boron nitride by strong oxidizers and evidence for the metallic nature of the products," *Journal of Solid State Chemistry*, vol. 147, no. 1, pp. 74–81, 1999.

[71] N. I. Kovtyukhova, Y. Wang, R. Lv, M. Terrones, V. H. Crespi, and T. E. Mallouk, "Reversible intercalation of hexagonal boron nitride with brønsted acids," *Journal of the American Chemical Society*, vol. 135, no. 22, pp. 8372–8381, 2013.

[72] G. Doll, J. Speck, G. Dresselhaus, M. Dresselhaus, K. Nakamura, and S.-I. Tanuma, "Intercalation of hexagonal boron nitride with potassium," *Journal of applied physics*, vol. 66, no. 6, pp. 2554–2558, 1989.

[73] A. Sumiyoshi, H. Hyodo, and K. Kimura, "Li-intercalation into hexagonal boron nitride," *Journal of Physics and Chemistry of Solids*, vol. 71, no. 4, pp. 569–571, 2010.

[74] A. Sumiyoshi, H. Hyodo, and K. Kimura, "Structural analysis of Li-intercalated hexagonal boron nitride," *Journal of Solid State Chemistry*, vol. 187, pp. 208–210, 2012.

[75] A. Sumiyoshi, H. Hyodo, Y. Sato, M. Terauchi, and K. Kimura, "Good reproductive preparation method of Li-intercalated hexagonal boron nitride and transmission electron microscopy–electron energy loss spectroscopy analysis," *Solid State Sciences*, vol. 47, pp. 68–72, 2015.

[76] E. Budak and Ç. Bozkurt, "The effect of transition metals on the structure of h-BN intercalation compounds," *Journal of Solid State Chemistry*, vol. 177, no. 4, pp. 1768–1770, 2004.

[77] B. Altintas, C. Parlak, C. Bozkurt, and R. Eryiğit, "Intercalation of graphite and hexagonal boron nitride by lithium," *The European Physical Journal B*, vol. 79, no. 3, pp. 301–312, 2011.

[78] C.-H. Doh, B. Han, B.-S. Jin, and H.-B. Gu, "Structures and formation energies of Li_xC_6 (x= 1-3) and its homologues for lithium rechargeable batteries," *Bull. Korean Chem. Soc*, vol. 32, no. 6, pp. 2045–2050, 2011.

Chapter 2

Methods

2.1 Sample preparations

2.1.1 Properties of lithium

Lithium is one of the alkali metals and the lightest metal as it has a 0.534 g/cm^3 density at room temperature. Pure lithium metal is very soft, thus it can be cut using a knife. The atomic number of lithium is 3 in the periodic table and standard atomic weight is 6.941 mol/g. The crystal structure of lithium is body-centered cubic (BCC) (lattice parameter is a = 0.351 nm) and atomic radius is 0.150 $\sim$ 0.156 nm. Naturally, two stable isotopes of lithium exist as ^{6}Li (7.59%) and ^{7}Li (92.41%) [1].

Lithium is highly reactive and it burns in the air. Thus lithium reacts with nitrogen gas in dry air as seen in Eq. 2.1, while lithium hydroxide was formed in humid air (Eq. 2.2).

$$6\ \mathrm{Li} + \mathrm{N_2} \rightarrow 2\ \mathrm{Li_3N} \tag{2.1}$$

$$2\,\mathrm{Li} + 2\ \mathrm{H_2O} \rightarrow 2\ \mathrm{LiOH} + \mathrm{H_2} \tag{2.2}$$

For this reason, in nature lithium doesn't exist in the form of pure metal, but instead it can be obtained by lithium compounds. Pure lithium metal has to be stored in mineral oil or argon atmosphere [2]; in this thesis, the storage and treatment of lithium metal is conducted in glove box filled with argon gas (purity up to 99.9999%).

2.1.2 Ball milling (BM) and starting materials

Ball milling (BM) is a technique of a solid-state powder processing and one of the processes to produce supersaturated solid solutions, nano-crystal alloys and non-equilibrium phase alloys [3–8]. The finely dispersed powder can be manufactured using BM through welding and pulverizing in a solid state. This process was firstly developed by Benjamin and his colleagues (International Nickel Company, INCO) in 1966 in order to produce nickel-based oxide dispersion-strengthened alloys (ODS) for turbine blades of aircraft engines, and they were able to get improved mechanical properties of nickel-based superalloys. Then, Benjamin has reported it using the term of "mechanical alloying" [9]. There are two major terms for nomenclatures of BM as follows [8]:

▷ "Mechanical alloying" : the process when different materials are milled together and material transfer occurs with a homogeneous alloy.

▷ "Mechanical milling" : the process when uniform composition powders are milled with structure modification without chemical reaction.

Except for these two terms, many authors used various terms such as mechanical disordering, mechanical grinding, reaction milling, cryomilling, rod milling and so on, in order to easily know the detail processes using milling. In this thesis, "ball milling (BM)" was used because several means could be included [10].

The basic method of BM is that the starting materials and the grinding medium (balls) are put into the vessel (generally same material with balls) and milled for the desired durations. There are various parameters for BM processes such as types of mill, kinds of milling containers and balls, milling speeds, milling durations, milling atmosphere, ball-to-powder weight ratio(BPR) and ratios between starting materials etc. In this thesis, BM processes were used in the three Chapters, which are Chapter 3, 4 and 5. The common conditions of BM are as in the following.

▷ Types of milling: vibratory ball mill
NISSIN GIKEN Corporation, Super Misuni NEV-MA8 (Fig. 2.1)
Fig. 2.2 shows a mode of vibration.

▷ Kinds of milling containers and balls: stainless steel (AISI 304)

▷ Motor rotation speed: 710 rpm

▷ Milling atmosphere: argon gas

Fig. 2.1. Picture of a vibratory ball mill used for this thesis.

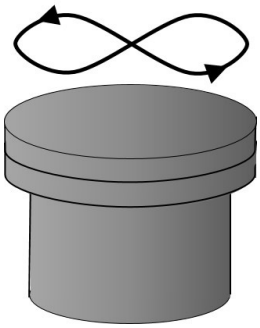

Fig. 2.2. Vibration mode of Super Misuni NEV-MA8.

▷ The weight of starting materials: 3g
▷ BPR: about 10 (9 AISI 304 balls (about 3.58 g per a ball))

The starting materials with their ratios and milling durations of respective Chapters are organized in Table 2.1: in the Chapter 3 the pieces of Li metal and h-BN powder with the molar ratio of 1 : 2.2 and milling durations of 1, 2.5, 5, 10, 35 and 60 hours for Li–BN system, in the Chapter 4 the pieces of Li metal, h-BN and graphite powder with a molar ratio of 1 : 1.1 : 1.1 and milling durations of 2.5 and 10 hours for Li–BN–graphite and in the Chapter 5 h-BN and graphite powder with a weight ratio of 8 : 1 and milling duration of 2.5 hours for electrochemical test.

The h-BN powder exhibits thin plate-like morphology as seen in Fig. 2.3 with purity up to 99.5% (NACALAI TESQUE, INC.) and graphite (purity up to 99.9%, KOJUNDO CHEMICAL Lab., CO., LTD). Li metal (purity up to 99.9999%, KOJUNDO CHEMICAL Lab., CO., LTD) was cut/sliced into a stick shape with dimension of 1 mm in length, 0.5 mm in thickness and width using a knife, from a bar-shaped Li bulk after removing the oxide scale (Oxide exists on the surface though it is kept in argon atmosphere) as seen in Fig. 2.4. In this study, all samples were kept and treated in a glove box filled with argon gas.

2.1.2.1 Sequential process of BM and heat treatment

In the Li–BN (Chapter 3) and Li–BN–graphite (Chapter 4) system, the milled samples were subject to heat treatment at 700 °C for 2 hours in argon atmosphere. The heating and cooling rate is 10 °C/min. The milled samples were put in a platinum holder in the glove box and capped by alumina with dome-like shape. It was moved into holder of DTA (Differential thermal analysis) machine with packing under argon atmosphere.

2.2 Sample analysis

2.2.1 X-ray diffraction (XRD)

X-ray powder diffraction (XRD) is an analytical technique to typically measure structural properties, such as crystal structure, defect structure and grain size etc., and it identifies phases of materials and provides information on unit cell dimensions. X-rays generated by a cathode ray tube are filtered to produce monochromatic radi-

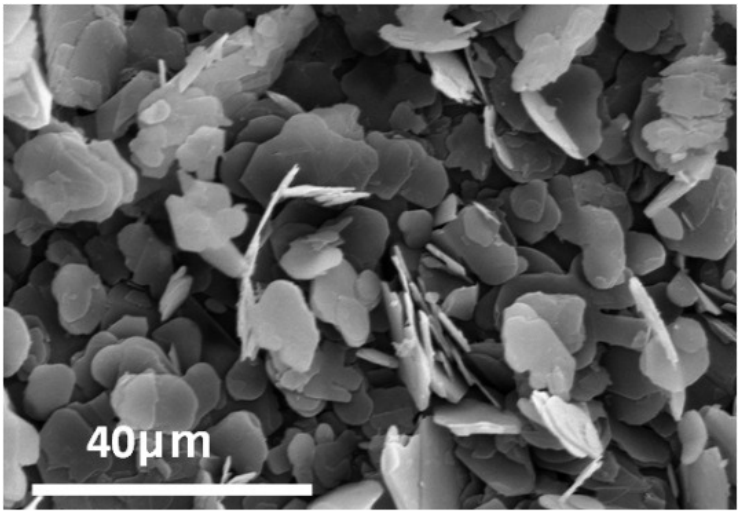

Fig. 2.3. SEM image of hexagonal boron nitride.

Table 2.1. The starting materials, their ratios and milling durations used in each Chapter.

	Chapter 3	Chapter 4	Chapter 5
Starting materials	Li + h-BN	Li + h-BN + graphite	h-BN ; graphite ; h-BN + graphite
Ratio	1 : 2.2 (molar) =1 : 7.9 (weight) =1 : 2 (volume)	1 : 1.1 : 1.1 (molar) =1 : 1 : 0.5 (volume)	8 : 1 (weight) for h-BN + graphite
Milling durations (h)	1, 2.5, 5, 10, 35, 60	2.5, 10	2.5

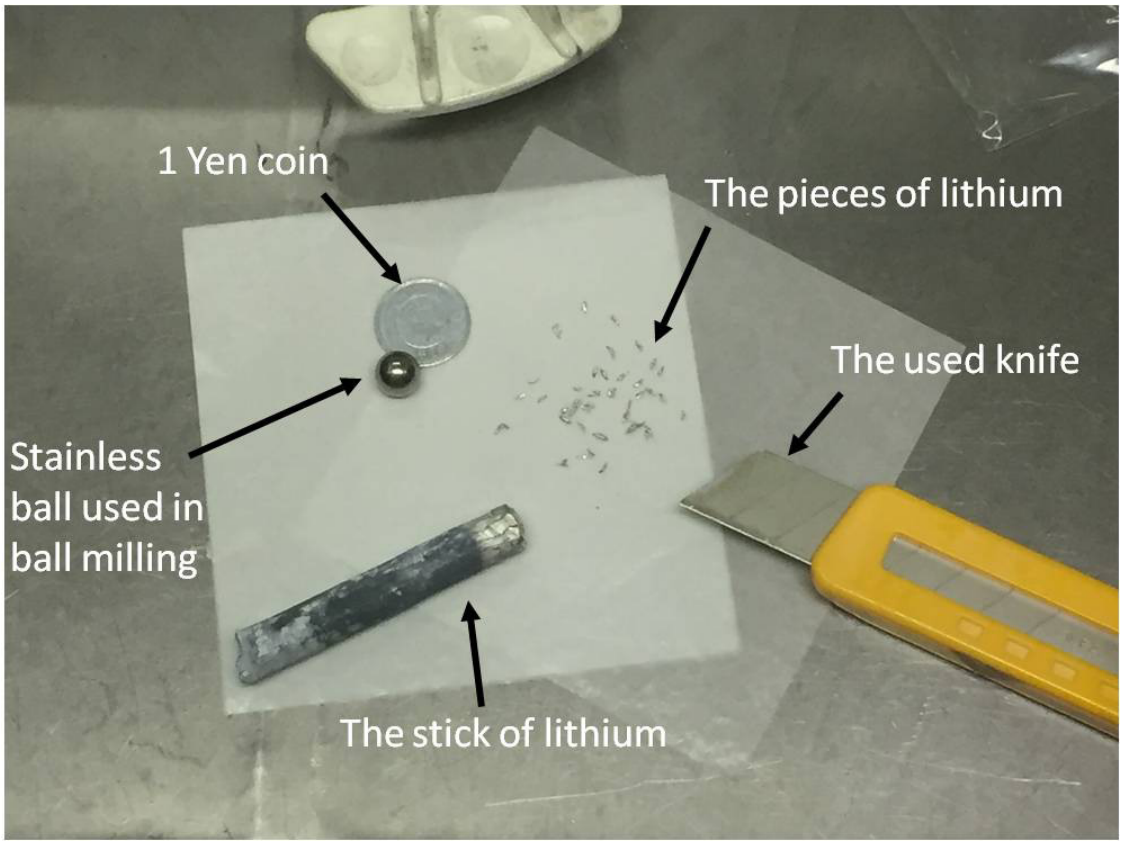

Fig. 2.4. Picture for cutting lithium.

ation, collimated to concentrate, and directed toward the sample. When these X-ray beam interacts with samples (planes of atoms), each part of the beam is transmitted, absorbed by the sample, refracted, scattered, and diffracted, respectively; and the interaction of the incident rays produces constructive interference with diffracted rays. The condition for constructive interference is given by Bragg's Law: $n\lambda = 2d \sin\theta$, where, the integer n is the order of the diffracted beam, λ is the wavelength of the incident X-ray beam, d is the interatomic spacing (the distance between adjacent planes of atoms, d-spacings), and θ is the diffraction angle. These diffracted X-rays are then detected, processed and counted. The various 2θ angles versus d-spacing for materials have been already investigated, and conversion of the diffraction peaks to d-spacings allow the identification of the material.

In this study, the crystal structures of samples prepared were characterized by XRD (RIGAKU Corporation, RINT-2100) with Cu-K_α radiation at 40 kV and 30 mA. Some samples including lithium (Chapter 3 and 4) were sealed in an airtight sample holder equipped with beryllium window to avoid sample exposure to air.

2.2.2 Differential thermal analysis (DTA)

The differential thermal analysis (DTA) is a typical thermo-analytical technique. In DTA, the temperature difference between the material (sample for measure) and an inert reference (usually alumina, Al_2O_3) is measured with thermocouple by simultaneously heating sample and reference. Thermal changes in the sample, such as exothermic or endothermic reaction, can be detected by comparing an inert reference, which is not changed. These changes, i.e. differential temperatures are plotted against time, or against temperature and is called DTA curve, or thermogram. From a DTA curve, transformations, such as glass transitions, crystallization, melting and sublimation can be identified.

In this study, DTA (RIGAKU Corporation, Thermo Plus 2 series TG 8120) was conducted to perform thermal analysis of the milled sample of Chapter 3 and Chapter 4. The conditions for DTA are selected as follows: a heating rate of 10 °C/min in a flowing argon gas from room temperature to 700 °C. In the Chapter 4, heating rates of 5, 10, 20, 30 and 50 °C/min were used for some samples in order to calculate activation energy using the Kissinger method with the following equation [11]:

$$\ln\left(\frac{\beta}{T_p^2}\right) = \ln\left(\frac{AR}{E_a}\right) - \frac{E_a}{RT_p} \tag{2.3}$$

where, β is the heating rate, T_p is the peak temperature of each DTA curve at different heating rate, A is a pre-exponential factor, R is a gas constant (8.314 $\mathrm{J{\cdot}K^{-1}mol^{-1}}$) and E_a is the activation energy. E_a can be estimated from the slope of E_a/R by fitting $1/T_p$ versus $\ln(\beta/T_p^2)$.

2.2.3 X-ray photoelectron spectroscopy (XPS)

X-ray photoelectron spectroscopy (XPS) is a widely used technique for surface analysis. A quantitative and chemical state information on the surface of the materials can be identified by irradiating the surface with a X-ray beam and measuring the kinetic energy of the inner or valence electrons (E_{kinetic}) emitted from X-ray photon. Because E_{kinetic} is measured and the energy of this X-ray photon with particular wavelength is known, for example E_{photon} is 1486.7 eV for Al-K_α, the electron binding energy for each of the emitted electrons (E_{binding}), which are characteristic of the chemical bonds of materials, can be calculated by the following equation:

$$E_{\mathrm{binding}} = E_{\mathrm{photon}} - (E_{\mathrm{kinetic}} + \phi) \tag{2.4}$$

where, ϕ is the work function dependent on both the spectrometer and the material.

In this study, XPS was performed with Al-K_α source operating at 10 kV and 20 mA. A pass-energy is 20 eV with 0.1 eV/200 ms steps. All the samples for XPS were kept in a transfer vessel filled with argon gas and transferred from the glove box to the XPS system under vacuum.

2.2.4 ^{7}Li nuclear magnetic resonance (NMR)

Nuclear magnetic resonance (NMR) is a physical phenomenon in which nuclei in a magnetic field resonate with electromagnetic wave of a specific frequency. This resonance is caused by the spinning of nuclei when the material is placed in a magnetic field; this energy depends on the strength of the magnetic field and the magnetic properties of the isotope of the atoms. Absorbed frequencies are different even at the same intensity of magnetic field, because the spinning intensities for nuclei of each atoms in a compound are different, thus, we can deduce which atoms exist. Through NMR phenomena, molecular physics, crystals, and non-crystalline materials etc. can

be studied and NMR is also routinely used in medical techniques, such as in magnetic resonance imaging (MRI).

For the lithium NMR, lithium has two useful nuclei, ^{6}Li and ^{7}Li, as mentioned in Section 2.1.1. The properties of them are organized in Table 2.2. ^{6}Li has a low quadrupolar moment and sharp signals although spin is 1, which is greater than 1/2 and means quadrupolar. Receptivity relative to that of ^{1}H for ^{6}Li is lower than ^{7}Li, so signals of ^{7}Li are broader.

In this study, Li states in the samples of Chapter 3 and Chapter 4 were examined by ^{7}Li NMR. NMR measurements were carried out under 4.65 T of magnetic field by using a standard phase coherent-type NMR pulsed spectrometer. Free induction decay (FID) signal was observed after a single pulse of 20 μs at room temperature. NMR spectra were measured by the fast Fourier transform (FFT) method of the FID. The samples for NMR were prepared by sealing in glass tubes in argon atmosphere and measured at 76.94 MHz with a repetition time of 6 $\sim$ 75 sec determined by the longitudinal relaxation times. LiCl aqueous solution was used as a reference. The samples were sealed in glass tubes with argon atmosphere to avoid their exposure to air.

2.2.5 Electrochemical test

This electrochemical test is a main method for Chapter 5.

2.2.5.1 Preparation of half cells

In this study, the electrochemical performances were conducted using a beaker cell with three electrodes in ethylene carbonate/dimethyl carbonate (EC-DMC 1 : 2 by vol.) containing 1 M $LiPF_6$. The schematic three electrode cell is shown in Fig. 2.5 and the roles of each electrode are defined as follows: the working electrode (WE), where the electrochemical reaction occurs, the auxiliary or counter electrode (CE), which supplies the current required for the electrochemical reaction at WE, and reference electrode (RE), which tracks the potential solution. The lithium ribbons were used as CE and RE, and 6 kinds of WEs were prepared. The details about WEs are shown in Table 2.3 and they are the pristine graphite (Pure C), the pristine h-BN (Pure BN), the milled graphite (Milled C), the milled h-BN (Milled BN), the mixture of milled graphite and milled h-BN on weight ratio of 1/8 (Milled BN8C1-s), and milled together graphite and h-BN by the same weight ratio (Milled BN8C1-

Table 2.2. The properties of ^{6}Li and ^{7}Li [12]

Isotope	^{6}Li	^{7}Li
Spin	1	3/2
Natural abundance (x/%)	7.59	92.41
Magnetic moment ($\mu/\mu N$)	1.162 5637	4.204 075 05
Magnetic ratio ($\gamma/10^{7}$ rad s^{1} T^{1})	3.937 1709	10.397 7013
Quadruple moment (Q/fm^{2})	0.0808	4.01
Frequency ratio (Ξ /%)	14.716 086	38.863 797
Receptivity relative to that of ^{1}H	6.45×10^{4}	0.271
Refernce sample	LiCl	

t). The conditions for the milled WEs can be seen in Table 2.1 and all starting materials, which are h-BN and graphite were milled separately or together, are 3g, respectively. The prepared 6 kinds of powders were coated on Cu foil by mixing with the binder, which is 5.34 wt% polyvinylidene fluoride (PVDF) with N-Methyl-2-pyrrolidone (NMP). Assembling the cell and all the electrochemical measurements were conducted in the glove box filled with Ar gas with moisture and oxygen level below 2 ppm.

2.2.5.2 Cyclic voltammetry (CV) and Galvanostatic cycling with potential limitation (GCPL)

The electrochemical properties were characterized by cyclic voltammetry (CV) and galvanostatic cycling with potential limitation (GCPL) using a potentiostat/galvanostat (Biologic Science Instruments, VMP3). CV is one of potentiodynamic methods and, in a CV experiment, a variation of electric current is measured by cycling electric potentials in the opposite direction to return to the initial potential [13]. Cyclic voltammogram shows a plot of the current versus the voltage (that is, potential) at the working electrode to give the cyclic voltammogram trace. CV is the most widely used method for investigation of electro-active species. In this study, range of 0∼2 V for potential and 1.0 mV/s scan rate was used.

GCPL is the method for measuring the variation of potential by applying a constant current to the electrochemical cell over fixed range of potential. The potential limit of 0.01 and 3.0 V vs. Li/Li^+ was used in this study. Through GCPL experiment, the quantity of electrical charge (C) per mass of active material (m) can be calculated by the following equation:

$$C = I \times t/m \tag{2.5}$$

where, t is the time under constant current (I) of each step. C represents the specific capacity and its unit is mAh/g.

Meanwhile, theoretical capacities (Q, mAh/g) can be typically calculated by Faraday's 2^{nd} law of electrolysis as follows:

$$Q = \frac{xF}{M} \tag{2.6}$$

Table 2.3. Constituted arrangement of working electrodes.

No.		Active and/or Conductive material		Binder	Weight (mg)	Sample name
		h-BN	graphite			
1	Category	-	Pure graphite	PVDF	1.95 ± 0.005	Pure C
	wt%	-	90	10		
2	Category	Pure BN	-	PVDF	1.3 ± 0.005	Pure BN
	wt%	90	-	10		
3	Category	-	2.5 h-milled graphite	PVDF	1.3 ± 0.005	Milled C
	wt%	-	80	20		
4	Category	2.5 h-milled BN	-	PVDF	0.95 ± 0.005	Milled BN
	wt%	90	-	10		
5	Category	2.5 h-milled BN	2.5 h-milled graphite	PVDF	1.2 ± 0.005	Milled BN8C1-s
	wt%	80	10	10		
6	Category	2.5 h-milled BN + 2.5 h-milled graphite		PVDF	0.9 ± 0.005	Milled BN8C1-t
	wt%	80	10	10		

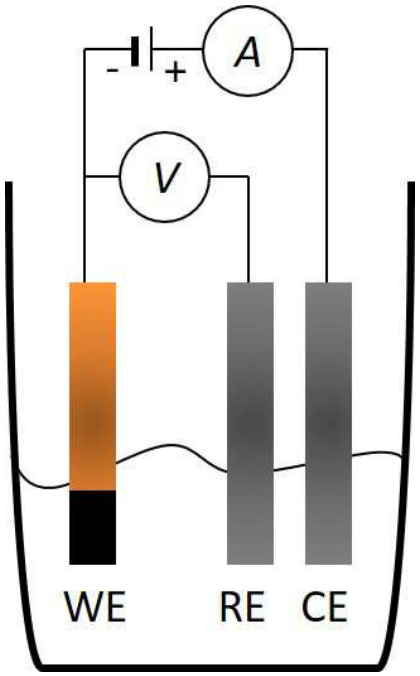

Fig. 2.5. The schematic diagram of three electrodes cell.

where, x is the (max.) number of Li moles for reaction involved, M is a molar mass and F is Faraday constant (F = 96485 C (A· s) = 26800 mAh). The capacity of graphite was calculated as 372 mAh/g based on the following reaction (it is same to Eq. 1.1):

$$6\,\mathrm{C} + \mathrm{Li}^+ + \mathrm{e}^- \rightarrow \mathrm{LiC}_6 \tag{2.7}$$

On the other hand, in case of BN, the reaction(s) involved and the Li concentration(s) have not been reported. Therefore, a hypothetical reaction similar to graphite reaction for producing LiC_6 was tentatively written as follows;

$$3\,(\mathrm{BN}) + \mathrm{Li}^+ + \mathrm{e}^- \rightarrow \mathrm{Li(BN)_3} \tag{2.8}$$

From Eq. 2.8, the calculated capacity for BN is 360 mAh/g and this estimated capacity value will be used for calculating C-rate.

2.3 Structure modeling

2.3.1 Phase model

In this thesis, various hypothetic Li-BNICs, which are Li(BN), $Li_2(BN)_3$, $Li(BN)_3$, $Li(BN)_4$, $Li_2(BN)_9$ and $Li(BN)_9$, were predicted in order to investigate Li concentration in synthesized Li-BNICs through DFT calculation. Fig. 2.6 shows their atomic structures (left figures exhibit unit cells). All compounds are 1^{st} stage phase and they are referred as Li-GICs. Also, both 2L- and 1L-model structures will be calculated because the atomic structure for Li-BNICs have been suggested 1L model as mentioned in Chapter 1.5 and it should need to compare these two models. The reason for suggested phases of hypothetic Li-BNICs will be explained in Chapter 6 in detail.

2.3.2 Rietveld method

The Rietveld method (Rietveld analysis, Rietveld refinement) devised by Hugo Rietveld is an advanced analysis with whole XRD pattern fitting refinement [14] and it is based on minimizing the residual function, which is a weighted sum of squares, $S(x)$, using non-linear least squares as seen in Eq. 2.9 [15]:

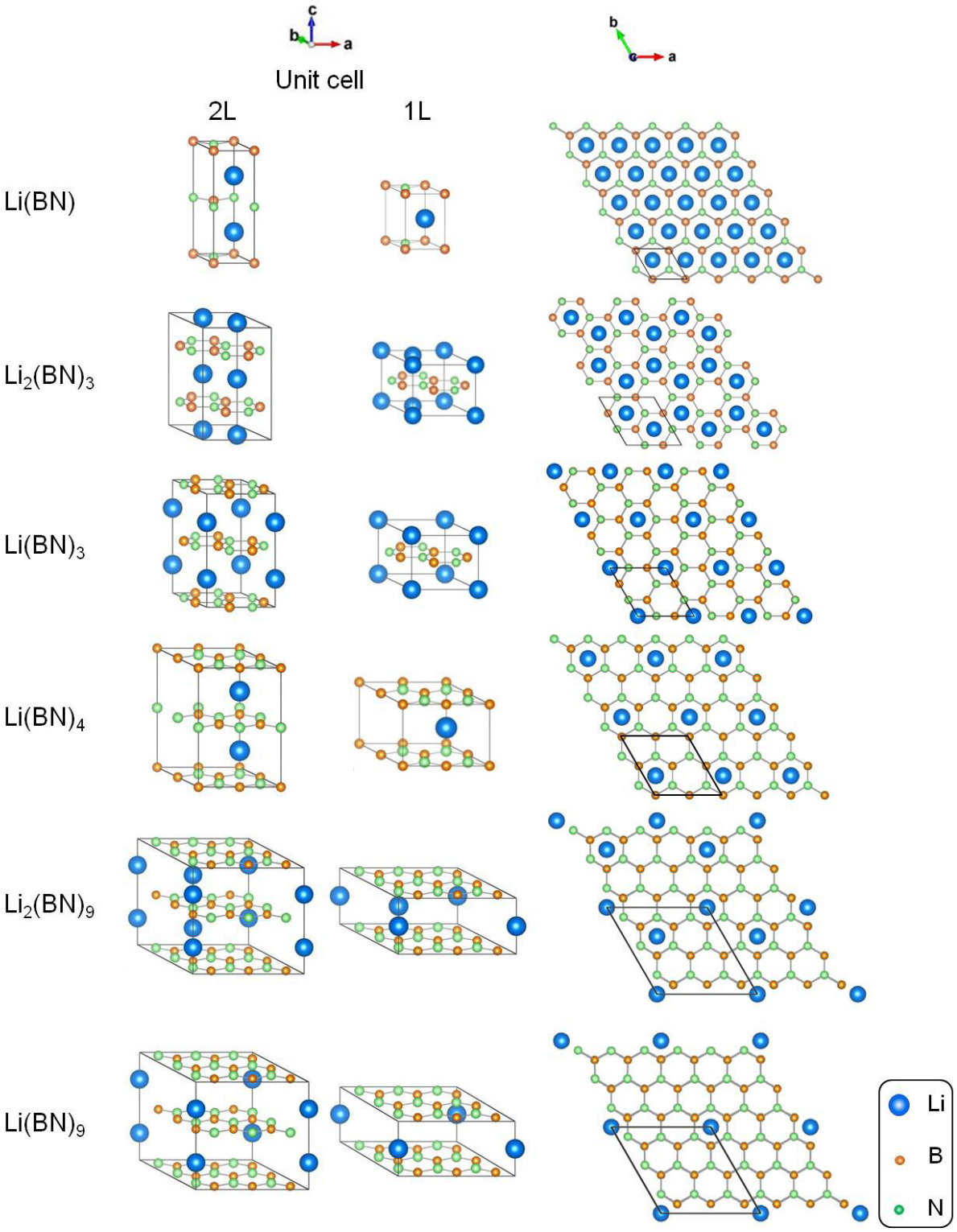

Fig. 2.6. Structures of hypothetic Li-BNICs.

$$S(x) = \sum_{i=1}^{N} w_i[y_i - f_i(x)]^2 \tag{2.9}$$

where, y_i is the observed intensity, i is $1 \sim N$, N is the number of data points, $f_i(x)$ is the calculated intensity and w_i is $w_i \equiv 1/y_i$. The indicators, which are the reliability factors (R-factor) and the goodness of fit (S), are obtained when the calculation is finished for estimating the result of Rietveld analysis. The most universal R-factor is R_{wp}, which is the weighted-profile R-factor, and it is defined as the following:

$$R_{wp} = \left\{ \frac{\sum_{i=1}^{N} w_i[y_i - f_i(x)]^2}{\sum_{i=1}^{N} w_i y_i^2} \right\}^{1/2} \tag{2.10}$$

However, it depends on the background, thus, it is easier to get low values with a high background. Due to this problem, expected R-factor, R_e, which is statistically predicted value, is also considered. This R-factor can be calculated on the same denominator with R_{wp} as the weighted-profile one, using N with minus the number of used parameters (P) for a numerator as following:

$$R_e = \left\{ \frac{N - P}{\sum_{i=1}^{N} w_i y_i^2} \right\}^{1/2} \tag{2.11}$$

The ratio between the R_{wp} and R_e is called S:

$$S = \frac{R_{wp}}{R_e} = \left\{ \frac{\sum_{i=1}^{N} w_i[y_i - f_i(x)]^2}{N - P} \right\}^{1/2} \tag{2.12}$$

Other R-factor that did not involve the peak-shape function, is intensity or bragg R-factor, R_I or R_B and it is probably useful of the non-profile. Its equation is as:

$$R_B = \frac{\sum_K |I_K(\text{“o”}) - I_K|}{\sum_K I_K(\text{“o”})} \tag{2.13}$$

where, $I_K(\text{“o”})$ is the observed intensity and I_K is the calculated intensity.

Rietveld method can be computed by conducting curve-fitting XRD reflections and several structural information of samples, such as lattice parameter, atom coordinates, etc., which can be identified through this method. However it is not for

determining the crystal structure but it is for refining the crystal structure of a compound. Thereby, a model for crystal structure is needed before the analysis.

In this study, Rietveld method was conducted using RIETAN-FP developed by F. Izumi's group [16]. The used XRD patterns for Rietveld analysis and detailed results can be seen in Chapter 3 and 6.

2.3.3 Density functional theory (DFT) calculation

Hypothetical Li-BNICs structures were calculated using ABINIT package [17], which is a program for implementing density functional theory (DFT) [18, 19] based on a pseudopotential method of first principles calculation using a plane-wave basis about wave functions. Norm-conserving pseudopotential, which is most common forms of pseudopotential for plane-wave electronic structure codes and local-density approximation (LDA) [20,21] generated from FHI98PP program [22] for the exchange-correlation function using Perdew and Wang [23] were used. The total energies was well converged at 1 meV level when the cutoff energy for plane-wave expansion was set to 35 Hartree and the k-points grid of real space length, which is represented to kptrlen input parameter of ABINIT was approximately 85. Lattice parameters were calculated from structural optimization using the Broyden-Fletcher-Goldfarb-Shanno (BFGS) minimization.

Formation energy (E_f) are calculated from total energies computed by DFT and defined as:

$$E_f = E_{Product} - \sum_n E_{Reactant} \tag{2.14}$$

where, $E_{Product}$ and $E_{Reactant}$ are the total energy of a product and reactant from calculation, respectively. The formation energy calculated by DFT is different Gibbs free energy (or enthalpy) of formation because the energies obtained from DFT calculation are potential within the framework of the Born-Oppenheimer approximation [24]. Namely, the energies of the system for the fixed positions of the nuclei in the DFT are calculated as the sum of the kinetic energies of the electronic clouds, where they are from the Coulomb interactions between electrons and nuclei.

The equilibrium voltage difference ($V(x)$) between the two electrodes depends on the difference of the Li chemical potential (μ_{Li}) between the anode (no Li metal) and cathode as:

$$V(x) = -\frac{\mu_{Li(x)}^{cathode} - \mu_{Li(x)}^{anode}}{zF} \tag{2.15}$$

where, z is the charge transported by lithium in the electrolyte. Usually z is 1 for Li intercalation in most nonelectronically conducting electrolytes and F is the Faraday constant.

From these hypothetic Li-BNICs, the reaction of Li intercalation into h-BN (in the half cell including electrodes of Li metal and h-BN) is implied as following equation:

$$x\mathrm{Li} + 3\,(\mathrm{BN}) \rightarrow \mathrm{Li_x(BN)_3} \tag{2.16}$$

Thereby, Eq. 2.15 in the above reaction can be rewritten as:

$$V(x) = -\frac{\mu_{Li(x)}^{BN} - \mu_{Li}^{metallic\ Li}}{zF} \tag{2.17}$$

The average voltage ($\bar{V}$) for Li intercalation of the intercalation compound have been detected by integrating Eq. 2.15 [25] and it can be simply determined by computing total energy (calculated by DFT) of $\mathrm{Li}_x(\mathrm{BN})_3$, BN, and Li metal on the assumption that the entropy (S) and $P\Delta V$ contributions are neglected.

$$\bar{V} = \frac{-[E(\mathrm{Li_x(BN)_3}) - E(3\,(\mathrm{BN})) - xE(\mathrm{Li})]}{xe} = \frac{-E_r(x)}{xe} \tag{2.18}$$

where, e is the electron charge and $E_r(x)$ is reaction energy.

The reactions for Li intercalation into graphite and h-BN according to the amount of Li concentrations are organized in Table 2.4.

Table 2.4. The intercalation reaction of lithium for Li-GIC (Li_xC_6) and Li-BNICs ($Li_x(BN)_3$).

Lithium concentration	Li-GICs		Li-BNICs	
	unit cell	reaction	unit cell	reaction
1/3	-	-	$Li(BN)_9$	1/3 Li+3(BN)-$Li_{1/3}(BN)_3$
2/3	LiC_9	2/3 Li+6C→$Li_{2/3}C_6$	$Li_2(BN)_9$	2/3 Li+3(BN)→$Li_{2/3}(BN)_3$
3/4	LiC_8	3/4 Li+6C→$Li_{3/4}C_6$	$Li(BN)_4$	3/4 Li+3(BN)→$Li_{3/4}(BN)_3$
1	LiC_6	1 Li+6C→LiC_6	$Li(BN)_3$	1 Li+3(BN)→$Li(BN)_3$
2	LiC_3	2 Li+6C→Li_2C_6	$Li_2(BN)_3$	2 Li+3(BN)→$Li_2(BN)_3$
3	LiC_2	3 Li+6C→Li_3C_6	Li(BN)	3 Li+3(BN)→$Li_3(BN)_3$

Reference

[1] M. Anderson and C. Swenson, "Experimental equations of state for cesium and lithium metals to 20 kbar and the high-pressure behavior of the alkali metals," *Physical Review B*, vol. 31, no. 2, p. 668, 1985.

[2] D. Jeppson, J. Ballif, W. Yuan, and B. Chou, "Lithium literature review: lithium's properties and interactions," *Hanford Engineering Development Laboratory*, 1978.

[3] K. Uenishi, K. Kobayashi, K. Ishihara, and P. Shingu, "Formation of a supersaturated solid solution in the Ag–Cu system by mechanical alloying," *Materials Science and Engineering: A*, vol. 134, pp. 1342–1345, 1991.

[4] M. Zdujic, K. Kobayashi, and P. Shingu, "Preparation of amorphous Ni-50 at.% Mo alloy powder by mechanical alloying," *Zeitschrift für Metallkunde*, vol. 83, no. 2, pp. 136–139, 1992.

[5] K. Uenishi, K. F. Kobayashi, K. N. Ishihara, and P. H. Shingu, "Non-equilibrium phase formation in Fe-Ag-Cu system by mechanical alloying," in *Materials Science Forum*, vol. 88, pp. 459–466, Trans Tech Publ, 1992.

[6] M. Zdujić, D. Skala, L. Karanović, M. Krstanović, K. Kobayashi, and P. Shingu, "Thermal behaviour of mechanically alloyed $Ni_{50}Mo_{50}$ powders and associated kinetics of amorphous phase transformation," *Materials Science and Engineering: A*, vol. 161, no. 2, pp. 237–246, 1993.

[7] M. Zdujić, D. Poleti, L. Karanović, K. Kobayashi, and P. Shingu, "Intermetallic phases produced by the heat treatment of mechanically alloyed Al–Mo powders," *Materials Science and Engineering: A*, vol. 185, no. 1, pp. 77–86, 1994.

[8] C. Suryanarayana, "Mechanical alloying and milling," *Progress in materials science*, vol. 46, no. 1, pp. 1–184, 2001.

[9] J. S. Benjamin, "Dispersion strengthened superalloys by mechanical alloying," *Metallurgical transactions*, vol. 1, no. 10, pp. 2943–2951, 1970.

[10] R. Janot and D. Guerard, "Ball-milling in liquid media: Applications to the preparation of anodic materials for lithium-ion batteries," *Progress in Materials Science*, vol. 50, no. 1, pp. 1–92, 2005.

[11] H. E. Kissinger, "Reaction kinetics in differential thermal analysis," *Analytical chemistry*, vol. 29, no. 11, pp. 1702–1706, 1957.

[12] R. K. Harris, E. D. Becker, S. M. Cabral de Menezes, R. Goodfellow, and P. Granger, "NMR nomenclature. Nuclear spin properties and conventions for chemical shifts (IUPAC recommendations 2001)," *Pure and Applied Chemistry*, vol. 73, no. 11, pp. 1795–1818, 2001.

[13] P. T. Kissinger and W. R. Heineman, "Cyclic voltammetry," *J. Chem. Educ*, vol. 60, no. 9, p. 702, 1983.

[14] H. Rietveld, "Line profiles of neutron powder-diffraction peaks for structure refinement," *Acta Crystallographica*, vol. 22, no. 1, pp. 151–152, 1967.

[15] F. Izumi, "The Rietveld method and its applications to synchrotron X-ray powder data," *Analytical Spectroscopy Library*, vol. 7, pp. 405–452, 1996.

[16] F. Izumi and K. Momma, "Three-dimensional visualization in powder diffraction," in *Solid State Phenomena*, vol. 130, pp. 15–20, Trans Tech Publ, 2007.

[17] X. Gonze, B. Amadon, P.-M. Anglade, J.-M. Beuken, F. Bottin, P. Boulanger, F. Bruneval, D. Caliste, R. Caracas, M. Cote, *et al.*, "ABINIT: First-principles approach to material and nanosystem properties," *Computer Physics Communications*, vol. 180, no. 12, pp. 2582–2615, 2009.

[18] P. Hohenberg and W. Kohn, "Inhomogeneous electron gas," *Physical review*, vol. 136, no. 3B, p. B864, 1964.

[19] W. Kohn and L. J. Sham, "Self-consistent equations including exchange and correlation effects," *Physical review*, vol. 140, no. 4A, p. A1133, 1965.

[20] D. C. Langreth and M. Mehl, "Beyond the local-density approximation in calculations of ground-state electronic properties," *Physical Review B*, vol. 28, no. 4, p. 1809, 1983.

[21] R. O. Jones and O. Gunnarsson, "The density functional formalism, its applications and prospects," *Reviews of Modern Physics*, vol. 61, no. 3, p. 689, 1989.

[22] M. Fuchs and M. Scheffler, "*Ab initio* pseudopotentials for electronic structure calculations of poly-atomic systems using density-functional theory," *Computer Physics Communications*, vol. 119, no. 1, pp. 67–98, 1999.

[23] J. P. Perdew and Y. Wang, "Accurate and simple analytic representation of the electron-gas correlation energy," *Physical Review B*, vol. 45, no. 23, p. 13244, 1992.

[24] M. Born and R. Oppenheimer, "Zur quantentheorie der molekeln," *Annalen der Physik*, vol. 389, no. 20, pp. 457–484, 1927.

[25] M. Aydinol, A. Kohan, G. Ceder, K. Cho, and J. Joannopoulos, "*Ab initio* study of lithium intercalation in metal oxides and metal dichalcogenides," *Physical Review B*, vol. 56, no. 3, p. 1354, 1997.

Chapter 3

Intercalation of hexagonal boron nitride with lithium by sequential process of ball milling and heat treatment

3.1 Introduction

h-BN has been receiving lots of attention due to similar lattice structure to graphite, i.e. both exhibiting a characteristic layered structure as mentioned in Section 1.3 and 1.4. Through making good use of this property, various intercalation compounds have been synthesized by inserting atoms or molecules into the interlayers, which are still being discussed and researched. Especially, alkali-metal GICs (graphite intercalation compounds) have been actively studied due to their interesting properties including superconductivity and electrochemical intercalation of anodes for Li-ion batteries [1]. Also, in case of h-BN, various intercalation compounds (BNICs) has been reported using several kinds of intercalants such as alkali metal [2–6], transition metal [7] or molecules [8–12] as explained in Section 1.4, although the intercalation into h-BN is more difficult than graphite. This difficulty is from the stronger interaction for interlayer of h-BN than that of graphite due to partial ionic characteristics of h-BN originating from the charge transfer from N to B.

The various BNICs were mainly synthesized under high temperatures and at high

pressure such as hot press or using a two-zone vapor transport technique, which is one of the synthesis methods for GICs and other intercalations. However, no report has been issued on the ball milling (BM) process for producing BNICs, while Li-GICs are reported to be synthesized by ball milling [13–16].

BM is a technique of a solid-state powder processing and one of the processes to produce supersaturated solid solutions, nano-crystal alloys, non-equilibrium phase alloys and so on [17]. This process also enables to induce a reaction that would take place in a finely dispersed powder through welding and pulverizing in a solid state. It is thus expected that Li be intercalated into BN by means of BM.

However, after ball milling of h-BN and other medium, borides and/or nitrides are generally formed, e.g. for BN–Ti system formed δ-TiN_{χ} [18] or TiN and TiB_2 [19], for BN–Fe formed ε-$Fe_{\chi}N$ [20], and for BN–Al produced Al–B–N solid solution [21]. In case of BN–Al system, the milled BN–Al formed AlB_2 and AlN after heat treating. Pure h-BN mainly transformed into amorphous [22–25] or turbostratic BN [26–28] when it was ball-milled with longer milling durations.

The purpose of this Chapter is then to investigate the effects of ball milling and post-annealing on h-BN/Li mixing state and phase formation. Particularly, it is interesting to see where Li is intercalated into h-BN, or boride and/or nitride are formed with lithium. The crystal structure of synthesized compounds will be discussed.

3.2 Results and discussion

Firstly, to investigate the variation for h-BN lattice by milling, h-BN without Li was ball-milled for several milling durations and XRD results can be seen in Fig. 3.1. Also the crystallite sizes (L) for h-BN milling (Fig. 3.2 and Table 3.1) were calculated using XRD peaks of Fig. 3.1 by Scherrer equation [29] as following:

$$L = \frac{K\lambda}{\beta cos\theta} \tag{3.1}$$

where, K is a shape factor (in the parallel layer group, $K = 0.9$ for $00l$ diffraction (L_c) and $K = 1.84$ for hkl diffraction (L_a) [30, 31]), λ is the X-ray wavelength (λ = 0.15406 nm in the case of Cu-$K_{\alpha 1}$), β is FWHM (full-width at half maximum) in radians, and θ is the Bragg angles. Diffraction contributions from Cu-$K_{\alpha 2}$ radiation are subtracted before calculation and L_c and L_a are calculated from (002) and (100) diffractions, respectively. For 35 h-milled h-BN and 60 h-milled h-BN, only L_c are

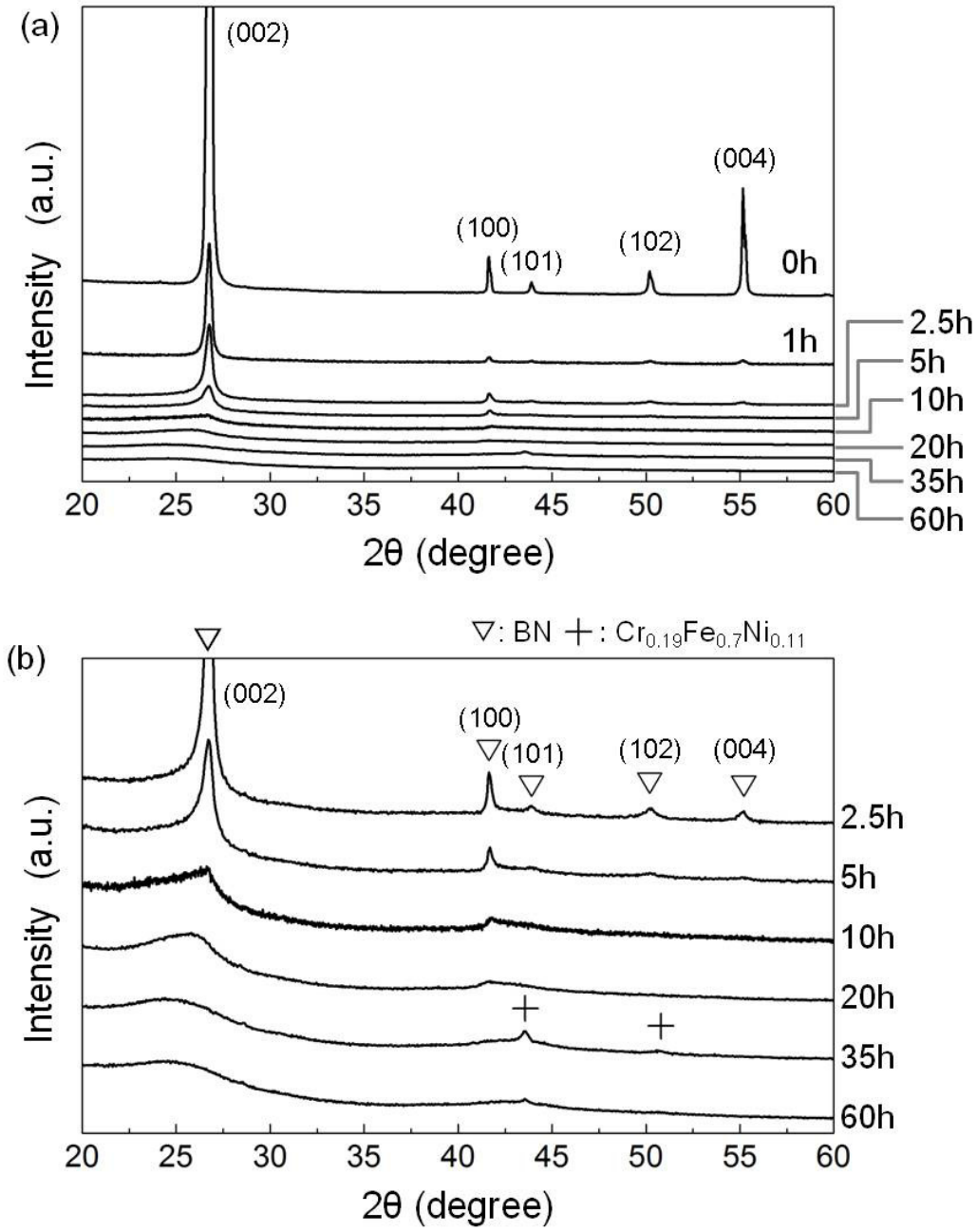

Fig. 3.1. (a) XRD peaks of the pristine and the milled h-BN for different durations. (b) Magnified XRD peaks of 2.5 $\sim$ 60 h-milled h-BN for the axis of intensity.

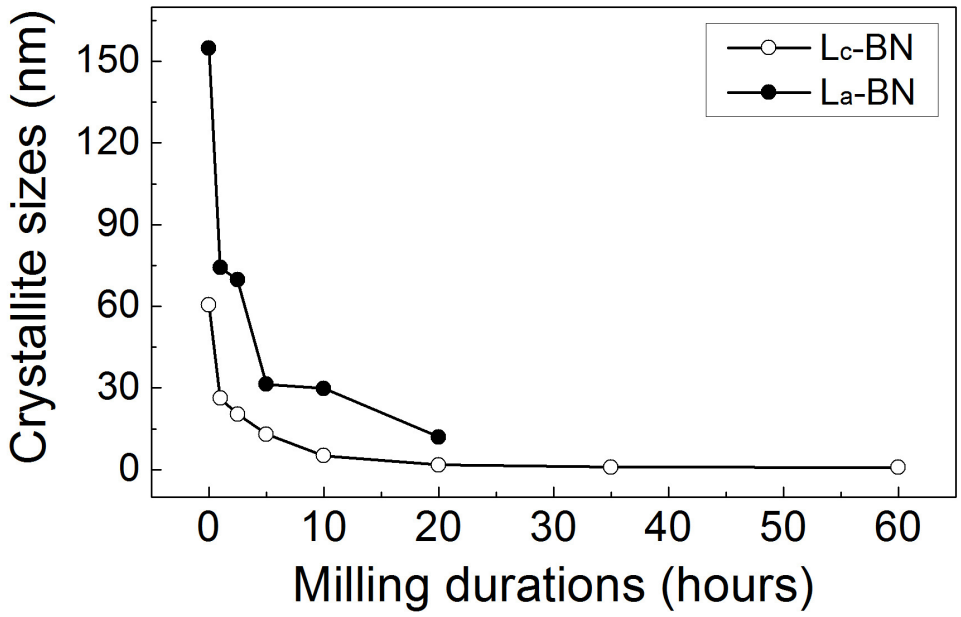

Fig. 3.2. The variation of the crystallite sizes (L) for h-BN according to milling durations.

Table 3.1. The crystallite sizes (L) for the pristine and the milled h-BN without lithium calculated by Scherrer equation.

Milling duration (h)	L_c (nm)	L_a (nm)
0	60.49	154.76
1	26.24	74.35-
2.5	20.36	69.66
5	13.00	31.36
10	5.15	29.83
20	1.75	11.96
35	0.90	-
60	0.79	-

calculated, as the (100) peaks were too broad, as seen in Fig. 3.1, to provide a credible L_a value. The L_c values are always smaller than L_a values, characteristic to the cleavage mechanism involved in the structure.

The h-BN peaks become broader and smaller with increasing milling time as seen in Fig. 3.1 because the crystallite sizes are decrease as seen in Fig. 3.2 and Table 3.1. The structural characteristics of the milled BN have been reported by several researchers [22–28]. The processes for deformation of h-BN structure during ball milling are accordingly divided into three steps as follows: For shorter milling durations (for 1 h using a planetary ball mill [23] or 5 h using a high-energy vibrational ball mill [24], mainly the crystallite size of h-BN was decreased with small amount of stacking faults due to cleavage along the basal plane. For intermediate milling durations (for 2 h [23] or $7 \sim 9$ h [24]), both slower reduction of crystallite size and formation of a number of defects such as simultaneous shearing of lattice planes, inhomogeneous strains, twin faults and stacking faults occurred. Finally, the nanocrystalline powders with amorphous, turbostratic or both structures were formed though accumulation of above defects. Meanwhile, for the 35 and 60 h-milled BN without Li (Fig. 3.1 (b)), the contamination, which is stainless steel composed by $Cr_{0.19}Fe_{0.7}Ni_{0.11}$, can be seen and this comes from the vessel and balls. The particle sizes of h-BN observed from SEM (scanning electron microscopy) images of the 0, 2.5, 5 and 60 h-milled h-BN (Fig. 3.3), become smaller with increasing milling durations.

Fig. 3.4 shows the results of XRD after ball milling h-BN with lithium (the molar ratio of BN/Li is 2.2 : 1) for different milling times. Also in this case, the intensities become smaller with milling durations as the crystallinity of h-BN becomes lower. The contamination obtained after milling BN without Li (Fig. 3.1 (b)), was not exhibited in the milled h-BN with Li as seen in Fig. 3.4. It indicates that Li plays a buffer action for mechanical energy transfer to h-BN from ball mill processing. The Li (110) peak disappears when milling time was more than 10 h as seen in Fig. 3.4. Very small Li_3N peaks can be seen when the milling time is longer than 5 h (Fig. 3.4 (b)), but all peaks disappear after 60 h of milling time due to amorphization. A small amount of Li possibly reacts with nitrogen atoms from BN by mechanical activation. It can be considered that the Li_3N formation might be due to the reaction between Li and air from adsorbed gas molecules on the ball mill container and the balls, or through inflowing. However, Li_2O, Li_2O_2 or Li_2CO_3 would be produced if Li reacts with air because the reactivity of O_2 with Li is higher than that of N_2 [32]. Thus, there is another possibility for activated Li and h-BN during ball milling. Streletskii

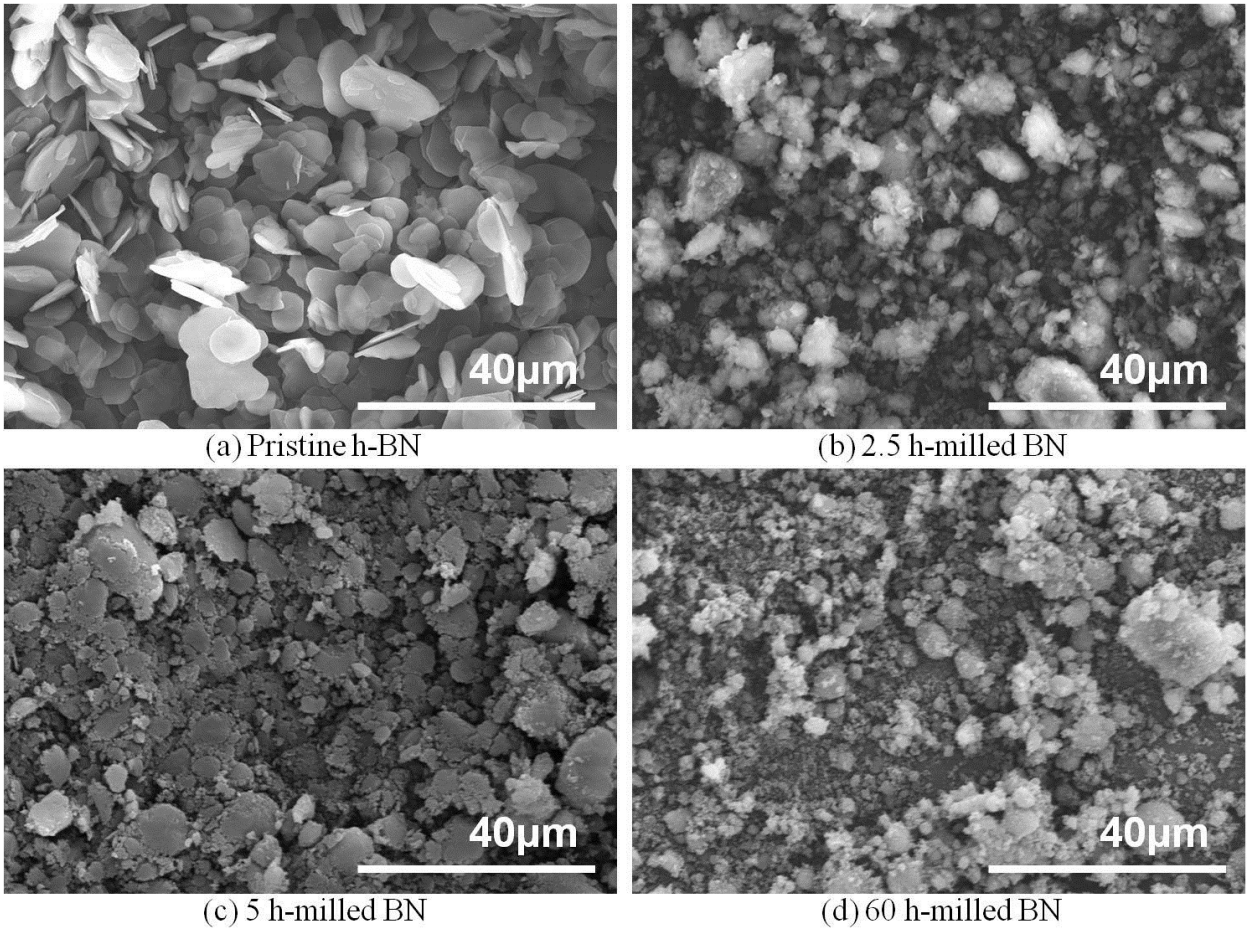

(a) Pristine h-BN (b) 2.5 h-milled BN

(c) 5 h-milled BN (d) 60 h-milled BN

Fig. 3.3. SEM image of (a) the pristine h-BN, (b) 2.5 h-milled BN, (c) 5 h-milled BN and (d) 60 h-milled BN.

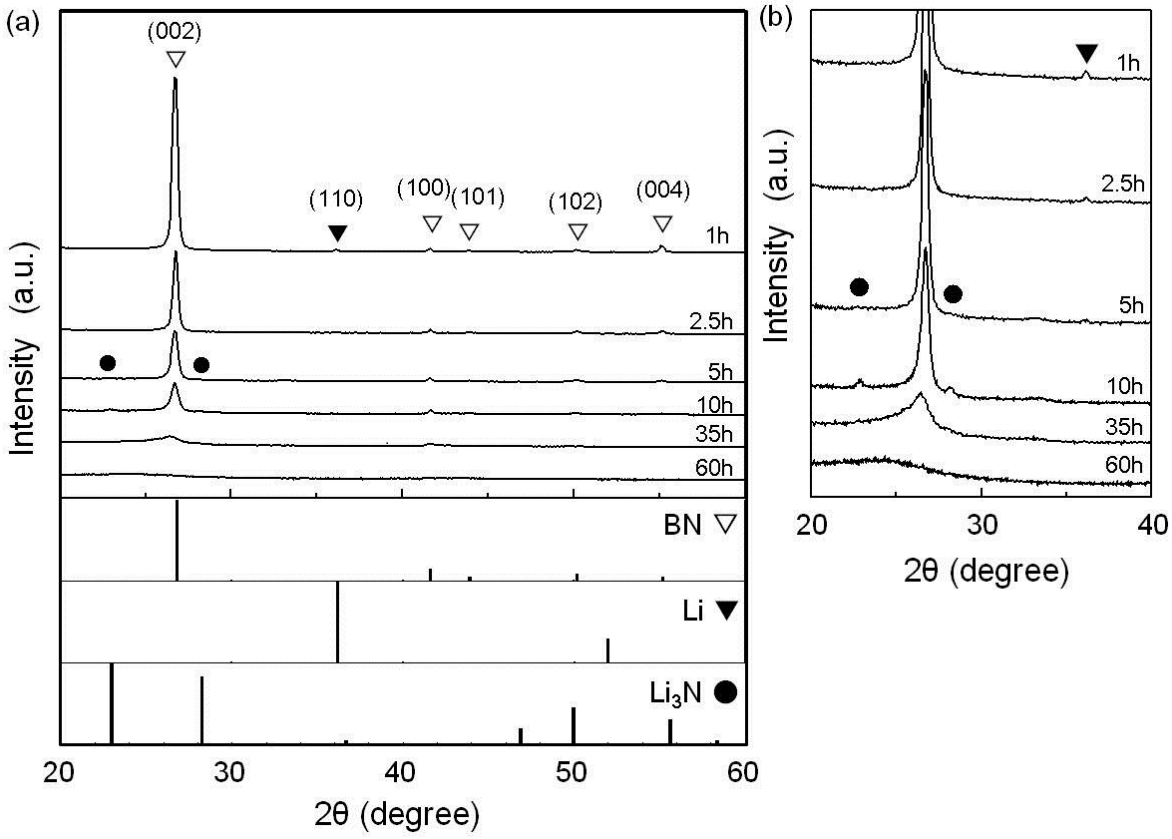

Fig. 3.4. (a) XRD peaks of the milled samples for different durations with the Li/BN molar ratio of 1 : 2.2. Common peaks of the pristine BN and Li are shown by bar chart. (b) Magnified XRD peaks from 20 to 40 degrees are represented.

et al. [25] and Gasgnier et al. [28] reported possible reaction of h-BN with H_2O when ball-milled h-BN is exposed to air because the mechanical milling increases the reactivity of h-BN. Also, the Li_3N formation strongly depends on the milling temperature, namely cooling-water temperature of milling machine. It was observed even after 2.5 h of milling time when the milling was carried out under relatively high ambient temperature. It can be said there is no intercalation during ball-milling.

Fig. 3.5 shows the XRD patterns of the milled samples after heat treatment at 700 °C for 2 hours. New peaks appeared after heat treatment except for the sample milled for 60 h. These new peaks can not be identified with the reported peaks for lithium borides or lithium nitrides. They are rather similar to Li-BNICs reported by Sumiyoshi et al. [4], indicating formation of a new phase through the mechanochemistry and heat treatment even in Li–BN system. The Li–BN system exhibits different tendency from Al–BN systems, where milling h-BN with Al would produce AlB_2 and AlN after heat treating [21].

To investigate the reaction during heat treatment of the milled samples, DTA was carried out. The DTA curves of the milled samples for several durations are shown in Fig. 3.6. The samples milled for 0, 1 and 2.5 h exhibit an endothermic peak around 180 °C representing lithium melting. It means that metallic Li is remained in the samples milled for less than 2.5 h. Clear exothermic peaks between 200 $\sim$ 500 °C are also seen (except for 60 h milling), which must be involved with Li atoms in the milled samples because the milled BN (w/o Li) does not exhibit any DTA peak. In order to understand whether these peaks correspond to synthesis of Li-BNICs or not, the samples milled for various milling time periods were heat-treated at several temperatures (350 $\sim$ 700 °C).

As the representative result, the XRD profiles for the sample milled for 2.5 h are shown in Fig. 3.7 (a), and the peak area and FWHM (full width at half maximum) at (002) plane for BN plotted as a function of annealing temperatures are shown in Fig. 3.7 (b). It is found that no new XRD peaks are observed when heat treatment temperature is below 600 °C. It should be noted that the areas of the BN peak are gradually decreased while FWHMs increased, as seen in Fig. 3.7 (b), with heat treatment temperature up to the exothermic peak observed in DTA (about 400 $\sim$ 500 °C in this case). This tendency, which seems to be out of ordinary trend, indicates that, when the milled samples are heat treated, the dispersed Li through milling (when the milling duration is longer than 2.5 h, Li are rather uniformly distributed through numerous folding processes of BN and Li powders: kneading effect.) and/or

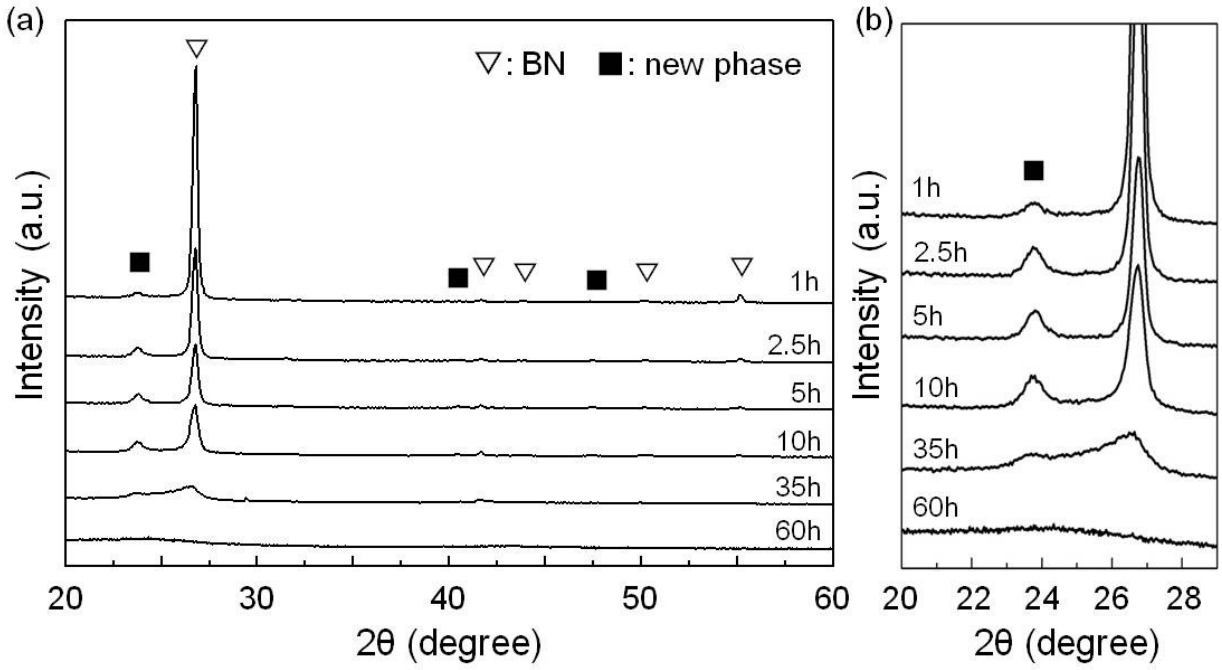

Fig. 3.5. (a) XRD peaks of the heat-treated samples at 700 °C for 2 hours after various milling durations. (b) Magnified XRD peaks from 20 to 29 degrees are represented.

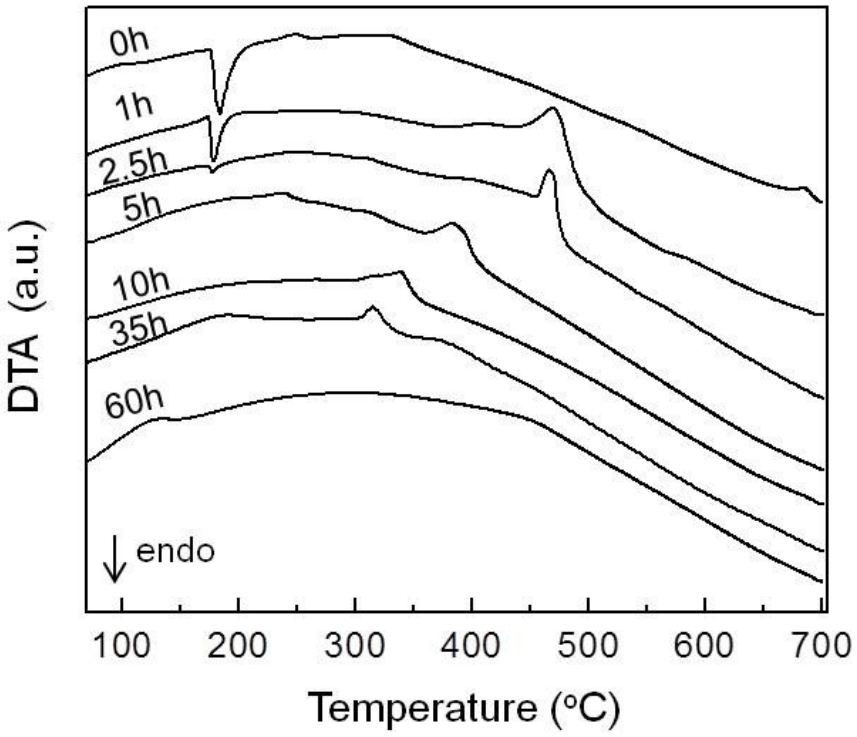

Fig. 3.6. DTA curves of Li/BN samples milled for several durations. (Appendix A shows the weight change before/after heat treatment.)

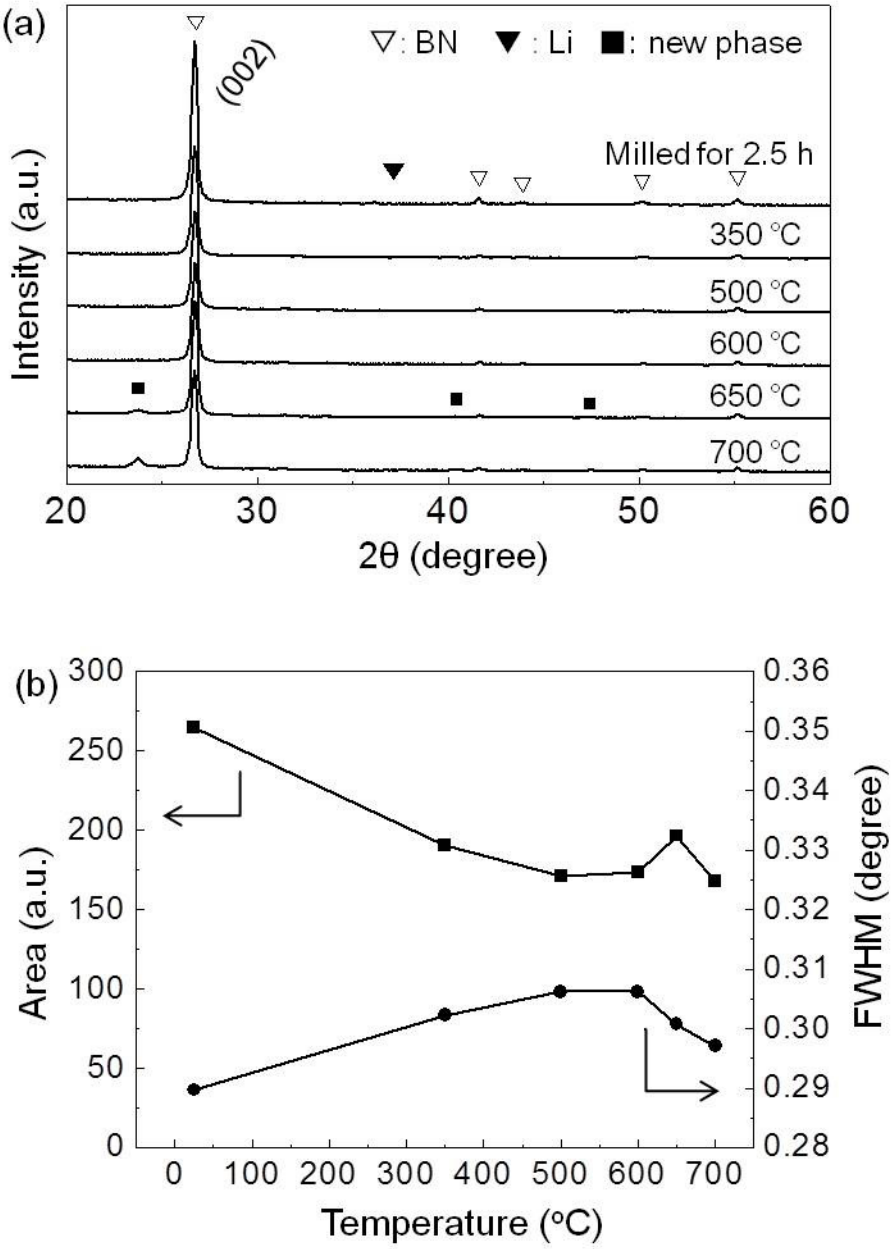

Fig. 3.7. (a) XRD peaks of Li/BN samples heat-treated (after 2.5 h milling) at several temperatures for 2 h, (b) peak area and FWHM at BN (002) plane diffractions represented as a function of temperature for heat treatment.

melting would erode BN structure and decrease h-BN peak intensity with broadening before the formation of intercalated phase at the exothermal reaction. Therefore it is suggested that; firstly, low-crystallized, such as glass-like Li-BNICs have been produced at the temperatures of exothermic DTA peaks, thus, XRD peaks for Li-BNICs are not observed at the temperatures right after exothermic peaks (500 °C in Fig. 3.7 (a)). Then, recovery for its crystallinity occurs with increasing temperatures, and finally, XRD peaks for Li-BNICs can be seen from 650 °C.

Figure 3.8 shows compositional dependence of XRD patterns exhibiting the new phase in addition to BN. The ratio of Li to BN during the milling process was changed from 1 : 2.2 to 1 : 3.3 (volume ratio of 1 : 3) or to 1 : 6.6 (volume ratio of 1 : 6), and the milling was carried out for 2.5 h, followed by heat treatment at 700 °C for 2 h. Observed XRD peak positions are not different with each other, indicating formation of the same phase even with changing the ratio. For decreasing XRD intensities of BN with increasing the BN ratio, it is speculated that the effect of ball milling on BN would be increased as the Li concentration decreases. Thereby, more destruction of BN would occur with increasing the BN molar ratio to Li (from (a) to (c)). The reason for decreasing the intensities of a new phase with the BN ratio would be that the amounts of Li for reaction decrease and the produced amount of new phase becomes smaller as well.

The ^{7}Li NMR study was conducted in order to investigate the Li state according to the ratio change. Fig. 3.9 shows the NMR spectra of the heat-treated samples after 2.5 h of milling, with the molar ratio of 1 : 2.2, 3.3 and 6.6 (Li/BN). The resonance frequency peaks are shifted to the lower delta (chemical shift: δ, ppm versus LiCl) from 7 ppm to –2 ppm with increasing the BN ratio (i.e. with decreasing the relative Li composition). The NMR spectrum of the sample with 3.3 and 6.6 ratio seems to exhibit multiple peaks. There might be possible inclusion of short-range-ordered impurities (local ordering) that are randomly-distributed throughout the sample. The sample with 2.2 ratio may also include the impurities, although the NMR spectrum seems to exhibit only one peak, as it is larger and broader than others. The chemical shift of the sample with 6.6 ratio exhibits the minus value. In case of Li-GICs, the chemical shift of gas-like GIC could be from –2.6 to +1.0 ppm [33]. Therefore, various Li-intercalated states may exist in the samples. Also, these widely broadened NMR peaks of the heat-treated samples are attributed to multiple Li sites with different atomic environments. If the structures of Li-BNICs exhibit a quasi-axial symmetry such as Li-GICs [33], the quadrupolar “wings” should be present.

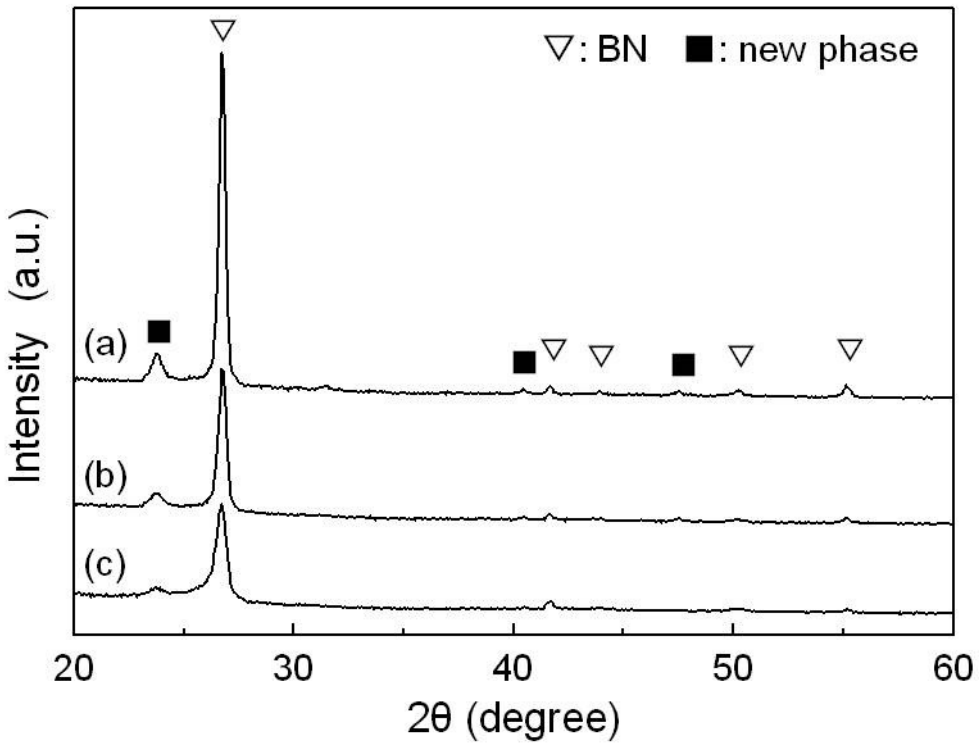

Fig. 3.8. XRD peaks of the heat-treated samples (at 700 °C for 2 h) after 2.5 h milling with Li/BN ratios of 1:2.2 (a), 1 : 3.3 (b) and 1 : 6.6 (c).

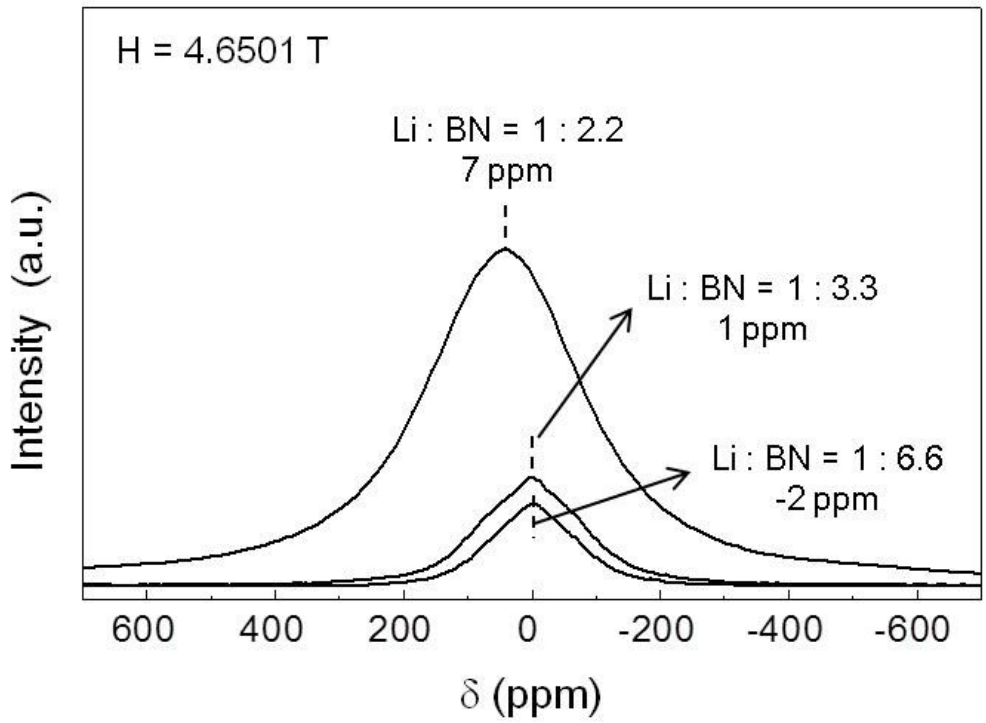

Fig. 3.9. ^{7}Li NMR spectra of the heat-treated samples (after 2.5 h milling) with the molar ratio of 1 : 2.2, 3.3 and 6.6 (Li/BN).

Based on this structural disorder, it is strongly indicated the XRD peaks for Li-BNICs, which were not distinguishable above the temperature of exothermic DTA peaks (Fig. 3.6) is also ascribed to the irregular structure of BN due to ball milling and Li intercalation. Hereby, the exothermic peaks of DTA might be due to the synthesis of Li-BNICs.

According to the XRD results, the peaks profiles of the heat-treated samples are similar although the amount of intercalated Li is decreased. It seems to produce same compounds, however, NMR spectra changed and shifted to lower delta with decreasing Li ratio. From these results, some can be inferred. First, Li-BNICs exhibit 1-stage compounds such as Brønsted-acids-BNIC [12]. In case of Li-GICs, structurally-different compounds have been synthesized by changing the ratio of Li to graphite, through not only electrochemical synthesis but also the heat treatment with pressure [16, 35] and ball milling [13, 16]. Namely, Li-GICs exhibit flexible-synthesized compounds through changing the amount of in-plane Li and staged intercalation. However, Li-BNICs do not exhibit this tendency of intercalation. This absence of higher stages in the BNICs is similar to intercalation of h-BN with $S_2O_6F_2$ reported by Ciping et al. [11] and Brønsted acids by Kovtyukhova et al. [12]. According to the former report there is no intermediate stage, i.e. this different intercalation behavior between graphite and h-BN is due to partial ionic state and poor π bonding in h-BN, thereby causing relatively weak flexibility of h-BN sheets than that of graphite. Secondly, it is assumed that the h-BN lattice is expanded to a same size when intercalation of Li occurs regardless the ratio of BN/Li. The (002) XRD peaks at 26.75 ° representing the layered distance of h-BN is changed to a lower angle side around 23.65 ° (from 0.333 to 0.376 nm). Also, other distinguished peaks corresponding to (100) and (102) planes are changed to about 40.43 ° and 47.55 °, respectively, due to Li intercalation.

Based on these two aspects, the XRD patterns of expanded h-BN and hypothetical Li-BNICs [$Li(BN)_3$ and $Li_2(BN)_3$] [34] are calculated and are shown in Fig. 3.10, where the layered states assumed are (a) "2L model", (b) "1L model" reported by Sumiyoshi et al. [5, 6]. They suggested that "2L model indicates two-layer stacking periodicity structure of the pristine h-BN" and "1L model indicates the structure without the two-layer stacking periodicity" [6]. The Rietveld method was conducted in order to analyze the structure of synthesized Li-BNICs. The XRD pattern used for the Rietveld analysis is obtained for the heat-treated samples at 700 °C for 2 h after milling for 2.5 h (X-ray radiation: Cu-$K_{\alpha 1}$, 2θ range: $20 \sim 70.01$ ° with 0.03 °

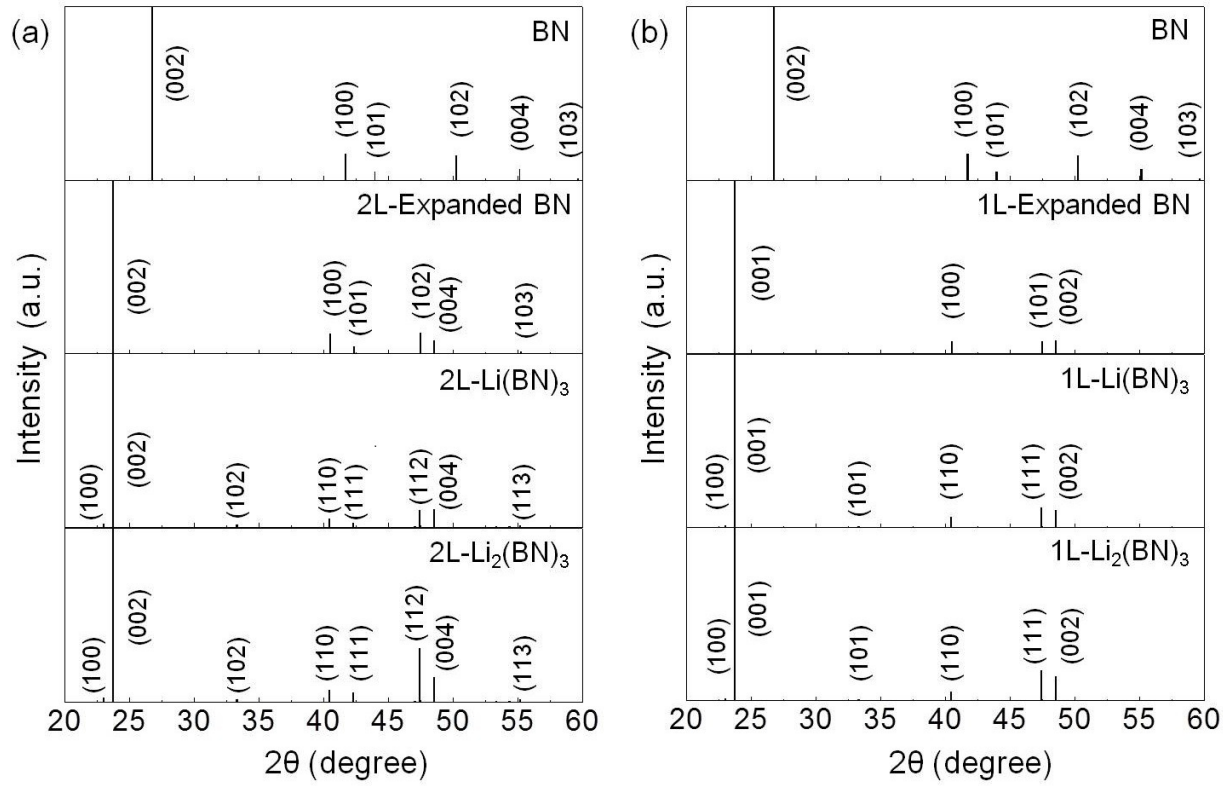

Fig. 3.10. Calculated XRD patterns of pure h-BN, expanded BN and Li-BNICs [$Li(BN)_3$ and $Li_2(BN)_3$)] based on layered states for (a) "2L" [5, 34] and (b) "1L" model [6].

step).

All Rietveld results are organized in Fig. 3.11 and Table 3.2. In Fig. 3.10 and 3.11, the outstanding three peaks of our experimental results about 23.65 °, 40.43 ° and 47.55 ° may correspond to (002), (100) and (102) for 2L model and (001), (100) and (101) for 1L model diffractions, respectively, of the expanded h-BN, while also to (002), (110) and (112) for 2L model and (001), (110) and (111) for 1L model diffractions, respectively, of the Li-BNICs, and they exhibit good fitting. The Rietveld analysis results of 1L model seem to show better fitting, as the R_{wp}, R_B (reliable factors) and S (good-to-fitness) values in Table 1 are smaller than those of 2L model for respective Li-BNICs phases. Compared with 2L and 1L model, for 2L model (Fig. 3.10 (a)), the diffractions (101) and (103) of expanded BN and the diffractions (111) and (113) of Li-BNICs (2L-$Li(BN)_3$ and 2L-$Li_2(BN)_3$) are not obtained in 1L model (Fig. 3.10 (b)). Also, these peaks are not observed in XRD experimental results as seen in Fig. 3.11. Therefore, 1L-model LiBNICs exhibits better fitting than 2L model for Rietveld analysis. In case of Li-BNICs, on the other hand, additional XRD peaks can be seen, unlike expanded BN, which are (100) at 23.0 ° and (102) at 33.2 ° for the 2L or (101) for the 1L model at 33.2 °, as observed in. Fig. 3.10 (a) or (b), respectively, for both $Li(BN)_3$ and $Li_2(BN)_3$ phases. Although they derive from Li intercalation, the intensities are relatively small due to weak scattering by a Li atom in character.

The lattice parameters of Li-BNICs, calculated by Rietveld analysis in this study, are a = 0.4465 ± 0.0001 nm, c = 0.7504 ± 0.0001 nm for the 2L and a = 0.4465 ± 0.0001 nm, c = 0.3751 ± 0.0001 nm for the 1L model. On the other hand, Sumiyoshi et al. reported a = 0.44437 nm, c = 0.37599 nm, for the 1L model and a = 0.44437 nm, c = 0.75198 nm for the 2L model [6]. This difference of lattice parameters may signify that different kinds of Li-BNICs were produced due to different methods of synthesis.

Meanwhile, it is difficult to determine the exact phases of Li-BNICs though the Rietveld method was conducted, as both $Li(BN)_3$ and $Li_2(BN)_3$ phases exhibit similar XRD peak patterns as seen in Fig. 3.11. Therefore, possible structures of Li-BNICs, Li concentrations/distribution, and detailed explanation on structural disorder in Li-BNICs will be discussed in Chapter 6 through theoretical calculation.

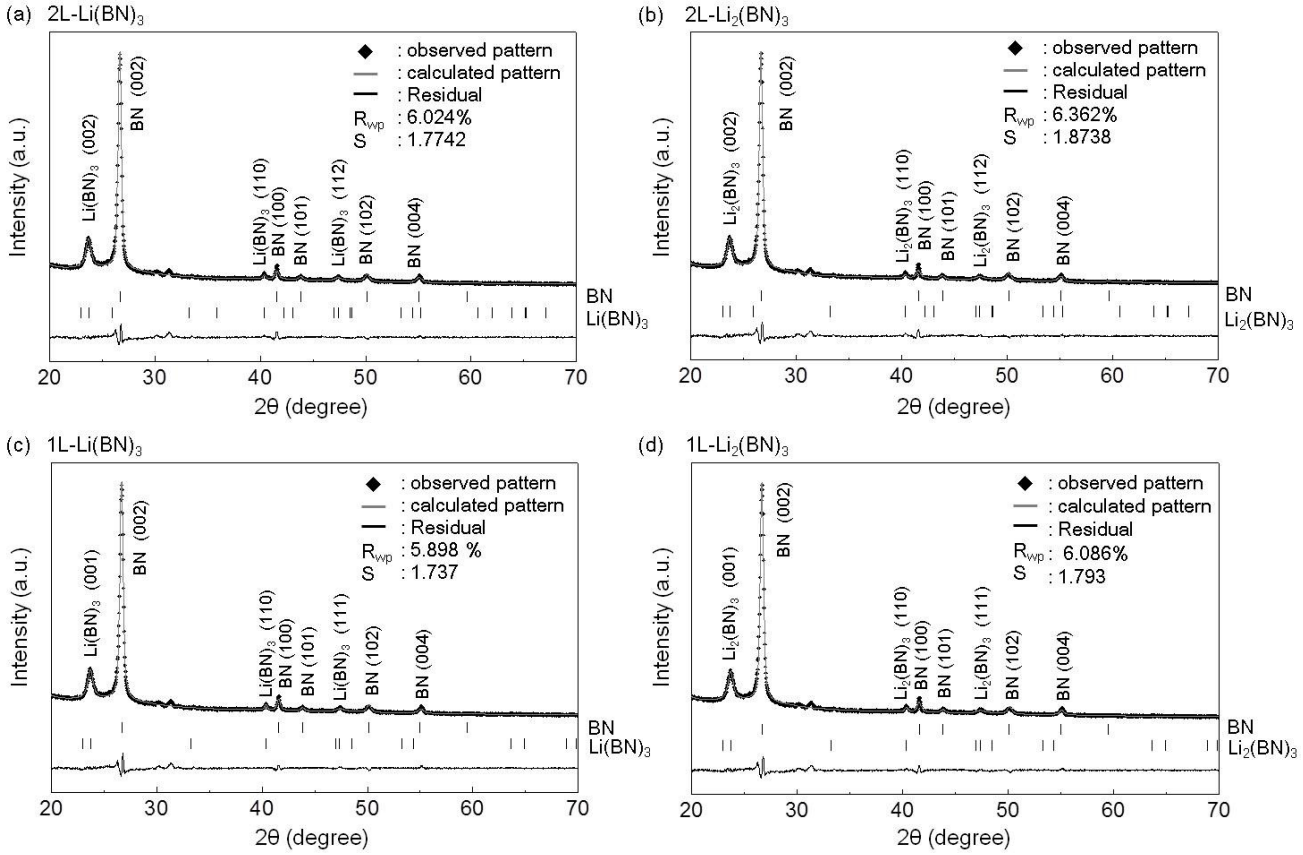

Fig. 3.11. Rietveld results of the heat-treated samples (after 2.5 h milling) for the (a) "2L" model of $Li(BN)_3$, (b) "2L model" of $Li_2(BN)_3$ [5,34], (c) "1L model" [6] of $Li(BN)_3$ and (d) "1L" model of $Li_2(BN)_3$.

Table 3.2. The results of Rietveld analysis.

		2L		1L	
		$Li(BN)_3$	$Li_2(BN)_3$	$Li(BN)_3$	$Li_2(BN)_3$
R_{wp}		6.024	6.362	5.898	6.086
S		1.774	1.874	1.737	1.793
BN	R_B	1.054	1.699	0.825	1.064
	a (nm)	0.2506	0.2506	0.2506	0.2506
	c (nm)	0.6678	0.6678	0.6678	0.6678
Li-BNIC	R_B	1.586	2.107	0.883	0.888
	a (nm)	0.4465	0.4465	0.4465	0.4466
	c (nm)	0.7505	0.7503	0.3751	0.3751

3.3 Conclusion

Li-BNICs are synthesized through a heat treatment at 700 °C for 2 h in Ar atmosphere after ball-milling of small lithium metal pieces and h-BN powder, where the samples contain both h-BN and Li-BNICs phases together. The DTA exothermic peaks observed between 200 $\sim$ 500 °C are supposed to be the synthesis temperatures of Li-BNICs, however, the XRD peaks of Li-BNICs are not detected due to the highly-disordered structure. The synthesized Li-BNICs as the XRD patterns of Li-BNICs are not changed although the amount of Li is decreased. The NMR spectra of Li-BNICs are changed according to the ratio of Li to BN. This difference between the results of XRD and NMR is supposed to derive from expansion of the h-BN lattice to a same size by intercalating Li regardless the amount of Li. Namely, the BN lattice might be changed from 0.333 nm to 0.375 nm of the layer distance and from 0.145 nm to 0.149 nm of the B–N atomic bond length. Also, the broadened XRD and NMR peaks of Li-BNICs indicate that the geometrical/topological state of intercalated Li exhibits irregular arrangement and/or multiple sites with expansion of BN lattice, not in each of the BN galleries. Also, many vacancies might exist in the expanded BN lattice or defective Li-BNICs could be synthesized.

Reference

[1] M. Dresselhaus and G. Dresselhaus, "Intercalation compounds of graphite," *Advances in Physics*, vol. 30, no. 2, pp. 139–326, 1981.

[2] A. Freeman and J. Larkindale, "Evidence for the formation of boron nitride-alkali metal intercalation compounds," *Inorganic and Nuclear Chemistry Letters*, vol. 5, no. 11, pp. 937–939, 1969.

[3] G. Doll, J. Speck, G. Dresselhaus, M. Dresselhaus, K. Nakamura, and S.-I. Tanuma, "Intercalation of hexagonal boron nitride with potassium," *Journal of applied physics*, vol. 66, no. 6, pp. 2554–2558, 1989.

[4] A. Sumiyoshi, H. Hyodo, and K. Kimura, "Li-intercalation into hexagonal boron nitride," *Journal of Physics and Chemistry of Solids*, vol. 71, no. 4, pp. 569–571, 2010.

[5] A. Sumiyoshi, H. Hyodo, and K. Kimura, "Structural analysis of Li-intercalated hexagonal boron nitride," *Journal of Solid State Chemistry*, vol. 187, pp. 208–210, 2012.

[6] A. Sumiyoshi, H. Hyodo, Y. Sato, M. Terauchi, and K. Kimura, "Good reproductive preparation method of Li-intercalated hexagonal boron nitride and transmission electron microscopy–electron energy loss spectroscopy analysis," *Solid State Sciences*, vol. 47, pp. 68–72, 2015.

[7] E. Budak and Ç. Bozkurt, "The effect of transition metals on the structure of h-BN intercalation compounds," *Journal of Solid State Chemistry*, vol. 177, no. 4, pp. 1768–1770, 2004.

[8] M. Sakamoto, J. Speck, and M. Dresselhaus, "Cesium and bromine doping into hexagonal boron nitride," *Journal of Materials Research*, vol. 1, no. 05, pp. 685–692, 1986.

[9] N. Bartlett, R. Biagioni, B. McQuillan, A. Robertson, and A. Thompson, "Novel salts of graphite and a boron nitride salt," *Journal of the Chemical Society, Chemical Communications*, no. 5, pp. 200–201, 1978.

[10] J. Hooley, "Intercalation by $(SO_3F)_2$ in various forms of graphite and boron nitride," *Carbon*, vol. 21, no. 3, pp. 181–188, 1983.

[11] C. Shen, S. G. Mayorga, R. Biagioni, C. Piskoti, M. Ishigami, A. Zettl, and N. Bartlett, "Intercalation of hexagonal boron nitride by strong oxidizers and evidence for the metallic nature of the products," *Journal of Solid State Chemistry*, vol. 147, no. 1, pp. 74–81, 1999.

[12] N. I. Kovtyukhova, Y. Wang, R. Lv, M. Terrones, V. H. Crespi, and T. E. Mallouk, "Reversible intercalation of hexagonal boron nitride with brønsted acids," *Journal of the American Chemical Society*, vol. 135, no. 22, pp. 8372–8381, 2013.

[13] R. Janot, J. Conard, and D. Gurard, "Ball milling: a new route for the synthesis of superdense lithium GICs," *Carbon*, vol. 39, no. 12, pp. 1931–1934, 2001.

[14] D. Guérard and R. Janot, "Structure of the superdense LiC_3 compound prepared by ball-milling," *Journal of Physics and Chemistry of Solids*, vol. 65, no. 2, pp. 147–152, 2004.

[15] R. Janot and D. Guerard, "Ball-milling in liquid media: Applications to the preparation of anodic materials for lithium-ion batteries," *Progress in Materials Science*, vol. 50, no. 1, pp. 1–92, 2005.

[16] R. L. Sacci, L. A. Adamczyk, G. M. Veith, and N. J. Dudney, "Dry synthesis of lithium intercalated graphite powder and fiber," *Journal of The Electrochemical Society*, vol. 161, no. 4, pp. A614–A619, 2014.

[17] C. Suryanarayana, "Mechanical alloying and milling," *Progress in materials science*, vol. 46, no. 1, pp. 1–184, 2001.

[18] Z. Ding, B. Yao, L. Qiu, S. Bai, X. Guo, Y. Xue, W. Wang, X. Zhou, and W. Su, "Formation of titanium nitride by mechanical milling and isothermal annealing of titanium and boron nitride," *Journal of alloys and compounds*, vol. 391, no. 1, pp. 77–81, 2005.

[19] J.-H. Shim, J.-S. Byun, and Y. W. Cho, "Mechanochemical synthesis of nanocrystalline TiN/TiB_2 composite powder," *Scripta materialia*, vol. 47, no. 7, pp. 493–497, 2002.

[20] J. Tao, B. Yao, J. Yang, S. Zhang, K. Zhang, S. Bai, Z. Ding, and W. Wang, "Mechanism of formation of Fe–N alloy in the solid-state reaction process between iron and boron nitride," *Journal of alloys and compounds*, vol. 384, no. 1, pp. 268–273, 2004.

[21] Z. Xia, Z. Li, C. Lu, B. Zhang, and Y. Zhou, "Structural evolution of Al/BN mixture during mechanical alloying," *Journal of alloys and compounds*, vol. 399, no. 1, pp. 139–143, 2005.

[22] Y. Du, F. Guo, and K. Lu, "Grain size distribution and morphologies of nanocrystalline boron-nitride during ball milling," *Nanostructured materials*, vol. 7, no. 5, pp. 579–589, 1996.

[23] J. Y. Huang, H. Yasuda, and H. Mori, "HRTEM and EELS studies on the amorphization of hexagonal boron nitride induced by ball milling," *Journal of the American Ceramic Society*, vol. 83, no. 2, pp. 403–409, 2000.

[24] J. Ghosh, S. Mazumdar, M. Das, S. Ghatak, and A. Basu, "Microstructural characterization of amorphous and nanocrystalline boron nitride prepared by high-energy ball milling," *Materials Research Bulletin*, vol. 43, no. 4, pp. 1023–1031, 2008.

[25] A. Streletskii, D. Permenov, B. Bokhonov, I. Kolbanev, A. Leonov, I. Berestetskaya, and K. Streletzky, "Destruction, amorphization and reactivity of nano-BN under ball milling," *Journal of Alloys and Compounds*, vol. 483, no. 1, pp. 313–316, 2009.

[26] J. Huang, X. Jia, H. Yasuda, and H. Mori, "Stacking disordering in hexagonal BN induced by shearing under ball milling," *Philosophical magazine letters*, vol. 79, no. 5, pp. 217–224, 1999.

[27] Z. P. Xia and Z. Q. Li, "Structural evolution of hexagonal BN and cubic BN during ball milling," *Journal of Alloys and Compounds*, vol. 436, no. 12, pp. 170–173, 2007.

[28] M. Gasgnier, H. Szwarc, and A. Ronez, "Low-energy ball-milling: Transformations of boron nitride powders. Crystallographic and chemical characterizations," *Journal of materials science*, vol. 35, no. 12, pp. 3003–3009, 2000.

[29] P. Scherrer, "Bestimmung der inneren Struktur und der Größe von Kolloidteilchen mittels Röntgenstrahlen," in *Kolloidchemie Ein Lehrbuch*, pp. 387–409, Springer, 1912.

[30] R. Nemanich, S. Solin, and R. M. Martin, "Light scattering study of boron nitride microcrystals," *Physical Review B*, vol. 23, no. 12, p. 6348, 1981.

[31] S. Le Gallet, G. Chollon, F. Rebillat, A. Guette, X. Bourrat, R. Naslain, M. Couzi, and J. Bruneel, "Microstructural and microtextural investigations of boron nitride deposited from BCl_3–NH_3–H_2 gas mixtures," *Journal of the European Ceramic Society*, vol. 24, no. 1, pp. 33–44, 2004.

[32] D. Jeppson, J. Ballif, W. Yuan, and B. Chou, "Lithium literature review: lithium's properties and interactions," *Hanford Engineering Development Laboratory*, 1978.

[33] F. Chevallier, F. Poli, B. Montigny, and M. Letellier, "*In situ* ^{7}Li nuclear magnetic resonance observation of the electrochemical intercalation of lithium in graphite: second cycle analysis," *Carbon*, vol. 61, pp. 140–153, 2013.

[34] B. Altintas, C. Parlak, C. Bozkurt, and R. Eryiğit, "Intercalation of graphite and hexagonal boron nitride by lithium," *The European Physical Journal B*, vol. 79, no. 3, pp. 301–312, 2011.

[35] V. Mordkovich, "Synthesis and XPS investigation of superdense lithium-graphite intercalation compound, lic 2," *Synthetic metals*, vol. 80, no. 3, pp. 243–247, 1996.

Chapter 4

Intercalation of hexagonal boron nitride and graphite with lithium by sequential process of ball milling and heat treatment

4.1 Introduction

In the previous Chapter, lithium boron nitride intercalation compounds (Li-BNICs) has been successfully synthesized through the sequential process of ball milling and heat treatment and the structural investigation has been carried out [1], It is difficult, however, to define the stoichiometry of Li-BNICs, due to irregular arrangement of Li ions in the BN host. The layered structures of Li-BNICs have been suggested to exhibit "1L model", but not "2L model", that is, possessing "a structure without two-layer stacking periodicity" of the pristine h-BN structure [2]. It is supposed that Li could be intercalated into the defective BN host structure. Sumiyoshi et al. have also reported that electrical conductivities of Li-BNICs are higher than the pristine h-BN [2, 3], however, it is still difficult to apply Li-BNICs for lithium ion batteries due to its easiness of returning into an insulator when Li is deintercalated.

On the other hand, lithium graphite intercalation compounds (Li-GICs) have been actively studied due to their application for anode material of lithium ion batteries and various phases, which are classified into stages such as gas-like stage 1', dilute LiC_{9n} type, dense LiC_{6n} type [4–12] and super-dense LiC_{2-3} [13–16], have been reported

as explained in section 1.2.1. These Li-GICs have been synthesized through various methods, such as electrochemical method [4–7, 9, 11, 17], mechanical milling [12, 14–16] and heat treatment with/without pressure control [10, 12, 13]. In case of heat treatment, temperatures below 400 °C have been usually selected to suppress synthesis of Li_2C_2, which is not an intercalation compound. Direct production of Li-GICs might be possible even at room temperature under high pressures ($10 \sim 20$ kbar), while in vacuum or under low pressures they can only be synthesized by annealing [8]. Except for LiC_6, which is a "1st stage" compound of dense LiC_{6n} type, the stoichiometry is thus sensitive to temperature when synthesized under lower pressures, whereas it becomes sensitive to pressure (less sensitive to temperature) under high-pressure preparative methods. As the thermodynamic stability of Li-GICs is controversial, there is no consensus on the temperature of their deintercalation(s) [5, 10, 17, 18], and it might depend on the methods of synthesis. In case of an electrochemical method, deintercalation of Li-GICs occurs at ∼80 °C [17]. Drüe et al. reported that, though LiC_6 was thermodynamically unstable above 330 °C, it has been produced by annealing at the same temperature (330 °C) and suggested a metastable Li–C phase diagram [10, 18]. As for thermodynamic stability of Li-GICs synthesized by mechanical milling there has not been a detailed report until now.

In this Chapter, a Li–BN–graphite ternary system has been then focused in order to overcome the problem for insulator of h-BN, as there is a paucity of available research on the field, particularly Li intercalation into a BN–graphite binary system. In the B–C–N system, graphite-like BC_2N (g-BC_2N) has been reported as a promising material for rechargeable Li batteries [19], and, among various methods of BC_2N synthesis, ball-milling was reported as one of the useful processes, using h-BN and graphite powders as starting materials [20,21]. Therefore, the purpose of this Chapter is to investigate firstly intercalation of combined BN–graphite with Li through milling and heating processes, which were used in previous Chapter, and to study their thermal stability.

4.2 Results and discussion

Fig. 4.1 shows XRD peak patterns of the milled samples at molar ratio of 1 : 1.1 : 1.1 (Li/BN/graphite) for 2.5 and 10 hours. After milling, all graphite reacted with lithium and mainly Li-GICs (LiC_6 and LiC_{12}) were produced, in addition to Li_3N as a minor phase. It appears that Li is not intercalated into BN and unreacted Li

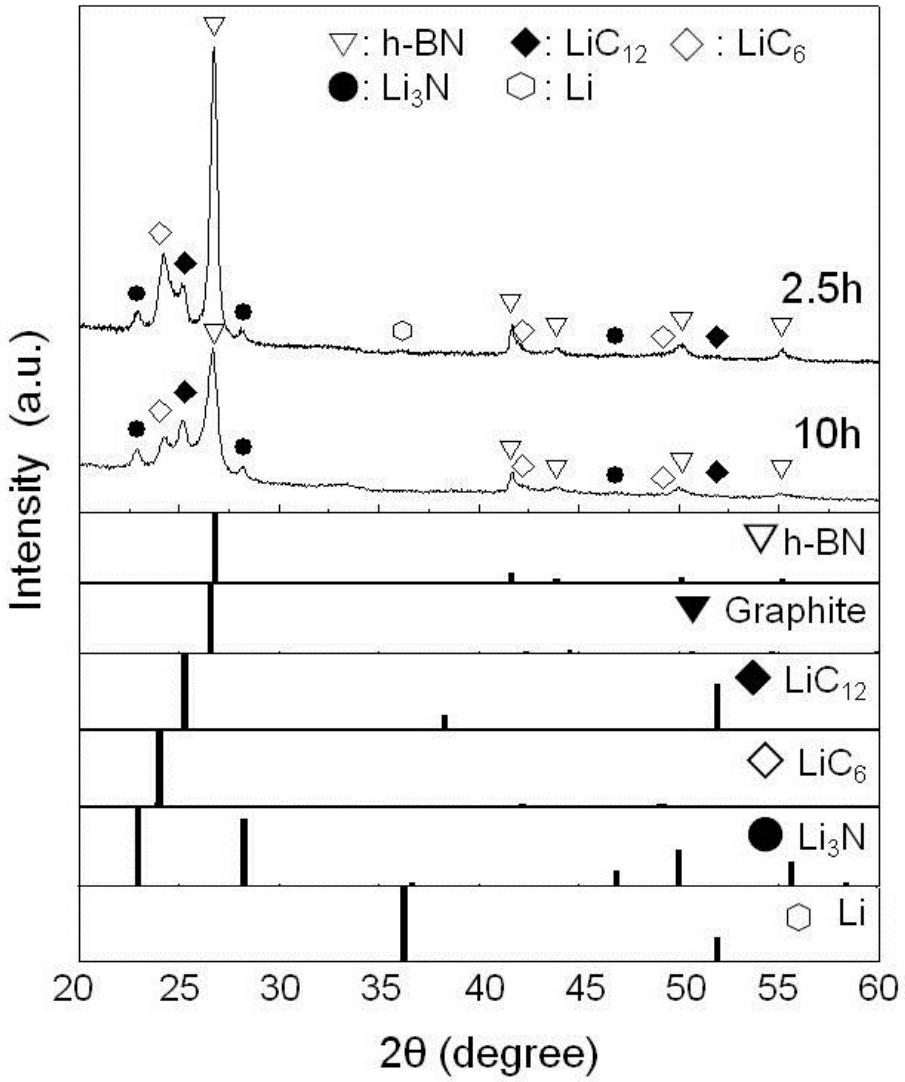

Fig. 4.1. XRD peaks of the milled samples with at a molar ratio of 1 : 1.1 : 1.1 (Li/BN/graphite) for 2.5 and 10 hours.

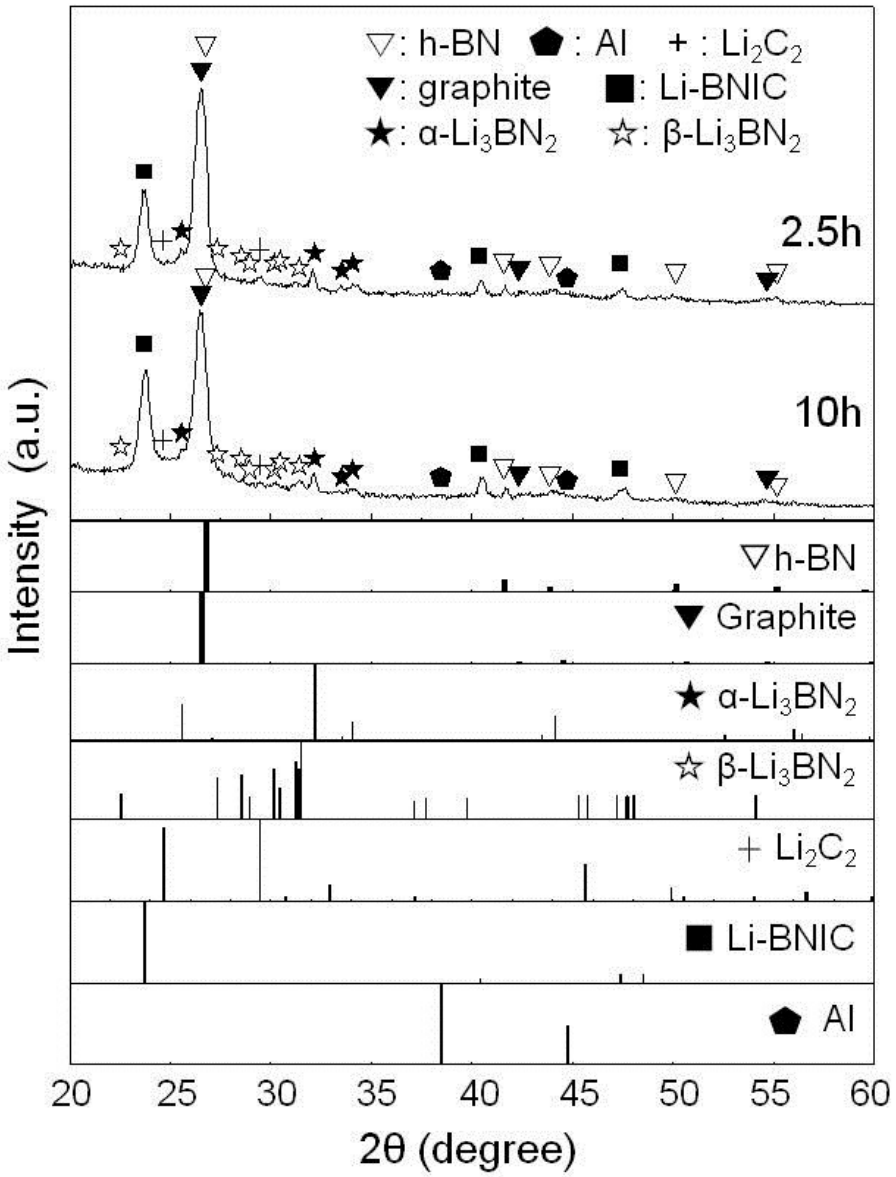

Fig. 4.2. XRD peaks of the heat-treated sample at 700 °C for 2 hours after milling for 2.5 and 10 hours.

metal is remained in the milled samples. The peak heights of h-BN decrease with longer milling durations due to destruction and/or amorphization of h-BN structure. The milled samples were heat-treated at 700 °C for 2 hours in Ar, and the results of XRD are shown in Fig. 4.2. After heat treatment, the peaks of Li-GICs phases disappeared, and instead, Li-BNICs were synthesized, with small amounts of Li_2C_2, lithium boron nitride (Li_3BN_2) and Al (Al was produced due to reduction of alumina crucible). Interestingly, it seems that Li atoms in Li-GICs diffused to BN during heat treatment, although unreacted Li metal after milling was also intercalated into BN. As for thermodynamic stability of Li-GICs, it is reported that LiC_6 could be deintercalated at several temperatures according to the synthesis method, as mentioned in Introduction of this Chapter, and transformed to Li_2C_2 and graphite during heating [10, 17]. Thus, it is strongly suggested that deintercalated Li atoms from Li-GICs have diffused into the BN layered structure, consistent with XRD peaks of graphite and Li_2C_2 exhibited after the post-annealing. With increasing milling durations the peak heights of Li-BNICs are increased because more Li could be intercalated into more-defective h-BN. Li_3BN_2 phases (α- and β-) were obtained after heat treatment possibly by the reaction between Li_3N and BN [22, 23]. Meanwhile, there is also a possibility that Li might be intercalated into the B–C–N matrix, however, through XRD study it is difficult to investigate it. Therefore, XPS was conducted on 2.5 h-milled samples before and after heat treatment, in order to investigate whether a B–C–N bond is obtained from reaction between BN and graphite by the processes in this study.

Fig. 4.3 shows XPS spectra (1s of B (a), N (b), C (c) and Li (d)) of 2.5 h-milled samples before/after heat treatment and the deconvoluted results (Fig. 4.3 (a) $\sim$ (d)). As for the milled samples, the peak-tops of the spectra at around 190.5 eV of B 1s and 398.0 eV of N 1s are attributed to the h-BN phase [24]. In case of C 1s profile, 3 peaks at around 284.9 (C–C), 286.4 (C–O–C) and 288.7 eV (O–C=O) were obtained, as shown in the fitted results in Fig. 4.4 (c). These 3 peaks may partially derive from adventitious carbon, and the third peak at 288.7 eV from Li-carbonate (Li_2CO_3) (it will be discussed later). Also, a small portion may derive from carbon tape attached on an Al stage to fix the powder samples, however, it seems negligible as the contained Si in the tape exhibited negligible Si 2p peak intensity. Therefore, the majority of the peak component should derive from the milled powder, and the first C–C binding energy (284.9 eV: main peak) corresponds attributable to Li-GICs, as the reported values are in a range of 284.7 $\sim$ 285.2 eV [25–28]. In case of lithium, on the other

hand, only one (but rather broad) Li 1s spectrum with a peak-top at around 55.0 eV was obtained, though rather broad. Although the peak position of Li metal is still controversial (even 52.9 eV has been reported), this should correspond to metallic lithium remained (Fig. 4.1) because 54.8 ± 0.3, or 54.5 ∼ 55.2 eV [24–28] peaks have been reported for Li metal. Additionally, our XRD data show Li-GICs as the major product after milling. In case of Li 1s for Li-GICs, various values have been reported, e.g. 56.3 [27], 57 [28], 57.1 [25], 57.6 [26] eV, which are higher than Li metal. In the Li 1s spectra of the milled sample shown in Fig. 4.3 (d), a small shoulder at about 56.3 eV represented by a blue bar might be attributed to Li-GICs, but it is difficult to explain due to low sensitivity for Li 1s. Furthermore, the measurement depth of XRD and XPS is significantly different (at least in 3 orders of magnitude). On considering that Li easily forms hydroxide, carbonate, or oxide, a few nanometers on powder surface may have reacted (even carefully treated in vacuum or Ar), resulting in the XPS data. Although controversial, the major peak at 55 eV may derive from LiOH and/or Li_2CO_3, which is consistent with C 1s results in that some free carbon may appear near the surface, as discussed.

After heat treatment some new peaks have emerged at the lower binding energies. A new C 1s binding energy at 284.0 eV (Fig. 4.3 (d)) is attributed to graphite due to deintercalation of Li-GICs. New peaks of B 1s at 188.7 eV and N 1s at 396.0 eV (Fig. 4.3 (a) and (b)) are supposed attributable to Li-BNICs. The binding energies are shifted by 1.8 eV for B 1s and 2.0 eV for N 1s, respectively, from those of h-BN. Intercalation of Li into the BN layered structure may decrease the bond strength/order of h-BN and increase the electron density on boron or nitrogen [29]. This may explain the lowered binding energies of B 1s and N 1s components. As for Li 1s component, the spectrum essentially does not change after heating except for the peak height. Although it is difficult to determine whether the 55.0 eV (orange line in Fig. 4.3 (d) for Li 1s) peak is attributed to Li-BNICs, as it may mainly derive from LiOH and/or Li_2CO_3 on the surface, there is some possibility. Any evidence on a reaction between BN and graphite was not obtained, which is consistent with absence of reported binding energies for a B–C–N system [21].

^{7}Li NMR spectra of the heat-treated samples after milling for 2.5 and 10 hours are shown in Fig. 4.5, where the central positions (chemical shifts: δ) are at 7 ppm and 14 ppm, respectively. The values and shapes of NMR spectra are similar to our previous study (Chapter 3) [1], in that the values would represent chemical shifts for Li-BNICs, and the widely broadened peaks indicate multiple Li sites exist with various electron

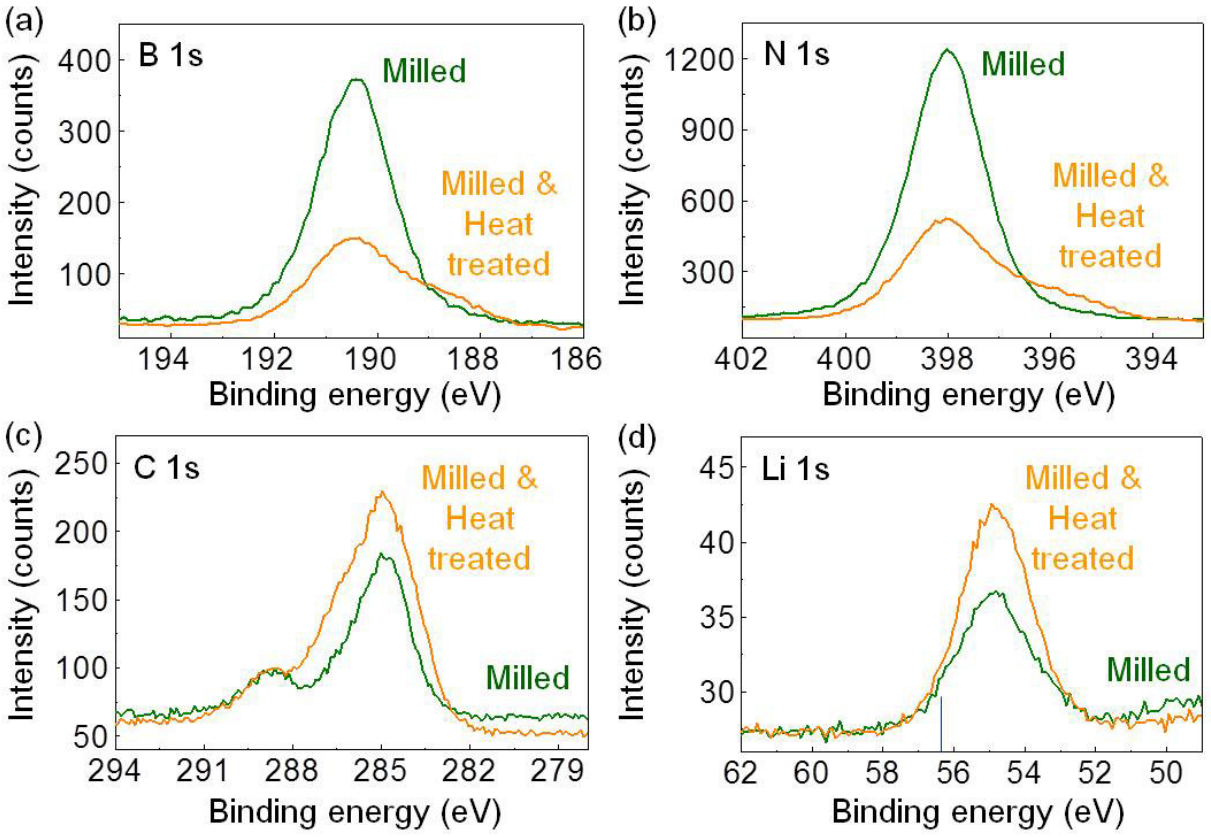

Fig. 4.3. XPS B 1s, N 1s, C 1s and Li 1s profiles of 2.5 h-milled samples before (green line) and after (orange line) heat treatment.

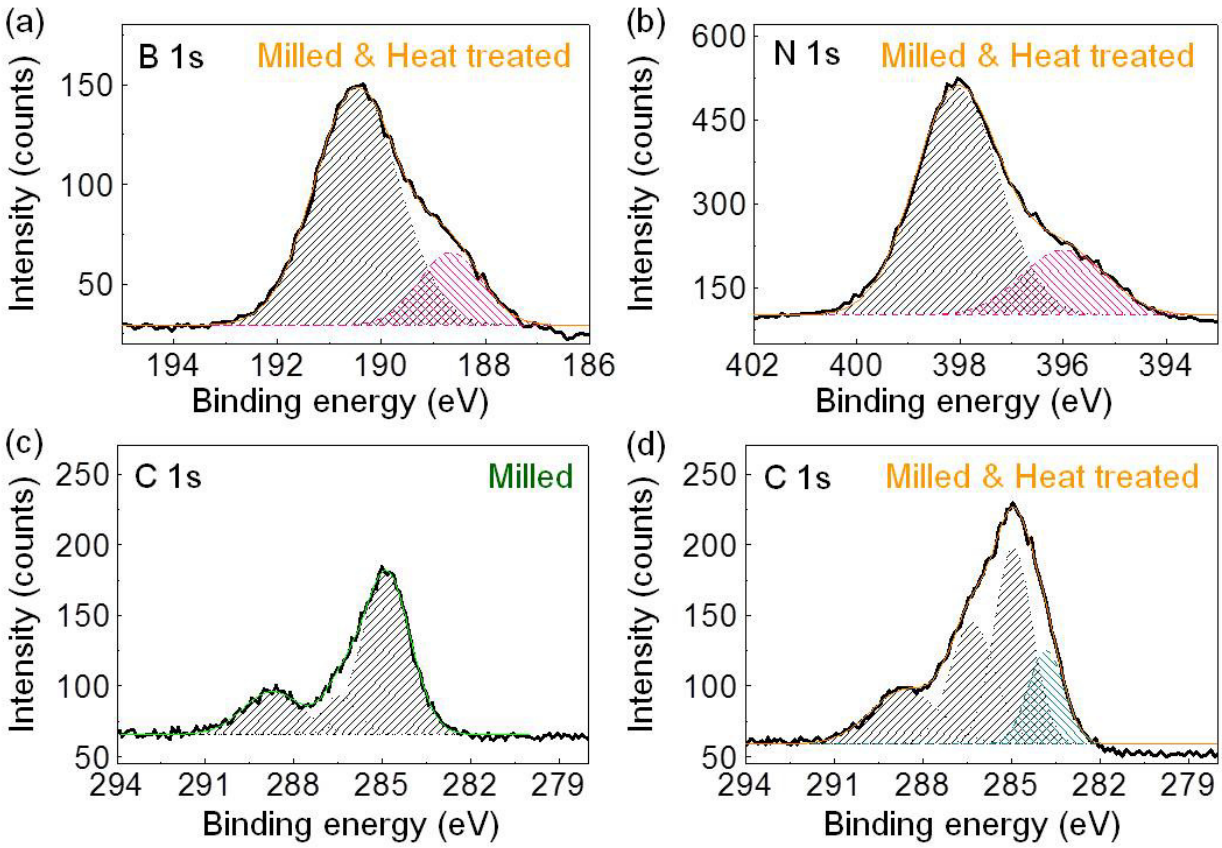

Fig. 4.4. Enlarged and/or deconvoluted XPS spectra for (a) B 1s and (b) N 1s of the heat-treated samples after milling, and C 1s spectra for (c) the milled sample and (d) the heat-treated sample after milling.

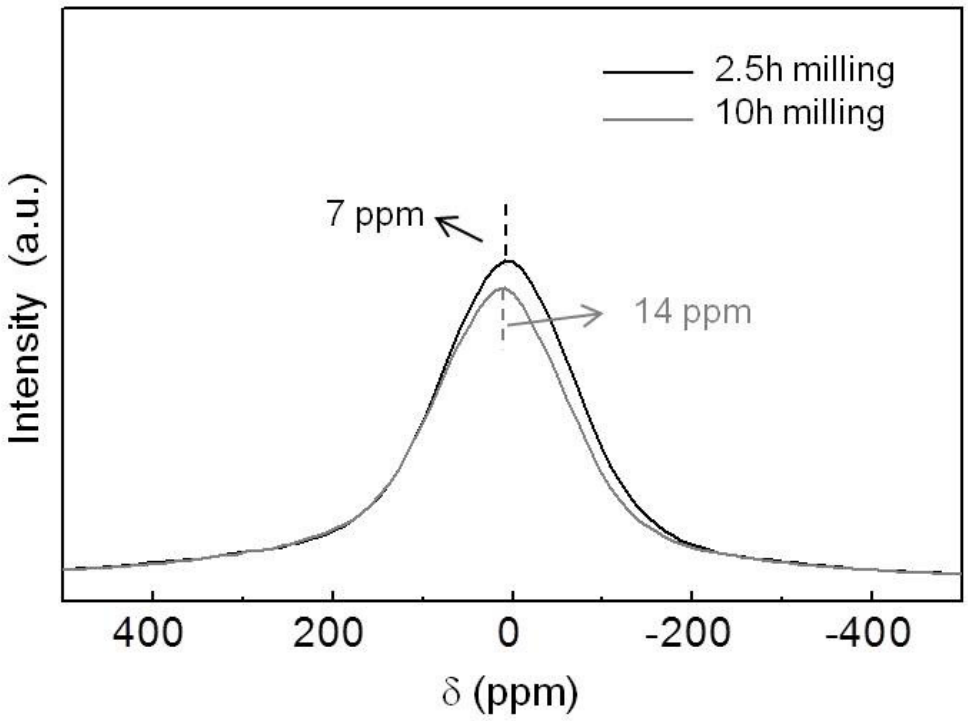

Fig. 4.5. ^{7}Li NMR spectra of the heat-treated samples after milling for 2.5 and 10 hours.

densities due to different atomic environments. With increasing milling duration, electron densities at Li nucleus would become more modified which is consistent with the XRD data in that more Li atoms are intercalated after heat treatment of longer-milled samples (Fig. 4.2). The NMR spectra might include chemical shifts of α-Li_3BN_2, β-Li_3BN_2 and/or Li_2C_2 as well in small quantity [30] (^{7}Li NMR for Li_3BN_2 has not been reported).

Thermal analysis was conducted in order to investigate the reaction when the milled samples were heat-treated. Fig. 4.6 (a) shows the DTA curves of 2.5 h-milled samples for a Li–BN–graphite system. Compared to DTA curves of this ternary system (Fig. 4.6 (a)) and BN–graphite binary system (Fig. 4.6 (b)), various peaks between 150 $\sim$ 700 °C on a heating curve (1st cycle) and 650 $\sim$ 700 °C on a cooling curve were obtained in a ternary system, which should derive from reactions involved with lithium. Fig. 4.6 (c) shows XRD patterns of the heat-treated samples (duration: 2 hours) at several temperatures represented in Fig. 4.6 (a). A very small endothermic peak around 180 °C is due to melting of lithium metal remained in the milled sample. Deintercalation of Li-GICs occurs in the temperature range of 310 $\sim$ 380 °C. Formation of Li_3BN_2 phases (both α and β) and Li_2C_2 occurs below 380 °C and 445 °C, respectively (but above deintercalation temperatures of Li-GICs). The XRD peaks of Li-BNICs are observed when annealed at 600 and 650 °C. Therefore, various broad exothermic peaks at the lower temperatures (below $\sim$380 °C) are attributed mainly to deintercalation of Li-GICs and formation of Li_3BN_2. For a large exothermic peak around 440 °C there seem no consistent XRD results, however, it might be attributed to synthesis of Li-BNICs because similar peaks have been observed in the Li–BN system of our previous study (Chapter 3) [1]. It is possibly explained that Li would erode BN structure during heat treatment, and firstly Li-BNICs with low crystallinity might be synthesized at the temperature of the exothermic peak (at around 440 °C), then, the XRD peaks of Li-BNICs can be observed at the higher temperature (in this case at 600 °C) due to crystallization. An endothermic peak about 650 °C on a heating curve and exothermic peaks between 650 $\sim$ 550 °C on a cooling curve are probably attributed to melting and crystallization of Al, respectively, which may come from an Al_2O_3 holder. This can explain XRD peaks of Al after heat treatment (Fig. 4.6 (c)).

Based on the whole results of this study, Li-GICs were firstly synthesized by milling, and then, by heat treatment the Li-GICs were deintercalated to produce Li-BNICs without any reaction between BN and graphite. It is then supposed that

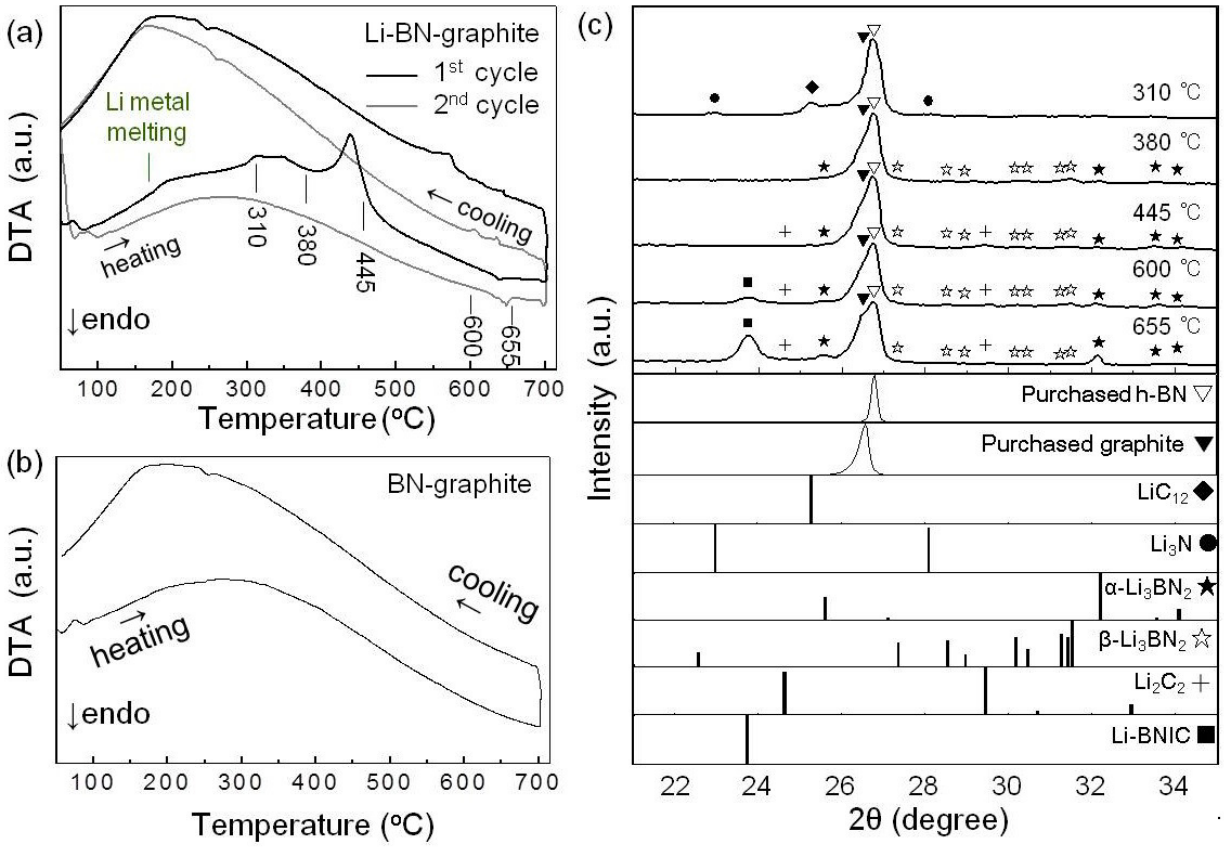

Fig. 4.6. DTA curves of 2.5 h-milled samples for (a) Li–BN–graphite ternary system, and (b) BN–graphite system by the ratio of 1:1, and (c) XRD patterns of samples heat-treated at several temperatures corresponding to (a) for 2 hours.

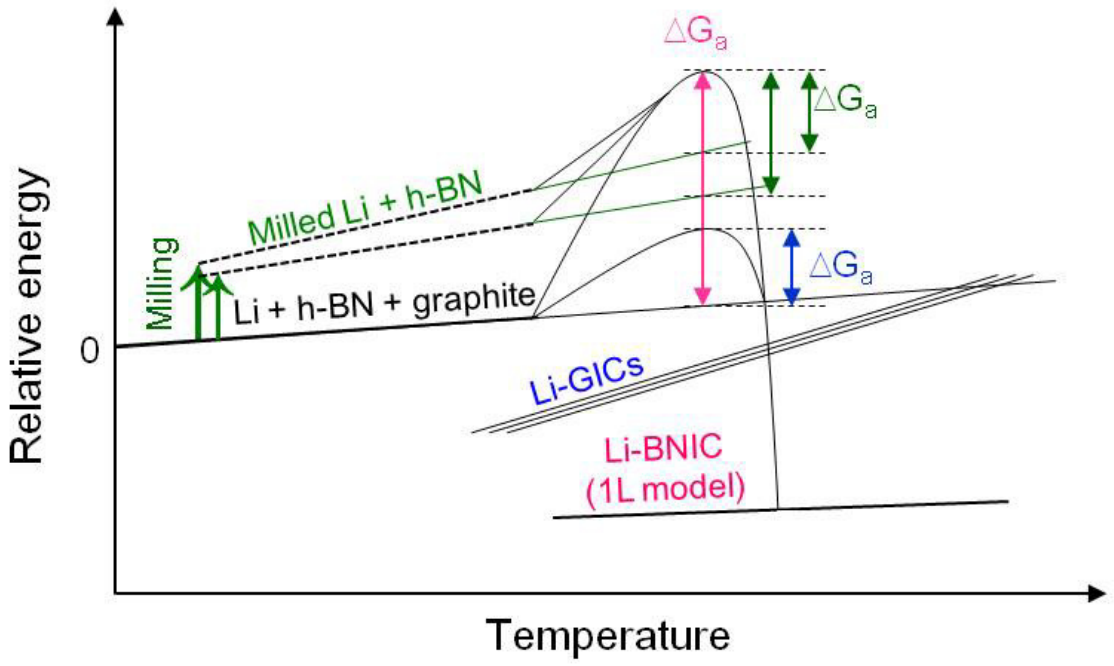

Fig. 4.7. Schematic diagram of relative energy profile for Li with h-BN and graphite.

Li-BNIC is more stable than Li-GICs, as seen Fig. 4.7, which shows a schematic diagram of relative energy profile for Li with h-BN and graphite. In this case, the criterion for relative energy is the pristine materials, which are lithium metal, h-BN and graphite, thus, the relative energy of these starting materials is zero. Li-GICs are easily synthesized by ball milling due to low activation barrier as seen by blue ΔG_a. On the other hand, a larger activation energy (pink ΔG_a) is required to produce Li-BNICs. Thereby, it is not synthesized by only milling. This pink ΔG_a can be lowered by milling-induced mechanochemical processes, as seen by green ΔG_a, and Li-BNICs are produced at lower temperatures when milling duration is longer, as reported by our previous study (Chapter 3) [1]. Meanwhile, three temperature-dependent lines for Li-GICs are represented with different energies in Fig. 4.7, because the thermal stability of Li-GICs might depend on synthesis processes, as mentioned in Introduction of this Chapter. Li-GICs synthesized by electrochemical method [17], milling (in this study) and heat treatment [10] would become more unstable in this order when evaluated from the temperature of deintercalation ($\sim$80, 310 and 330 °C).

In the DTA curves of Li–BN–graphite system (Fig. 4.6 (a)), an exothermic peak at around 440 °C is suggested attributable to Li-BNICs synthesis. Using this exothermic peak, an activation energy for Li intercalation into 2.5 h-milled h-BN (for a Li–BN–graphite ternary system) was estimated through the Kissinger method. Fig. 4.8 (a) shows DTA curves of 2.5 h-milled samples for a Li–BN–graphite ternary system with several heating rates between 5 and 50 °C/min, and Fig. 4.8 (b) shows the corresponding Kissinger plot. The activation energy was estimated to be 119.6 kJ/mol and it can be supposed that an activation energy of Li intercalation into the pristine h-BN would be higher than this value. For Li-GICs, activation energies for Li diffusion in various carbonaceous materials have been reported through electrochemical processes [31, 32]. Ping Liu et al. have reported activation energies in pyrolytic poly (furfural alcohol) (PFA), coke and MCMB (mesophase carbon, prepared at 1000 °C) to be about 10 $\sim$ 170 kJ/mol, as the activation energy is highly dependent on Li concentration. The activation energies at a lithium intercalation degree of $\sim$0.5, i.e. similar to LiC_{12}, are about 24 $\sim$ 50 kJ/mol. Kulova et al. have reported activation energies in graphite to be 35 kJ/mol calculated by the Arrhenius equation. Thus, the activation energy estimated in this study is in the same order of magnitude, and the values for Li-GICs (24 $\sim$ 50 kJ/mol are considered because the synthesized Li-GICs are LiC_6 and LiC_{12} in this study) are smaller than 119.6 kJ/mol, which is supportive of our discussion and analysis. This higher activation energy for Li-BNICs than Li-

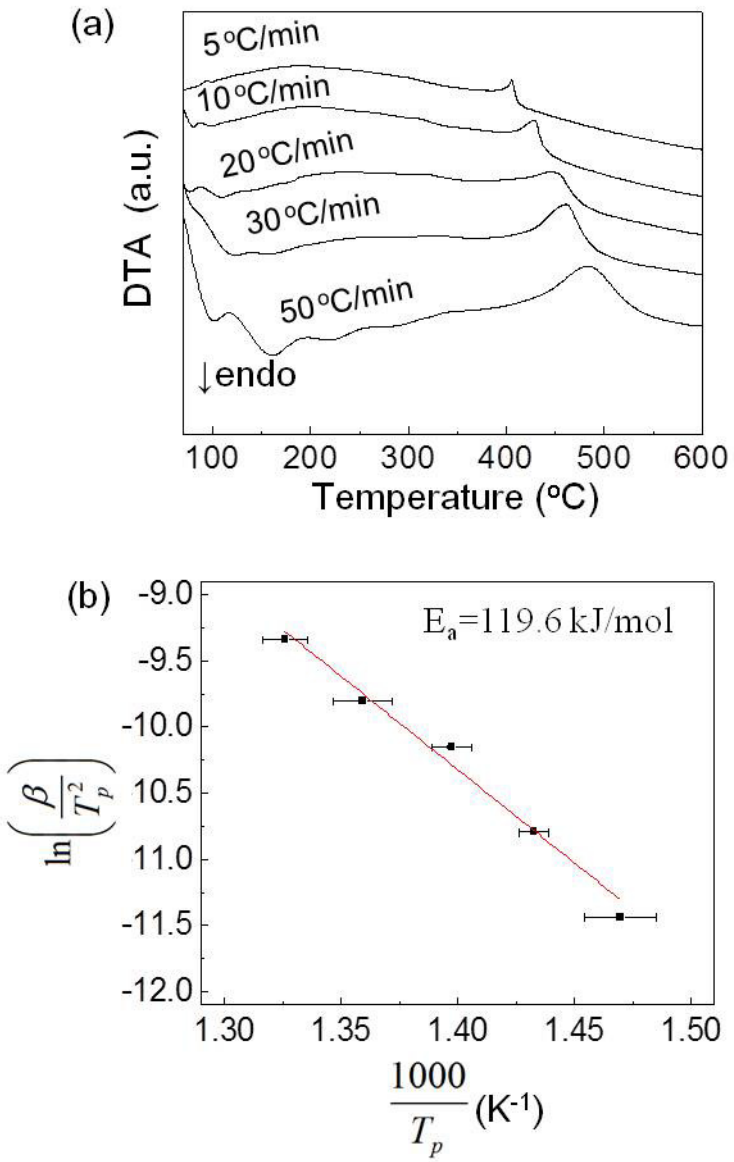

Fig. 4.8. (a) DTA curves (heating rate: 5 $\sim$ 50 °C/min) of 2.5 h-milled samples for a Li–BN–graphite ternary system and (b) Kissinger plot.

GICs is due to higher interlayer binding energy for h-BN as 85.9 meV/atom [33] than for graphite as 56 meV/atom [34] calculated by DFT. Therefore, Li intercalation and diffusion for h-BN are more difficult to occur than for graphite.

4.3 Conclusion

Pieces of lithium metal, h-BN and graphite powders, with a 1/1.1/1.1 molar ratio, were ball-milled using a vibratory ball mill machine and annealed at 700 °C for 2 h under argon atmosphere. After milling, Li-GICs and a small amount of Li_3N were produced, as well as some unreacted and defective Li metal and h-BN. After heat treatment of the milled samples, Li-BNICs a small amount of Li_2C_2, Li_3BN_2 and Al were synthesized, with graphite from deintercalation of Li-GICs. The deintercalation reaction occurs at lower temperatures (below 310 °C) and the deintercalated Li atoms seem to be diffused from graphite to BN. That is, Li-BNICs are more stable than Li-GICs at an ambient condition, while the activation energy for producing Li-GICs might be smaller than Li-BNICs. No reaction took place between BN and graphite powders during either process. Through elongation of milling duration, more Li could be intercalated because the structure of h-BN would become more defective.

Reference

[1] J. Kim, E. Yamasue, H. Okumura, K. N. Ishihara, and C. Michioka, "Structures of boron nitride intercalation compound with lithium synthesized by mechanical milling and heat treatment," *Journal of Alloys and Compounds*, vol. 685, pp. 135–141, 2016.

[2] A. Sumiyoshi, H. Hyodo, Y. Sato, M. Terauchi, and K. Kimura, "Good reproductive preparation method of Li-intercalated hexagonal boron nitride and transmission electron microscopy–electron energy loss spectroscopy analysis," *Solid State Sciences*, vol. 47, pp. 68–72, 2015.

[3] A. Sumiyoshi, H. Hyodo, and K. Kimura, "Structural analysis of Li-intercalated hexagonal boron nitride," *Journal of Solid State Chemistry*, vol. 187, pp. 208–210, 2012.

[4] D. Billaud, F. Henry, M. Lelaurain, and P. Willmann, "Revisited structures of dense and dilute stage II lithium-graphite intercalation compounds," *Journal of Physics and Chemistry of Solids*, vol. 57, no. 6, pp. 775–781, 1996.

[5] V. V. Avdeev, A. P. Savchenkova, L. A. Monyakina, I. V. Nikol'skaya, and A. V. Khvostov, "Intercalation reactions and carbide formation in graphite-lithium system," *Journal of Physics and Chemistry of Solids*, vol. 57, no. 6, pp. 947–949, 1996.

[6] K. Zaghib, K. Tatsumi, Y. Sawada, S. Higuchi, H. Abe, and T. Ohsaki, "^{7}Li-NMR of well-graphitized vapor-grown carbon fibers and natural graphite negative electrodes of rechargeable lithium-ion batteries," *Journal of The Electrochemical Society*, vol. 146, no. 8, pp. 2784–2793, 1999.

[7] Y. Reynier, R. Yazami, and B. Fultz, "The entropy and enthalpy of lithium intercalation into graphite," *Journal of power sources*, vol. 119, pp. 850–855, 2003.

[8] J. Sangster, "C-Li (Carbon-Lithium) system," *Journal of Phase Equilibria and Diffusion*, vol. 28, no. 6, pp. 561–570, 2007.

[9] F. Chevallier, F. Poli, B. Montigny, and M. Letellier, "*In situ* ^{7}Li nuclear magnetic resonance observation of the electrochemical intercalation of lithium in graphite: second cycle analysis," *Carbon*, vol. 61, pp. 140–153, 2013.

[10] M. Drüe, M. Seyring, A. Kozlov, X. Song, R. Schmid-Fetzer, and M. Rettenmayr, "Thermodynamic stability of Li_2C_2 and LiC_6," *Journal of Alloys and Compounds*, vol. 575, pp. 403–407, 2013.

[11] C. Sole, N. E. Drewett, and L. J. Hardwick, "*In situ* raman study of lithium-ion intercalation into microcrystalline graphite," *Faraday discussions*, vol. 172, pp. 223–237, 2014.

[12] R. L. Sacci, L. A. Adamczyk, G. M. Veith, and N. J. Dudney, "Dry synthesis of lithium intercalated graphite powder and fiber," *Journal of The Electrochemical Society*, vol. 161, no. 4, pp. A614–A619, 2014.

[13] C. Bindra, V. A. Nalimova, D. E. Sklovsky, Z. Benes, and J. E. Fischer, "Super dense LiC_2 as a high capacity Li intercalation anode," *Journal of the Electrochemical Society*, vol. 145, no. 7, pp. 2377–2380, 1998.

[14] R. Janot, J. Conard, and D. Gurard, "Ball milling: a new route for the synthesis of superdense lithium GICs," *Carbon*, vol. 39, no. 12, pp. 1931–1934, 2001.

[15] D. Guérard and R. Janot, "Structure of the superdense LiC_3 compound prepared by ball-milling," *Journal of Physics and Chemistry of Solids*, vol. 65, no. 2, pp. 147–152, 2004.

[16] R. Janot and D. Guerard, "Ball-milling in liquid media: Applications to the preparation of anodic materials for lithium-ion batteries," *Progress in Materials Science*, vol. 50, no. 1, pp. 1–92, 2005.

[17] A. M. Andersson, K. Edström, and J. O. Thomas, "Characterisation of the ambient and elevated temperature performance of a graphite electrode," *Journal of power sources*, vol. 81, pp. 8–12, 1999.

[18] A. Kozlov, M. Seyring, M. Drüe, M. Rettenmayr, and R. Schmid-Fetzer, "The Li–C phase equilibria," *International Journal of Materials Research*, vol. 104, no. 11, pp. 1066–1078, 2013.

[19] M. Morita, T. Hanada, H. Tsutsumi, Y. Matsuda, and M. Kawaguchi, "Layered-structure BC_2N as a negative electrode matrix for rechargeable lithium batteries," *Journal of The Electrochemical Society*, vol. 139, no. 5, pp. 1227–1230, 1992.

[20] B. Yao, W. Chen, L. Liu, B. Ding, and W. Su, "Amorphous B–C–N semiconductor," *Journal of applied physics*, vol. 84, pp. 1412–1415, 1998.

[21] Y. Xiong, C. Xiong, S. Wei, H. Yang, Y. Mai, W. Xu, S. Yang, G. Dai, S. Song, J. Xiong, *et al.*, "Study on the bonding state for carbon–boron nitrogen with different ball milling time," *Applied Surface Science*, vol. 253, no. 5, pp. 2515–2521, 2006.

[22] H. Yamane, S. Kikkawa, H. Horiuchi, and M. Koizumi, "Structure of a new polymorph of lithium boron nitride, Li_3BN_2," *Journal of solid state chemistry*, vol. 65, no. 1, pp. 6–12, 1986.

[23] B. Xu, M.-Z. Lv, H.-M. Yang, and Z.-X. Wen, "Thermodynamic analysis of the V-shaped area of high pressure and high temperature in cubic boron nitride synthesis with Li_3N as a catalyst," *Entropy*, vol. 16, no. 2, pp. 912–920, 2014.

[24] J. Moulder and J. Chastain, *Handbook of X-ray Photoelectron Spectroscopy: A Reference Book of Standard Spectra for Identification and Interpretation of XPS Data*. Physical Electronics, 1995.

[25] G. Wertheim, P. T. M. Van Attekum, and S. Basu, "Electronic structure of lithium graphite," *Solid State Communications*, vol. 33, no. 11, pp. 1127–1130, 1980.

[26] V. Mordkovich, "Synthesis and XPS investigation of superdense lithium-graphite intercalation compound, lic 2," *Synthetic metals*, vol. 80, no. 3, pp. 243–247, 1996.

[27] H. Momose, H. Honbo, S. Takeuchi, K. Nishimura, T. Horiba, Y. Muranaka, Y. Kozono, and H. Miyadera, "X-ray photoelectron spectroscopy analyses of lithium intercalation and alloying reactions on graphite electrodes," *Journal of power sources*, vol. 68, no. 2, pp. 208–211, 1997.

[28] C. M. Lee, S.-H. Yang, B.-J. Mun, and P. N. Ross, "Surface structure of lithiated graphite by X-ray photoelectron diffraction," *Surface science*, vol. 477, no. 2, pp. 126–132, 2001.

[29] N. I. Kovtyukhova, Y. Wang, R. Lv, M. Terrones, V. H. Crespi, and T. E. Mallouk, "Reversible intercalation of hexagonal boron nitride with brønsted acids," *Journal of the American Chemical Society*, vol. 135, no. 22, pp. 8372–8381, 2013.

[30] B. Ruprecht, H. Billetter, U. Ruschewitz, and M. Wilkening, "Ultra-slow Li ion dynamics in Li_2C_2–on the similarities of results from ^{7}Li spin-alignment echo NMR and impedance spectroscopy," *Journal of Physics: Condensed Matter*, vol. 22, no. 24, p. 245901, 2010.

[31] P. Liu and H. Wu, "Diffusion of lithium in carbon," *Solid state ionics*, vol. 92, no. 1, pp. 91–97, 1996.

[32] T. Kulova, A. Skundin, E. Nizhnikovskii, and A. Fesenko, "Temperature effect on the lithium diffusion rate in graphite," *Russian Journal of Electrochemistry*, vol. 42, no. 3, pp. 259–262, 2006.

[33] N. Marom, J. Bernstein, J. Garel, A. Tkatchenko, E. Joselevich, L. Kronik, and O. Hod, "Stacking and registry effects in layered materials: the case of hexagonal boron nitride," *Physical review letters*, vol. 105, no. 4, p. 046801, 2010.

[34] L. Spanu, S. Sorella, and G. Galli, "Nature and strength of interlayer binding in graphite," *Physical review letters*, vol. 103, no. 19, p. 196401, 2009.

Chapter 5

Intercalation of hexagonal boron nitride and graphite with lithium by electrochemical method

5.1 Introduction

As explained in Section 1.1.2, graphite is widely used as anode materials for lithium-ion secondary batteries, where it can intercalate and deintercalate lithium ions based on the layered-structure characteristics [1, 2]. In a fully charged state, LiC_6 is formed, and its theoretical capacity is 372 mAh/g with a potential below 0.3 V versus Li/Li^+.

Recently, for improvement battery abilities, especially higher capacity, many carbonaceous materials have been studied such as the milled graphite [3–6], carbon nanotubes [7–10], superdense Li-GICs [11–13] and so on. For the milled graphite, on the whole, the capacities are increased, whereas there are problems such as larger potential hysteresis [4] and smaller charge-transfer resistance [6]. C. Natarajan et al. suggested short milling duration (< 5 h) because "the extended milling destroys surface and increases the basal plane surface area, which reduces the reversible capacity and increases the irreversible capacity" [5]. Superdense Li-GICs (LiC_2 and LiC_3) were reached to high capacity (about 1 Ah/g), but reversible capacities correspond to that of LiC_6. Therefore Janot et al., who have studied LiC_3 synthesized by ball milling and its electrochemical properties, suggested superdense Li-GICs can be used for primary batteries [13].

Meanwhile, the successful synthesis of the lithium boron nitride intercalation compounds (Li-BNICs) through sequential processes of ball milling and heat treatment [14] have been investigated in Chapter 3. Still, it is difficult to investigate the exact atomic structure and Li concentration of Li-BNIC. Li could be intercalated into defective BN due to suggestion of "1L model" [14, 15]. However, similar I_c values for Li-BNIC have been reported, e.g. 0.37599 nm [15] and 0.3752 nm [14], which was unchanged with different ratios of Li/BN. Variations of I_c between the pristine and intercalated graphite (LiC_6: 0.37 nm) are quite similar to h-BN. Both are thus comparable, and the detailed structure of Li-BNIC is worth investigating. Li-BNIC is more stable than Li-GICs at higher temperatures as studied in Chapter 4. Thereby, h-BN can be considered as a potential battery material for high-temperature application.

In spite of this potential and successful production of Li-BNIC, electrochemical lithiation of h-BN has not been reported by now. Electrochemical properties of intercalation compounds of h-BN are extremely important for investigating possibility of application in terms of Li-ion battery. Therefore, the purpose of this study is to investigate the potential physical/chemical properties relating to electrical conductivity using the pristine and the milled h-BN with/without graphite.

5.2 Results and discussion

Firstly, the milled samples were characterized by XRD (Fig. 5.1), FE-SEM (field emission-scanning electron microscope, Fig. 3.3 and Fig. 5.2), BET (for specific surface area, Table 5.2) and XPS (etching by 300 V for 0, 30 and 180 seconds, Fig. 5.3) to investigate reaction between h-BN and graphite by milling.

Fig. 5.1 shows XRD patterns of graphite (a) and h-BN (b) before and after milling (The milling was separately performed for 2.5 hours.). After milling, high-crystallinity structures in the pristine graphite and BN were destroyed and their XRD peaks were broadened with decreased intensities. As seen in Table 3.1 and Table 5.1 for calculated crystallite sizes (L) using a Scherrer equation, the milled h-BN and graphite show smaller L than the pristine powders. Although L_c of the milled h-BN is still larger than that of the milled graphite, the reduction rate for h-BN before and after milling is larger than for graphite. It is supposed that ball milling has greater influences on h-BN for shorter milling durations than on graphite, possibly due to the differences in hardness and chemical bonding.

As seen in SEM images for the pristine and the milled samples (Fig. 3.3 and

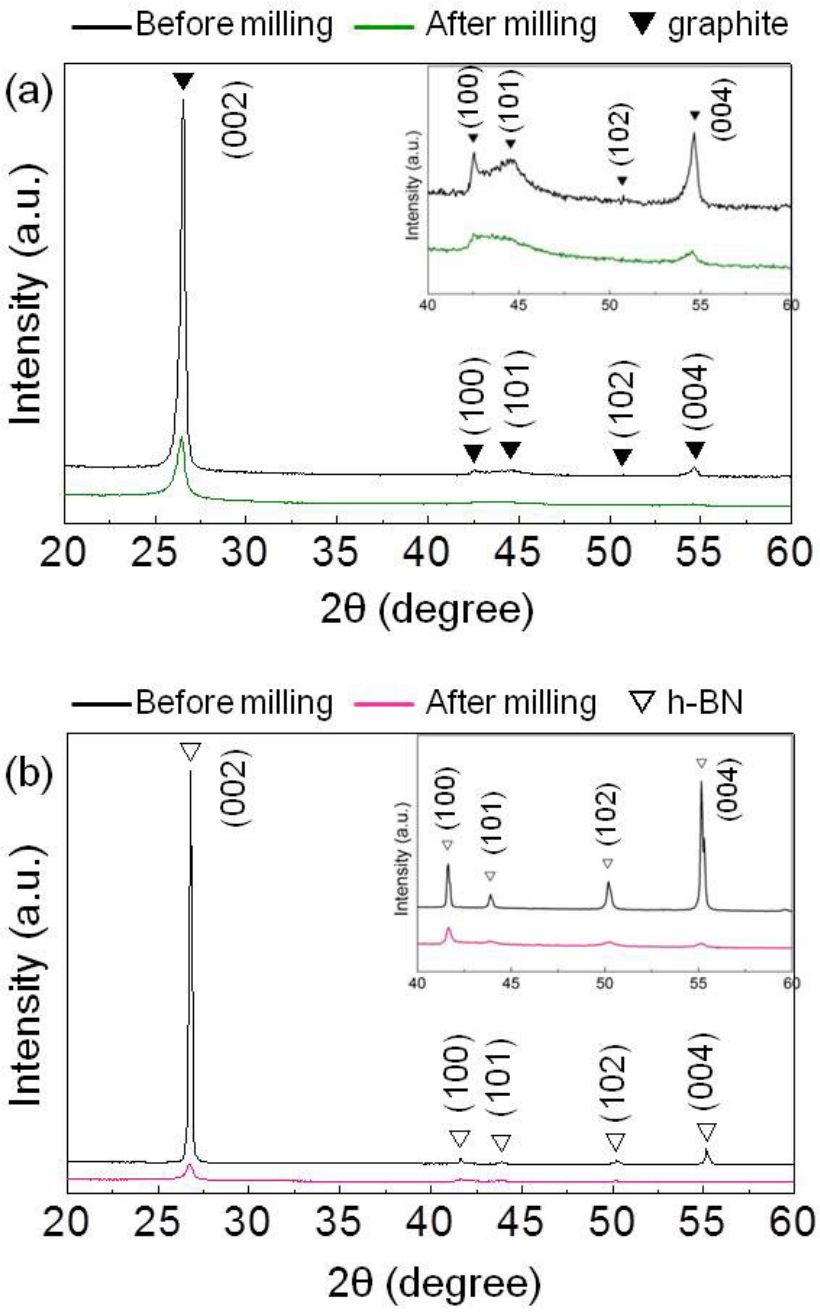

Fig. 5.1. XRD patterns of the pristine (Before milling) and 2.5 h-milled (After milling) powders: (a) graphite and (b) h-BN with including the expanded figures by intensity axis from 40 to 60 degrees.

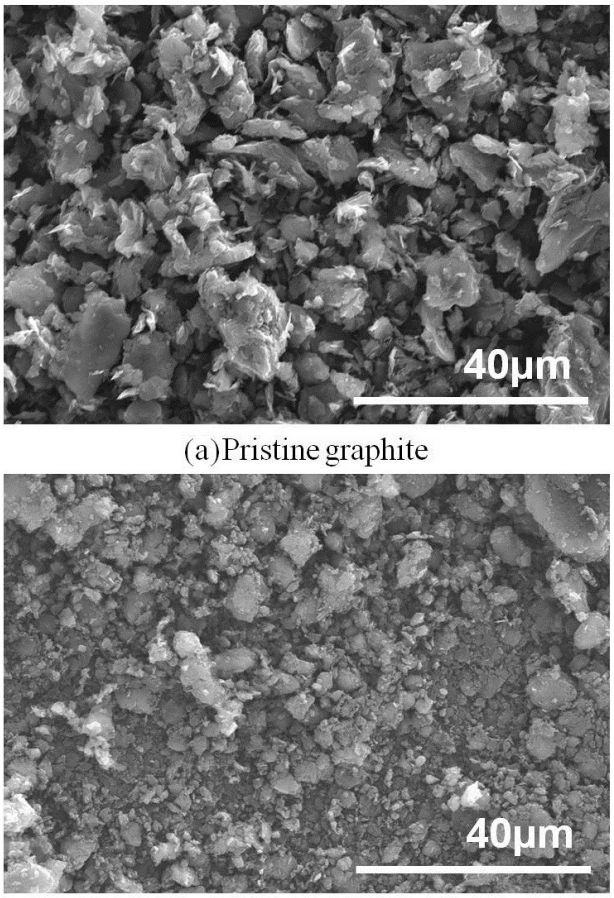

Fig. 5.2. SEM image of (a) the pristine graphite and (b) 2.5 h-milled graphite.

Table 5.1. The crystallite sizes (L) for the pristine and the milled graphite calculated by Scherrer equation. For the milled graphite, only L_c are calculated, as the (100) peaks were too broad, as seen in Fig. 5.1.

Milling duration (h)	L_c (nm)	L_a (nm)
0	30.54	50.31
2.5	16.78	-

Table 5.2. The specific surface areas of the pristine (0h-milled) and 2.5 h-milled samples for h-BN and graphite.

Milling	Hexagonal BN		graphite	
duration (h)	0 h	2.5 h	0 h	2.5 h
Specific surface areas (m^2/g)	1.2	258.7	9.7	259.8

$*$ Specific surface areas of samples were estimated using BET (FlowSorb III 2305, Micromeritics Instrument Corporation), which is the method based on the physical adsorption of gas, developed by the Brunauer, Emmer and Teller (BET) [16]. Here, the samples were purified by degassing at 180 °C for 30 min, followed by the BET measurement using the mixed gas of N_2 30% and He 70%.

Fig. 5.2), the particle sizes (or agglomerates) of the pristine h-BN and graphite are much larger than 2.5 h-milled h-BN and graphite, respectively, where the change appears more significant for the former. Also, the specific surface area of 2.5 h-milled h-BN is significantly increased from 1.2 to 258.7 m^2/g, as seen in Table 5.2, consistent with SEM observations. The variation of surface area for the milled h-BN has also been reported by Streletskii et al., where it has increased from 12 (0h milling) to 400 m^2/g [17]. Thus, the set milling duration of 2.5 h in this study for h-BN may correspond to the initial step of deformation processes (please refer Chapter 3), involving large reduction of both crystallite size and particle size, which leads to the significant increase in the specific surface area.

The XRD patterns for various milled samples (milled graphite; Milled C, milled h-BN; Milled BN, milled BN and graphite together by the ratio of 8 : 1; Milled BN8C1-t) are shown in Fig. 5.3 (a) on the left, and the XPS (C 1s, B 1s and N 1s) profiles for Milled BN8C1-t with etching times of 0, 30 and 180 s are shown in Fig. 5.3 (b) on the right. The XRD patterns of Milled C and Milled BN are duplicated in Fig. 5.1 and 5.3 for comparison. It seems that BN and graphite did not react after milling because: first, as seen in an enlarged figure of Fig. 5.3 (a), a shoulder XRD peak for the milled graphite can be seen at the lower angle side, and second, in Fig. 5.3 (b) the XPS spectra are mostly unchanged (except for the intensities) for graphite (at around 284.0 eV of C 1s) and h-BN (at around 190.5 eV of B 1s and 398.0 eV of N 1s [18]) regardless of etching times. The reason of no reaction between h-BN and graphite is because provided energies in the powder are not enough to break the in-plane bonding of B–N for h-BN and/or C–C for graphite by milling for 2.5 hours.

The galvanostatic cycles with potential limitation (GCPL) of the pristine graphite and h-BN are shown in Fig. 5.4 (a) and (b), respectively. The GCPLs were conducted on the pristine graphite (Pure C) and h-BN (Pure BN), where for the former using the 1 C-rate calculated by the theoretical capacity of graphite (372 mAh/g), while for the latter 1/80 C with the capacity of h-BN (360 mAh/g). In the case of BN, a very slow rate 1/80 C was selected as it was difficult to measure GCPL with 1 C that was used for the pristine graphite. Fig. 5.4 (a) shows typical galvanostatic cycles of graphite. On the other hand, significantly small capacities were obtained for Pure BN though the C-rate is very small, as seen in Fig. 5.4 (b). Accordingly, it is supposed that Li intercalation into the pristine h-BN is extremely difficult through an electrochemical method.

The GCPL of only-milled h-BN (Milled BN) was also conducted in order to inves-

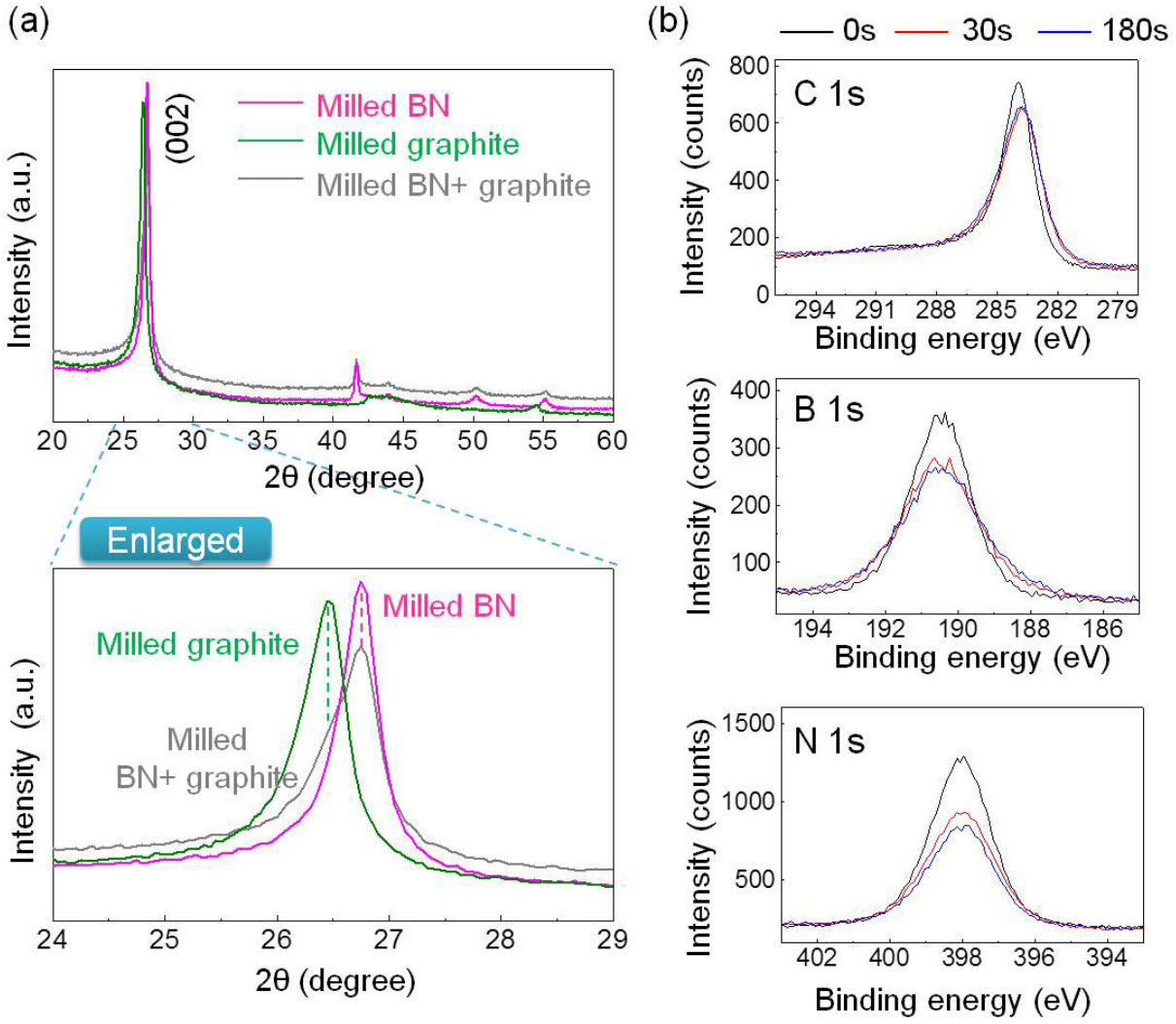

Fig. 5.3. (a) XRD patterns of 2.5 h-milled h-BN, graphite, and together (h-BN/graphite with weight ratio of 8 : 1) and below figure shows enlargement from 24 to 29 degrees. (b) XPS C 1s, B 1s and N 1s profiles of the milled-together h-BN and graphite with etching times of 0, 30 and 180 seconds.

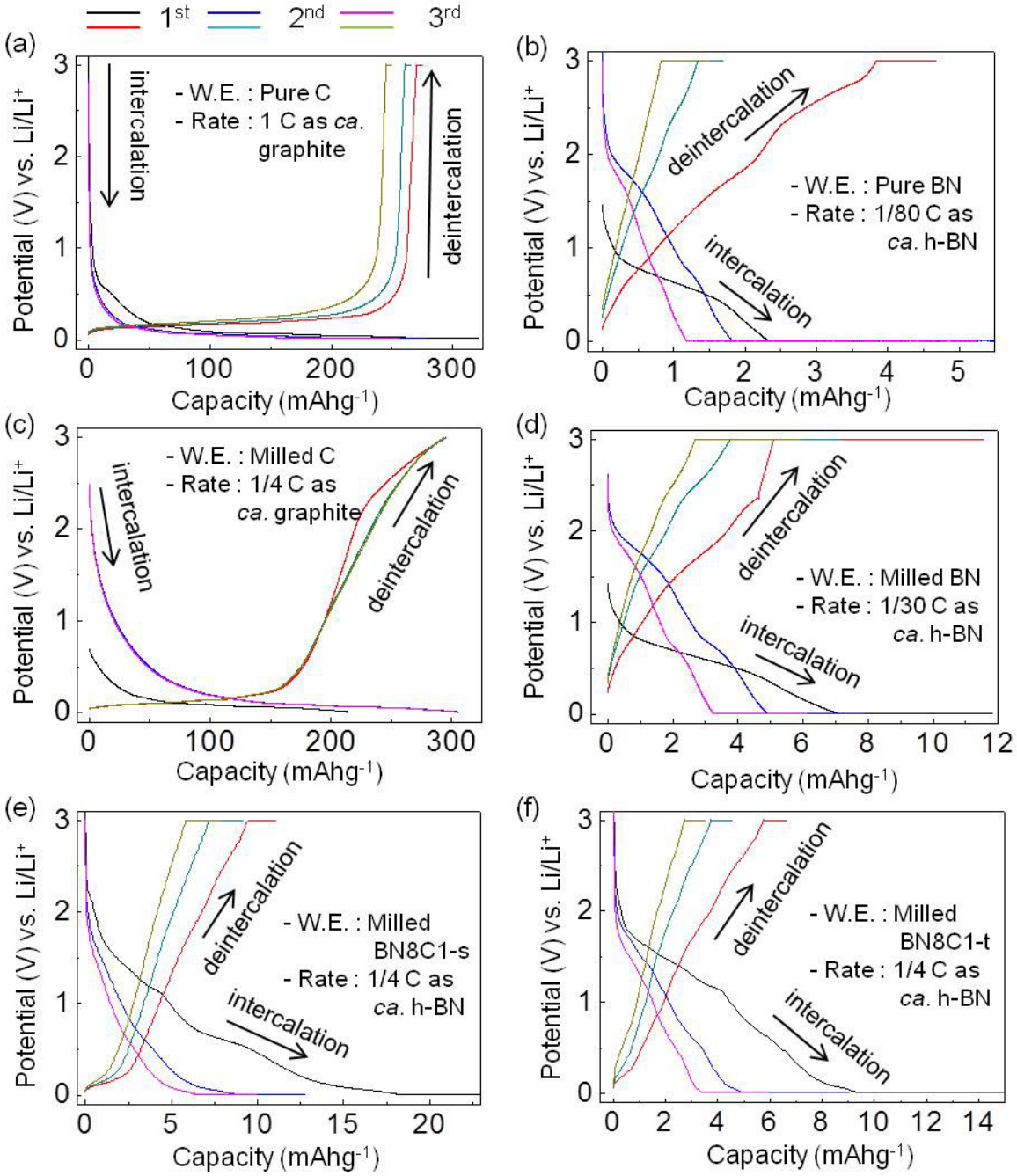

Fig. 5.4. Galvanostatic cycles for (a) the pristine graphite, (b) the pristine h-BN, (c) 2.5 h-milled graphite, (d) 2.5 h-milled h-BN, (e) the mixture of 2.5 h-milled h-BN and 2.5 h-milled graphite with a weight ratio of 8 : 1 and (f) 2.5 h-milled-together h-BN and graphite with the same weight ratio.

tigate the effect of ball milling using the C-rate of 1/30 C. The capacity of Milled BN is higher than that of Pure BN, although the C-rate is faster than that used for Pure BN, as shown in Fig. 5.4 (d). This might be due to increased surface area and/or formation of defective h-BN through milling. The enhanced capacity, however, still falls short of the capacity exhibited by graphite.

In order to improve the electrical conductivity of Milled BN, 2.5 h-milled graphite was added to 2.5 h-milled BN by weight ratio of 1 : 8 (Milled BN8C1-s), and the GCPL measurement was conducted using the rate of 1/4 C. The milled graphite (Milled C) and milled-together h-BN and graphite by the same ratio (Milled BN8C1-t) were also used for GCPL measurement with the same C-rate (1/4 C) to confirm an influence of milling on electrochemical properties. Fig. 5.4 shows the result of GCPL for (c) Milled C, (e) Milled BN8C1-s, and (f) Milled BN8C1-t. The Milled C shows a rather stable charge/discharge reaction behavior, where because the second and third cycle shapes are almost similar, as seen in Fig. 5.4 (c) in contrast with Pure C (5.4 (a)). The capacities of Milled BN8C1-s and Milled BN8C1-t are higher than Pure BN and Milled BN in Fig. 5.4 (b) and Fig. 5.4 (d), respectively, though it falls short of Pure C (5.4 (a)) and Milled C (5.4 (c)). The shapes of each curve for Milled BN8C1-s and Milled BN8C1-t exhibit a mixed behavior of h-BN and graphite. In charging reactions, Li intercalation into h-BN firstly occurs, as seen in the rapid curve shape, while the smooth curve shape should represent intercalation of Li into graphite. On the other hand, in the discharge reaction, Li was first deintercalated from graphite until about 2.5 mAh/g for Milled BN8C1-s, or about 1 mAh/g for Milled BN8C1-t at the first cycle, and then from h-BN. On comparing Milled BN8C1-s with Milled BN8C1-t, the capacities of the latter are smaller and more similar to Milled BN than that of the former. All GCPL results show that lithium intercalation/deintercalation into BN is rather fast but in a small quantity. The difficulty of an intercalation process involving only a small amount of Li is probably ascribed to the reaction occurring only near the surface region of BN through the electrochemical method, besides that Li atoms diffuse very slowly into BN.

Fig. 5.5 shows the cyclic voltammograms of (a) Pure C, (b) Pure BN, (c) Milled C, (d) Milled BN, (e) Milled BN8C1-s and (f) Milled BN8C1-t. The Pure and Milled C exhibit the typical cyclic voltammograms of graphite: the lithium intercalation reaction starts at about 0.2 V vs. Li/Li^+ and deintercalation finishes at about 0.3 V vs. Li/Li^+ [13]. A solid-electrolyte interphase (SEI) should form for both cases at around 0.5 V vs. Li/Li^+, which does not exhibit from the second cycle. The equilibrium

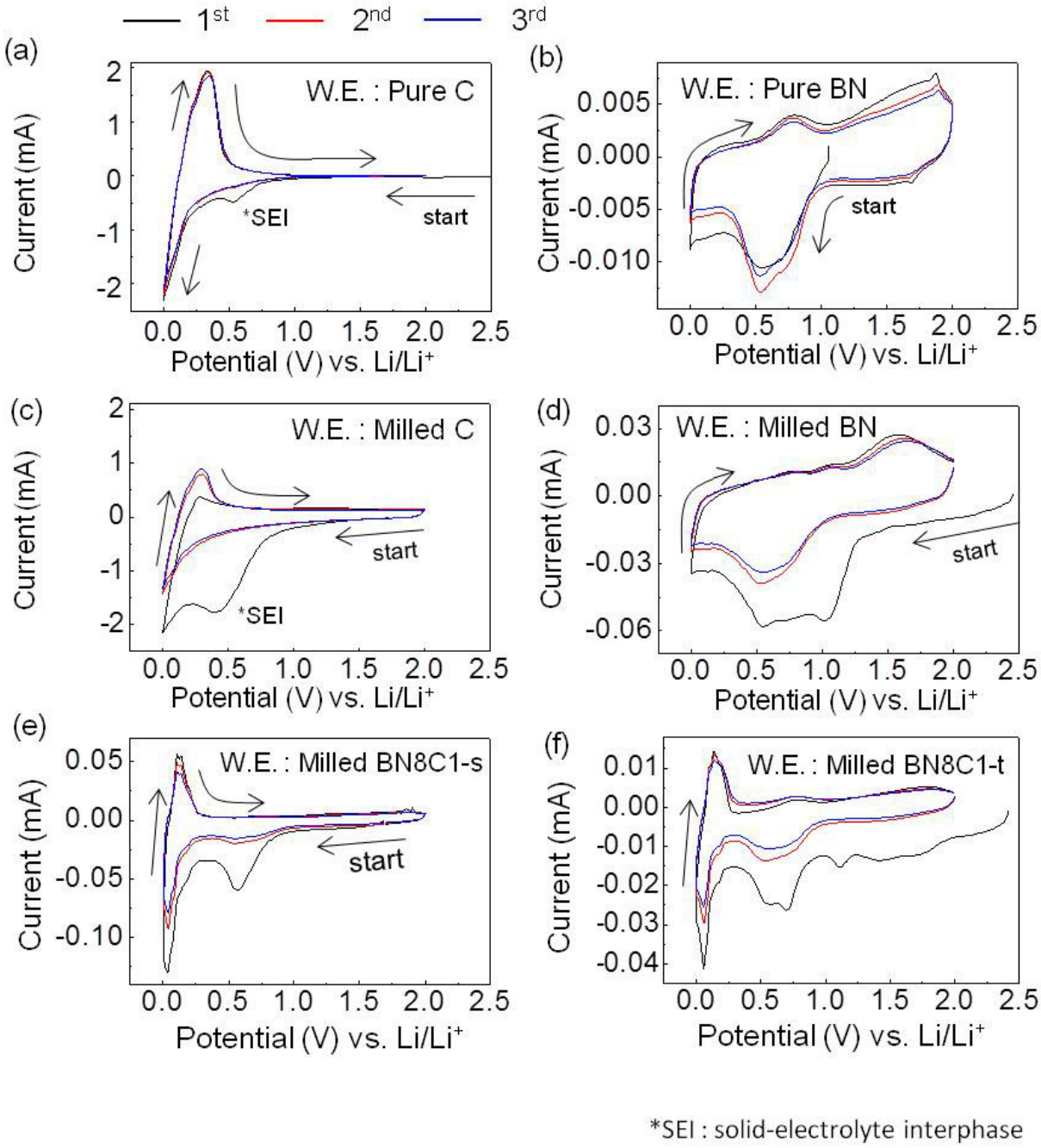

Fig. 5.5. Cyclic voltammograms for the pristine ((a) graphite and (b) h-BN) and 2.5 h-milled ((c) graphite, (d) h-BN) materials, (e) the mixture of 2.5 h-milled h-BN (Milled BN) and graphite (Milled C) by weight ratio of 8 : 1 and (f) 2.5 h-milled-together h-BN and graphite by the same ratio. (Scan rate: 1.0 mV/s)

intercalation potential of h-BN is around 1.0 V vs. Li/Li^+ and it was also obtained in the milled h-BN. The CV shapes of Pure and Milled BN indicate a two-phase reaction, where unlithiated and lithiated phases coexist during the charge/discharge process [19–21]. For the Milled BN, Milled BN8C1-s and Milled BN8C1-t, the reason that their first cycles are different to second and third cycles is due to the metastable surface of the milled samples. Thus, their first cycles exhibit several kinds of shoulders. In both Milled BN8C1-s and Milled BN8C1-t samples, except for the first cycle, two kinds of lithium intercalation reaction for h-BN and graphite were obtained at 1.0 V and 0.2 V, respectively, which correspond to each equilibrium intercalation potentials. This mixture of electrochemical behaviors of CVs is consistent with the galvanostatic cycles of Milled BN8C1-s and -t (Fig. 5.4 (e) and (f)).

Fig. 5.6 shows estimated chemical potentials, vs. Li/Li^+ and vs. SHE (standard hydrogen electrode), of h-BN and graphite. In order to calculate EMF (electromotive force) from these CV results, $LiCoO_2$ (or CoO_2), which is a typical cathode material of Li-ion batteries, is also shown for comparison. The diagram can be explained as that Li-BNICs are more stable than Li-GICs in terms of thermodynamics and Li intercalation into h-BN occurs more quickly than into graphite. It is consistent with the thermal stability of Li-GICs and Li-BNIC as mentioned in the Section 5.1.

As a whole, the milled h-BN is better than the pristine one in terms of the electrochemical properties, although the mixtures with graphite are unaffected by ball milling. It implies that there is a possibility of improving the electrochemical performance of defective h-BN. Further detailed study on Li concentration in Li-BNICs is required for determining the specific capacity.

5.3 Conclusion

Electrochemical experiments of CV and GCPL under an ambient condition were conducted on the pristine graphite, the pristine h-BN, and 2.5 h-milled various counterparts. The chemical potential of graphite is found 0.2 V vs. Li/Li^+, while of h-BN 1.0 V vs. Li/Li^+, regardless of pristine or milled. Thus, Li-BNIC is more stable than Li-GICs in terms of thermodynamics under an ambient condition. The Li intercalation occurs on the surface of BN, and Li atoms/ions are very slowly diffused inside BN particles. Accordingly, Li intercalation into BN is more difficult than into graphite through an electrochemical process, and CV curves indicate two-phase reaction.

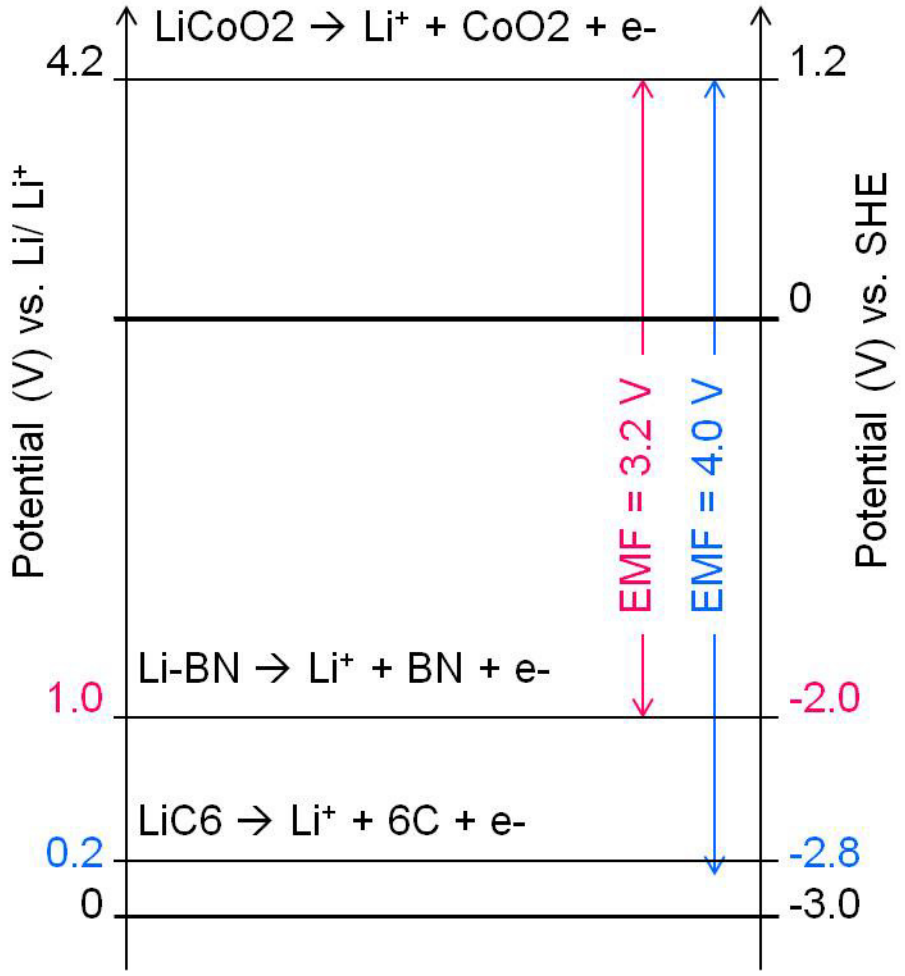

Fig. 5.6. Suggested chemical potentials of h-BN compared with graphite and CoO_2.

Reference

[1] Z. Shu, R. McMillan, and J. Murray, "Electrochemical intercalation of lithium into graphite," *Journal of The Electrochemical Society*, vol. 140, no. 4, pp. 922–927, 1993.

[2] T. Ohzuku, Y. Iwakoshi, and K. Sawai, "Formation of lithium-graphite intercalation compounds in nonaqueous electrolytes and their application as a negative electrode for a lithium ion (shuttlecock) cell," *Journal of The Electrochemical Society*, vol. 140, no. 9, pp. 2490–2498, 1993.

[3] F. Disma, L. Aymard, L. Dupont, and J.-M. Tarascon, "Effect of mechanical grinding on the lithium intercalation process in graphites and soft carbons," *Journal of the Electrochemical Society*, vol. 143, no. 12, pp. 3959–3972, 1996.

[4] C. Wang, G. Wu, and W. Li, "Lithium insertion in ball-milled graphite," *Journal of Power Sources*, vol. 76, no. 1, pp. 1–10, 1998.

[5] C. Natarajan, H. Fujimoto, A. Mabuchi, K. Tokumitsu, and T. Kasuh, "Effect of mechanical milling of graphite powder on lithium intercalation properties," *Journal of power sources*, vol. 92, no. 1, pp. 187–192, 2001.

[6] T. Ong and H. Yang, "Lithium intercalation into mechanically milled natural graphite: electrochemical and kinetic characterization," *Journal of The Electrochemical Society*, vol. 149, no. 1, pp. A1–A8, 2002.

[7] B. Gao, A. Kleinhammes, X. Tang, C. Bower, L. Fleming, Y. Wu, and O. Zhou, "Electrochemical intercalation of single-walled carbon nanotubes with lithium," *Chemical Physics Letters*, vol. 307, no. 3, pp. 153–157, 1999.

[8] G. Maurin, C. Bousquet, F. Henn, P. Bernier, R. Almairac, and B. Simon, "Electrochemical intercalation of lithium into multiwall carbon nanotubes," *Chemical Physics Letters*, vol. 312, no. 1, pp. 14–18, 1999.

[9] Z.-h. Yang and H.-q. Wu, "Electrochemical intercalation of lithium into carbon nanotubes," *Solid State Ionics*, vol. 143, no. 2, pp. 173–180, 2001.

[10] Z.-h. Yang and H.-q. Wu, "Electrochemical intercalation of lithium into raw carbon nanotubes," *Materials chemistry and physics*, vol. 71, no. 1, pp. 7–11, 2001.

[11] C. Bindra, V. A. Nalimova, D. E. Sklovsky, Z. Benes, and J. E. Fischer, "Super dense LiC_2 as a high capacity Li intercalation anode," *Journal of the Electrochemical Society*, vol. 145, no. 7, pp. 2377–2380, 1998.

[12] D. Guérard and R. Janot, "Structure of the superdense LiC_3 compound prepared by ball-milling," *Journal of Physics and Chemistry of Solids*, vol. 65, no. 2, pp. 147–152, 2004.

[13] R. Janot and D. Guerard, "Ball-milling in liquid media: Applications to the preparation of anodic materials for lithium-ion batteries," *Progress in Materials Science*, vol. 50, no. 1, pp. 1–92, 2005.

[14] J. Kim, E. Yamasue, H. Okumura, K. N. Ishihara, and C. Michioka, "Structures of boron nitride intercalation compound with lithium synthesized by mechanical milling and heat treatment," *Journal of Alloys and Compounds*, vol. 685, pp. 135–141, 2016.

[15] A. Sumiyoshi, H. Hyodo, Y. Sato, M. Terauchi, and K. Kimura, "Good reproductive preparation method of Li-intercalated hexagonal boron nitride and transmission electron microscopy–electron energy loss spectroscopy analysis," *Solid State Sciences*, vol. 47, pp. 68–72, 2015.

[16] S. Brunauer, P. H. Emmett, and E. Teller, "Adsorption of gases in multimolecular layers," *Journal of the American chemical society*, vol. 60, no. 2, pp. 309–319, 1938.

[17] A. Streletskii, D. Permenov, B. Bokhonov, I. Kolbanev, A. Leonov, I. Berestetskaya, and K. Streletzky, "Destruction, amorphization and reactivity of nano-BN under ball milling," *Journal of Alloys and Compounds*, vol. 483, no. 1, pp. 313–316, 2009.

[18] J. Moulder and J. Chastain, *Handbook of X-ray Photoelectron Spectroscopy: A Reference Book of Standard Spectra for Identification and Interpretation of XPS Data*. Physical Electronics, 1995.

[19] T. Ichitsubo, K. Tokuda, S. Yagi, M. Kawamori, T. Kawaguchi, T. Doi, M. Oishi, and E. Matsubara, "Elastically constrained phase-separation dynamics competing with the charge process in the $LiFePO_4/FePO_4$ system," *Journal of Materials Chemistry A*, vol. 1, no. 7, pp. 2567–2577, 2013.

[20] A. Hashem, M. Askar, M. Winter, J. Albering, and J. Besenhard, "Two-phase reaction mechanism during chemical lithium insertion into α-MoO3," *Ionics*, vol. 13, no. 1, pp. 3–8, 2007.

[21] H. Zhou *et al.*, "Two-phase transition of Li-intercalation compounds in Li-ion batteries," *Materials Today*, vol. 17, no. 9, pp. 451–463, 2014.

Chapter 6

Discussion: Atomic structures and phase stability of lithium boron nitride intercalation compounds

6.1 Introduction

Although Li-BNICs have been successfully synthesized by experimental methods such as heat treatment [1–3] in Chapter 3 and electrochemical intercalation in Chapter 5, it is still difficult to investigate exact amount of Li concentration in Li-BNIC. Some reports about structure of Li-BNICs are as following:

1. Similar interplanar distance (I_c) values for Li-BNIC have been reported, e.g. 0.37599 nm [1, 2] and 0.3752 nm [3].

2. According to report by Kim, the interplanar distance of Li-BNIC was unchanged with different ratios of Li/BN [3]. On the other hand, Li-GICs exhibit various structures with changes of Li concentration and stage phases as explained in Chapter 1.2.

3. Variations of I_c between the pristine and intercalated graphite (LiC_6: 0.37 nm) are quite similar to h-BN. Both are thus comparable, and the detailed structure of Li-BNIC is worth investigating.

4. The layered structures of Li-BNICs have been suggested to exhibit "1L model", but not "2L model". The 1L model involves "a structure without two-layer stacking periodicity", while the 2L model "two-layer stacking periodicity of the pristine

h-BN" [2].

From these, it can be assumed that Li-BNIC might exhibit no stage phase, i.e. only 1^{st} stage phase, which is different behavior with Li-GICs. Therefore, 1^{st} stage phases with different Li concentrations are considered for calculation as seen in Section 2.3.1.

As above fourth reports, it can be supposed that Li could be intercalated into defective BN. Also, Li was more easily intercalated into the milled BN than the pristine BN as shown in the results of Chapter 5. Therefore, disordered phase for Li-BNICs have to be considered. For disorder of the DFT calculation, several different approaches have been developed such as supercell method, virtual crystal approximation (VCA) [4], coherent potential approximation (CPA) [5, 6] and special quasi-random structures (SQS) [7, 8]. SC method is to use large supercells with one or more disordered configurations, but the disadvantage of this approach is required to use long durations of calculation. CPA approach is to introduce the multiple scattering theory using coherent Green function to approximate a random alloy with an effective medium. This method is a very successful mean-field approach for random alloys, but is not well suited to total-energy calculations for first principle methods. The SQS calculation constructs an optimum periodic supercell approximation by minimizing the interatomic Hellmann-Feynman forces during the first-principles calculations and relaxing atomic positions in the supercell. Lastly, VCA is technically the simplest approach speaking and it can be used to study a crystal with the primitive periodicity. It is assumed that a potentially disordered site is composed of virtual atoms which interpolate the behavior of the parent compounds. The atoms occupying random sites in the A–B sublattice for a concentration of $x\%$ of A atom, is defined as:

$$V_{VCA}(x) = xV_A + (1-x)V_B \tag{6.1}$$

where, V_A and V_B the pseudopotentials of A and B atoms. In this study, disordered sites of B atoms and N atoms in h-BN and Li-BNICs without vacancies will be considered. Thereby, Eq. 6.1 is rewritten as:

$$V_{VCA}(x) = 0.5V_B + 0.5V_N \tag{6.2}$$

The purpose of this Chapter is to investigate the atomic structures and phase stabilities of hypothetic Li-BNICs with/without disorder calculation comparing with

Li-GICs and to contribute to the research for possible Li concentration in Li-BNICs.

6.2 Results

6.2.1 Lattice parameter

Usually, in the case of graphite and h-BN, whose interlayers are bonded by van der Waals (vdW) forces, GGA (generalized gradient approximations) exchange correlation potentials have been reported to give bad predictions to the c-axis of lattice parameter [9–12], due to absence of considering vdW interactions, (dispersion forces) in GGA calculation. Therefore, in this thesis, only LDA calculation is conducted.

In this Chapter, the calculated phases are BCC lithium, graphite, h-BN, 1L-model h-BN with VCA calculation (Fig. 6.1), Li-GICs (Table 2.4), 2L-model Li-BNICs (Fig. 2.6), 1L-model Li-BNICs (Fig. 2.6) and disordered 1L-model Li-BNICs with VCA calculation (Fig. 6.1).

The calculated lattice parameters for BCC lithium, graphite, h-BN and 1L-model h-BN with VCA calculation are given in Table 6.1. Table 6.2 and 6.3 show the lattice parameters of Li-GICs and Li-BNICs , respectively. In case of the Li-BNICs, 2L and 1L model are considered as seen in Fig. 2.6 and VCA calculation, which is disorder DFT calculation, is conducted for the 1L-model as seen in Fig. 6.1. The measured lattice parameters experimentally [13–20] and theoretically [9, 11, 12, 21–27] are also organized in respective tables. The information on the unit cell and space group is referred from several literatures [9–12]. In this study, the range of error is from 0.69% (a-lattice of graphite) to 4.96% (a-lattice of BCC lithium). In case of c parameter for LiC_6, the error is about 4.78%.

Fig. 6.2 shows the distances of in-plane C–C and B–N bond for graphite, h-BN, Li-GICs and Li-BNICs calculated in this study and experimentally from literatures [3,14–17, 19, 20] and that of experimental Li-BNIC obtained from Chapter 3 is represented by (dotted) line due to unknown Li concentration. Actually these in-plane bonds become inconsistent after intercalating Li into graphite or BN, namely, the bond lengths of C–C and B–N in the intercalation compounds are different depending on whether they are adjacent to Li atoms or not. In this calculation the relative error between these in-plane distances is within approximately 2.5%. In order to compare their bonding lengths according to Li concentration, Fig. 6.2 shows the distances calculated from a-values of lattice parameters in Table 6.1, 6.2 and 6.3. These in-

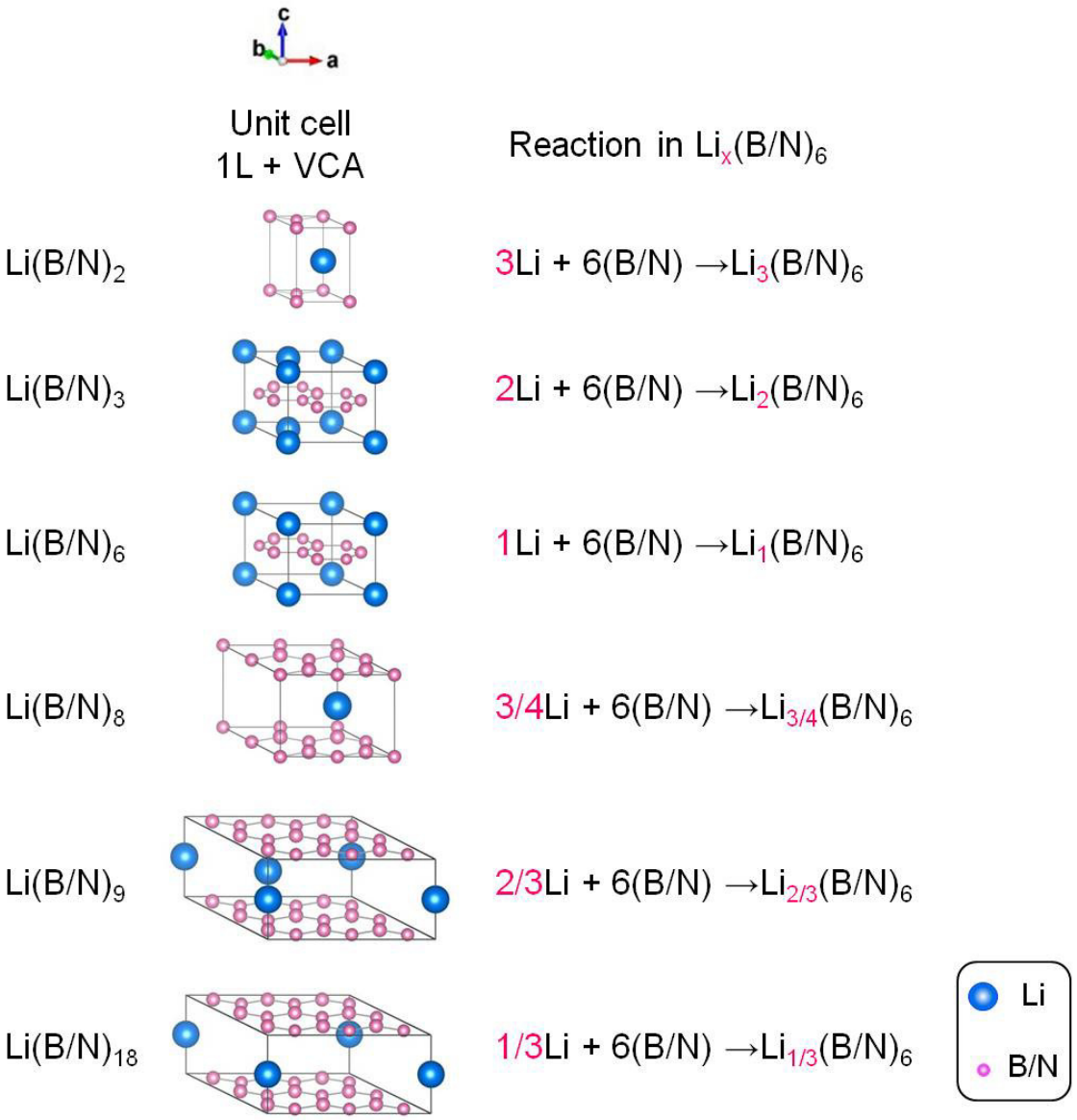

Fig. 6.1. The unit cells of Li-BNICs for VCA calculation and their reactions in $\mathrm{Li}_x(\mathrm{B/N})_6$

Table 6.1. Lattice parameters of BCC lithium, graphite and h-BN.

Phases		Lithium (BCC)	Graphite	h-BN	VCA-1L h-BN
Space group		229	194	194	194
This work	a (nm)	0.3336	0.2433	0.2481	0.2478
	c (nm)		0.6640	0.6467	0.3612
Exp.	a / c (nm)	0.351[a]	0.245 / 0.670[f]	0.2505 /0.6660[l]	-
			0.2463 / 0.6712[g]	0.2506 / 0.6692[m]	
Cal.	a / c (nm)	0.340[b]	0.2439 / 0.6653[e]	0.2494 / 0.6511[e]	-
		0.3355[c]	0.244 / 0.664[h]	0.249 / 0.642[n]	
		0.3445[d]	0.2447 / 0.6660[i]	0.2490 / 0.6424[i]	
		0.559[e]	0.2445 / 0.6726[j]	0.248 / 0.656[k]	
			0.244 / 0.671[k]		

a [13], *b* [21], *c* [22], *d* [23], *e* [11], *f* [14], *g* [15],

h [24], *i* [25], *j* [9], *k* [12], *l* [16], *m* [17], *n* [26]

Table 6.2. Lattice parameters of Li-GICs (LiC_6 and hypothetic phase: LiC_2, LiC_3, LiC_8 and LiC_9).

Phases		LiC_2	LiC_3	LiC_6	LiC_8	LiC_9
Space group		191	191	191	191	191
This	a (nm)	0.2548	0.4330	0.4265	0.4910	0.7359
work	c (nm)	0.3397	0.3459	0.3523	0.3511	0.3494
Exp.	a / c	-	0.43 / 0.74[b]	0.4316 / 0.3703[c]	-	-
	(nm)	-		0.4305 / 0.3706[d]		
Cal.	a / c	0.4488	0.4395	0.4319 / 0.3672[a]	0.4893	-
	(nm)	/ 0.3513[a]	/ 0.7222[a]	0.4282 / 0.3690[e]	/ 0.6699[e]	
				0.4289 / 0.3547[f]		
				0.4258 / 0.3857[g]		

a [27], *b* [18], *c* [19], *d* [20], *e* [9], *f* [10], *g* [11]

Table 6.3. Lattice parameters of hypothetic Li-BNICs.

Phases			Li(BN)	$Li_2(BN)_3$	$Li(BN)_3$	$Li(BN)_4$	$Li_2(BN)_9$	$Li(BN)_9$
Space group		2L	174	176	189	174	174	174
		1L	174	174	174	174	174	174
This work	a (nm)	2L	0.2586	0.4412	0.4351	0.5009	0.7505	0.7474
	c (nm)		0.7416	0.7159	0.7031	0.7023	0.7027	0.6838
		1L	0.2593	0.4428	0.4358	0.5011	0.7508	0.7473
			0.3599	0.3368	0.3297	0.3341	0.3357	0.3392
		1L-VCA	0.2590	0.4407	0.4342	0.5000	0.7492	0.7462
			0.3410	0.3457	0.3528	0.3528	0.3521	0.3599
Cal.	a (nm)		0.45560[a]	0.44902[a]	0.44176[a]	-	-	-
				0.4449[b]	0.4369[b]			
	c (nm)		0.37696[a]	0.36121[a]	0.35223 [a]	-	-	-
				0.7434[b]	0.7880[b]			

a [27], *b* [11]

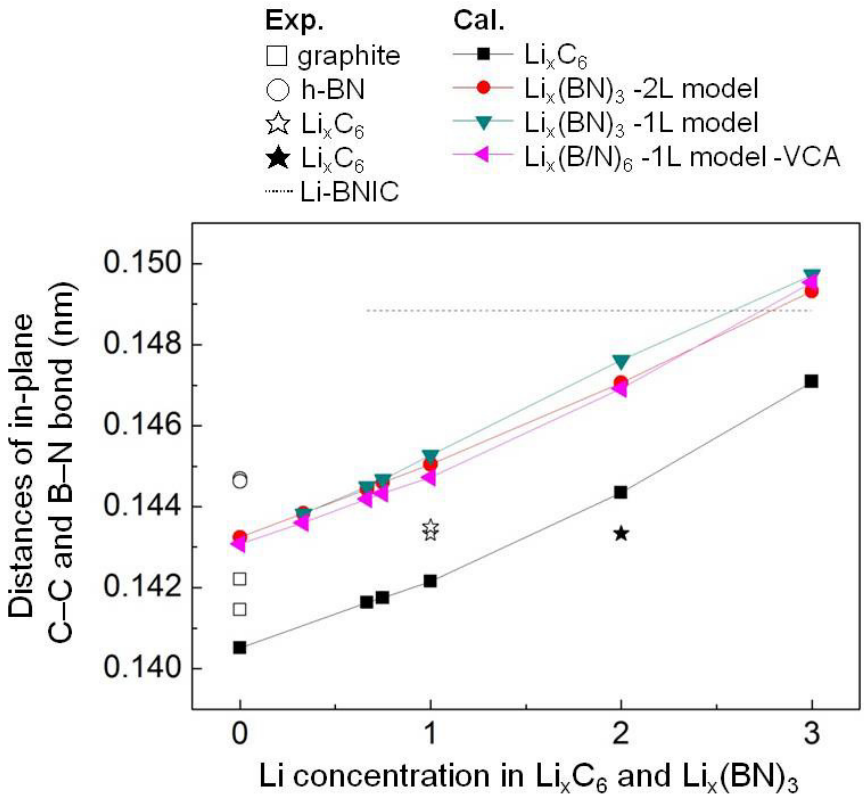

Fig. 6.2. Distances of in-plane C–C and B–N bond in graphite, Li-GICs, h-BN and Li-BNIC. The experimental values obtained from ref. [14, 15] for graphite, [16, 17] for h-BN, [19, 20] for LiC_6 and [3] for Li-BNIC.

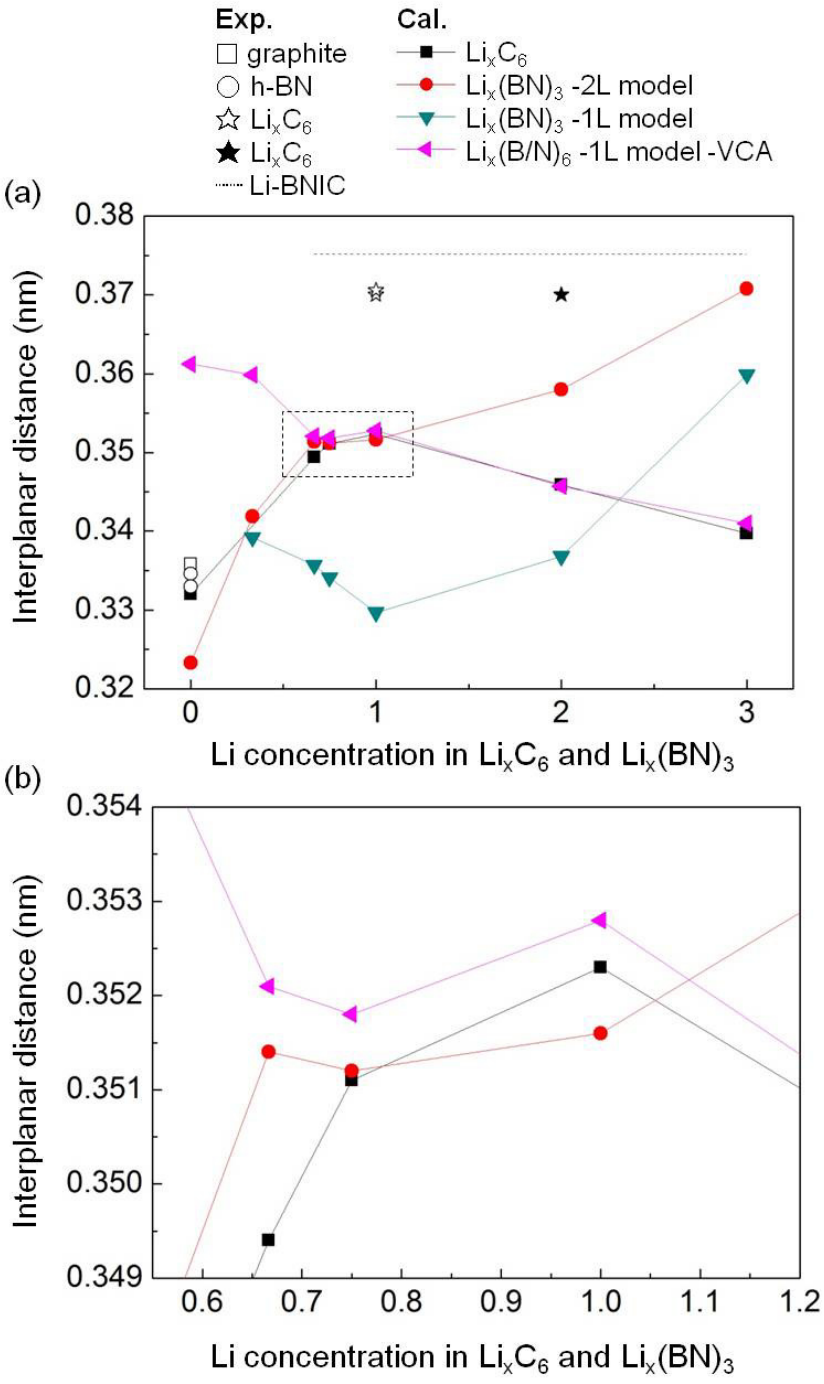

Fig. 6.3. (a) Interlayer distances in graphite, Li-GICs, h-BN and Li-BNIC and (b) is enlarged from the dotted-line rectangle in (a). The experimental values obtained from ref. [14, 15] for graphite, [16, 17] for h-BN and [19, 20] for LiC_6 and [3] for Li-BNIC.

plane bonding distances are well fitted with experimental values (the average error is about 0.9%) and increase with Li concentration.

On the other hand, the interplanar distances of Li-GICs and Li-BNICs are not dependent on the amount of Li intercalation as seen in Fig. 6.3 due to difficulty of calculation for the van der Waals forces between layers. It should be noted that calculated distances between layers of Li-BNICs have to be larger than Li-GICs for the same Li concentration because the experimental interlayer distances of LiC_6 is smaller than Li-BNIC.

6.2.2 Energy calculation

Formation energies (E_f), reaction energies (E_r) and reaction potentials of Li-GICs and Li-BNICs calculated in this study and experimentally [28, 29] and theoretically [9, 11, 27] obtained from literatures are given in Fig. 6.4 and Table 6.4, 6.5, 6.6. These energies for 1L-model phases of Li-BNICs without VCA calculation are calculated from 2L model, i.e. original h-BN, because h-BN for 1L model without VCA calculation was not calculated in this study. The tendencies according to Li concentrations for E_f and E_r are different as seen in Fig. 6.4 (a) and (b), because the number of atoms in unit cell and reaction in $Li_x(BN)_3$ are different as seen in Fig. 2.6, Fig. 6.1 and Table 2.4.

The positive values for formation and reaction energies mean that Li intercalation is difficult and additional energies such as high pressure or temperature are needed to synthesize a compound. In the contrary, the meaning of negative potentials is that Li deintercalation is easier than intercalation into graphite or h-BN. The calculated E_f of LiC_6 is about three times of the observed value (-13.9 and -11.1 kJ/mol) such as the report by Imai et al. [9]. They explained it is rather unusual in the LDA or GGA calculations, since the calculation by DFT methods often gives smaller values of formation enthalpies of various compounds than the values obtained experimentally. Li-GICs and Li-BNICs for VCA calculation under two Li concentration ($x \leq 2$) estimated negative E_f and E_r, and positive potentials as seen in Fig. 6.4 and Table 6.4, 6.5. Usually, the formation energy calculated by VCA method is not reliable due to the lack of one normalization constant energy term for each composition of the alloy for total energy [30]. However it can suggest that VCA calculation might be applied to ball-milled samples due to their metastable state and that calculated formation energies from VCA calculation in this study are well consistent with experimental tendency for thermal stability. Also, Li-BNIC is stable than Li-GICs

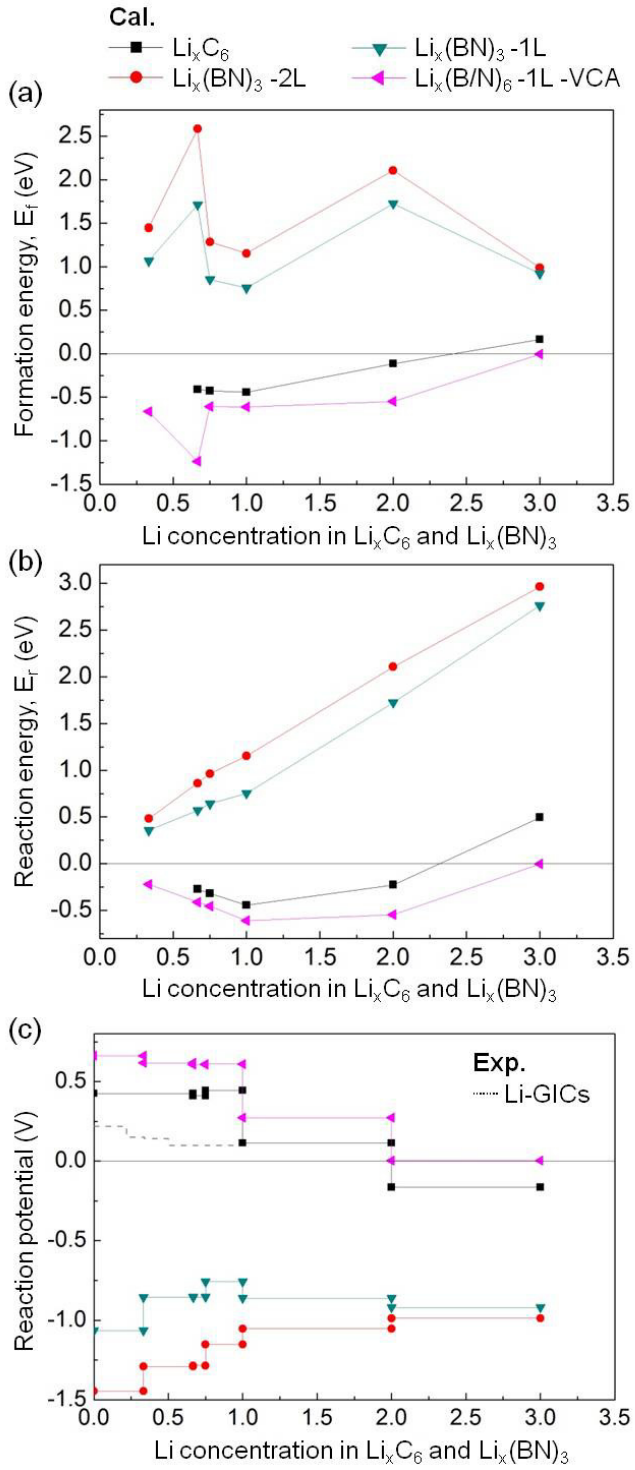

Fig. 6.4. (a) Formation energies (E_f), (b) Reaction energies (E_r) and (c) reaction potentials vs. Li concentration of Li-GICs and Li-BNICs calculated in this study.

Table 6.4. Formation (E_f) and reaction (E_r) energies and potentials of Li-GICs (LiC_6 and hypothetic phase: LiC_2, LiC_3, LiC_8 and LiC_9).

Phase	This work			Exp.	Cal.		
	E_f (eV)	E_r (eV)	Potential (V)	E_f (eV)	E_f (eV)	E_r (eV)	Potential (V)
LiC_9	-0.410	-0.273	0.410	-	-	-	-
LiC_8	-0.425	-0.319	0.425	-	1.13[c]	-	-
LiC_6	-0.444	-0.444	0.444	-0.144[a] -0.115[b]	-0.48[c] -0.082[d]	-0.141[e]	0.141[e]
LiC_3	-0.114	-0.227	0.114	-	-0.014[d]	0.493[e]	0.247[e]
LiC_3	0.116	0.499	-0.166	-	-	1.588[e]	0.529[e]

a [28], *b* [29], *c* [9], *d* [11], *e* [27]

Table 6.5. E_f, E_r and potentials of Li-BNICs for 2L and 1L model and for 1L model with VCA calculation was conducted.

	Without VCA						With VCA		
	2L model			1L model			1L model		
	E_f (eV)	E_r (eV)	Potential (V)	E_f (eV)	E_r (eV)	Potential (V)	E_f (eV)	E_r (eV)	Potential (V)
$Li(BN)_9$	1.446	0.482	-1.446	1.066	0.355	-1.066	-0.663	-0.221	0.663
$Li_2(BN)_9$	2.582	0.861	-1.291	1.711	0.570	-0.856	-1.236	-0.412	0.618
$Li(BN)_4$	1.285	0.964	-1.285	0.855	0.641	-0.855	-0.606	-0.455	0.606
$Li(BN)_3$	1.152	1.152	-1.152	0.757	0.757	-0.757	-0.610	-0.610	0.610
$Li_2(BN)_3$	2.107	2.107	-1.053	1.724	1.724	-0.862	-0.547	-0.547	0.273
Li(BN)	0.988	2.964	-0.988	0.921	2.762	-0.921	-0.003	-0.009	0.003

Table 6.6. Reference: E_f, E_r and potentials of Li-BNICs

Phase	E_f (eV)	E_r (eV)	Potential (V)
$Li(BN)_3$	0.112^a	1.236^b	-1.236^b
$Li_2(BN)_3$	0.253^a	2.548^b	-1.274^b
Li(BN)	-	4.993^b	-1.664^b

a [11], *b* [27]

thermodynamically in Chapter 4 and electrochemically in Chapter 5: formation energies of Li-BNICs are smaller than Li-GICs and potentials exhibit opposite tendency as seen in Fig. 6.4. From E_f, E_r and potential calculation, it can be supposed that Li intercalation into the defect BN is easier to occur than pure BN.

6.2.3 Band structure and DOS (density of states)

Fig. 6.5 (a) and (b) show band structures and density of states (DOS) for graphite and h-BN as LDA dispersion, respectively. It conforms to other reports [9, 11]: in case of graphite, over four electrons in graphite as explained in Chapter 1.3, three electrons form three strong in-plane σ bonds from 2s, $2p_x$ and $2p_y$ orbitals and σ energy bands at the high energy as seen in Fig. 6.5 (a). On the other hand, the other electron, which is the free electron, forms a relatively weak π bond from $2p_z$ orbital and results in π band at the lower energy. This π band crosses the Fermi energy (E_F). Namely, σ and π bonding orbitals build the valance bands and their anti-bonding ($\sigma*$ and $\pi*$) orbitals make conduction band with a band overlap of about 0.02 eV at the K point of the hexagonal Brillouin zone. Therefore graphite exhibits semi-metal properties. Meanwhile, the shape and ordering of band structure for h-BN is similar to that of graphite with σ, π and σ symmetry, although there are two big gaps in the band structure of h-BN: the first is between the valence and conduction band in Fermi energy, which is called band gap, and the second is between bottom σ band and other three bands (two σ and π bands). These energy gaps are caused by the partial ionic property due to heteroatom of boron and nitrogen. In this study, the band gap of h-BN is 4.04 eV as indirect band-gap semiconductor and this is well agreed with other reports for LDA calculations [11, 31, 32].

Fig. 6.5 (c) shows the band structures and DOS of h-BN for VCA calculation with 1L model. The band structure for1L-model h-BN with VCA calculation exhibits very similar ordering and energy distribution to graphite although its DOS shows almost half of states/eV due to the smaller number of band.

Fig. 6.6 (a)$\sim$(e) shows the band structures of LiC_6 and $Li(BN)_3$ for 2L model, 1L model and 1L model with VCA calculation. The band structure of LiC_6 in this study is also conforming with other studies done by Yoji and Altintas through LDA calculation: 1. Folding-back bands of graphite. 2. Degeneracy of the valence level for π and bottom σ from π and upper σ valence states at H and K points in graphite due to the perturbation of Li intercalation. 3. Raising up Fermi energy about 1.77 eV from graphite due to addition to electron from lithium. (In case of Altintas this

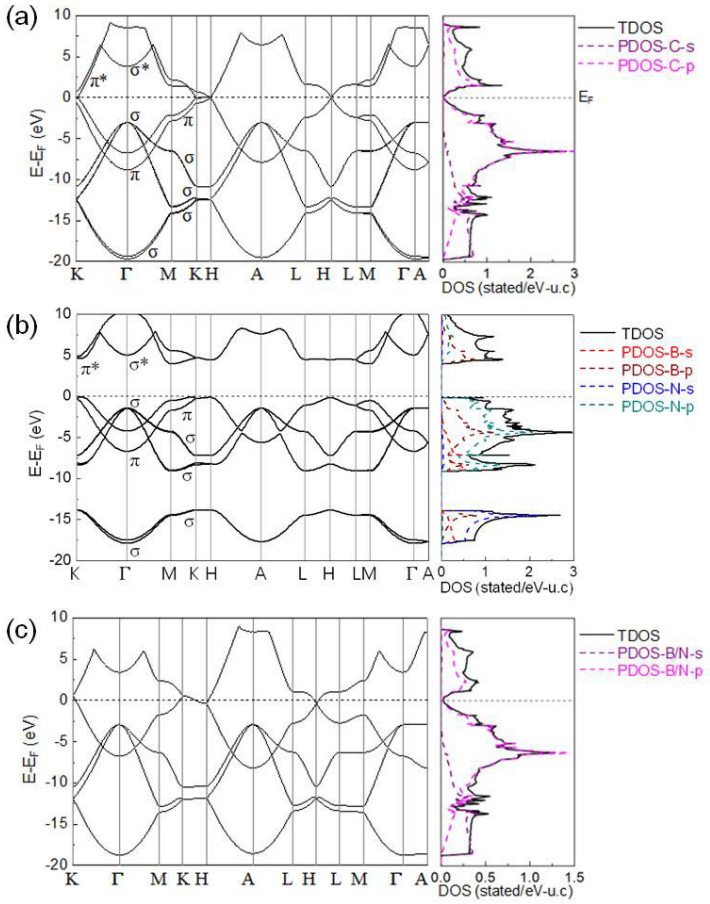

Fig. 6.5. Band structures and DOS for (a) graphite, (b) h-BN and (c) 1L-model h-BN with VCA calculation.

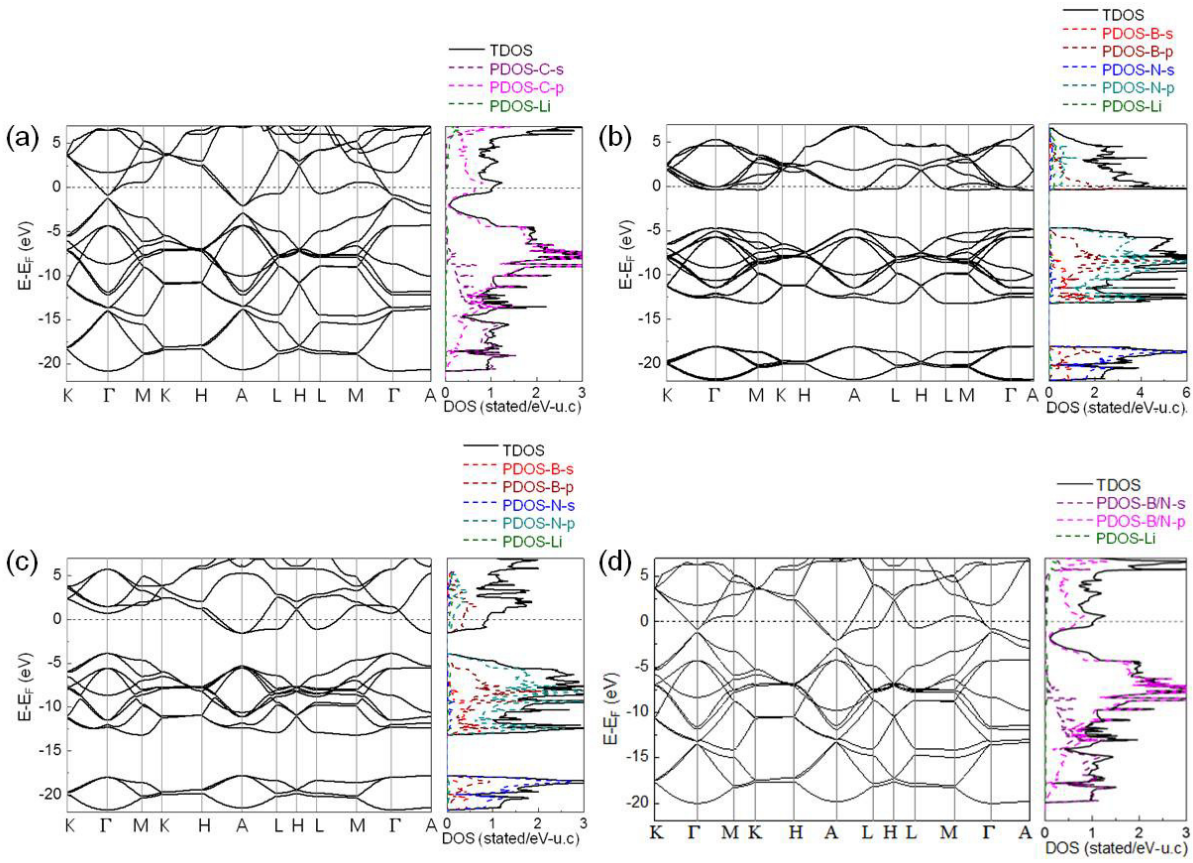

Fig. 6.6. Band structures and DOS for (a) LiC_6, (b) $Li(BN)_3$, (c) 1L-model $Li(BN)_3$ and (d) 1L-model $Li(BN)_3$ with VCA calculation.

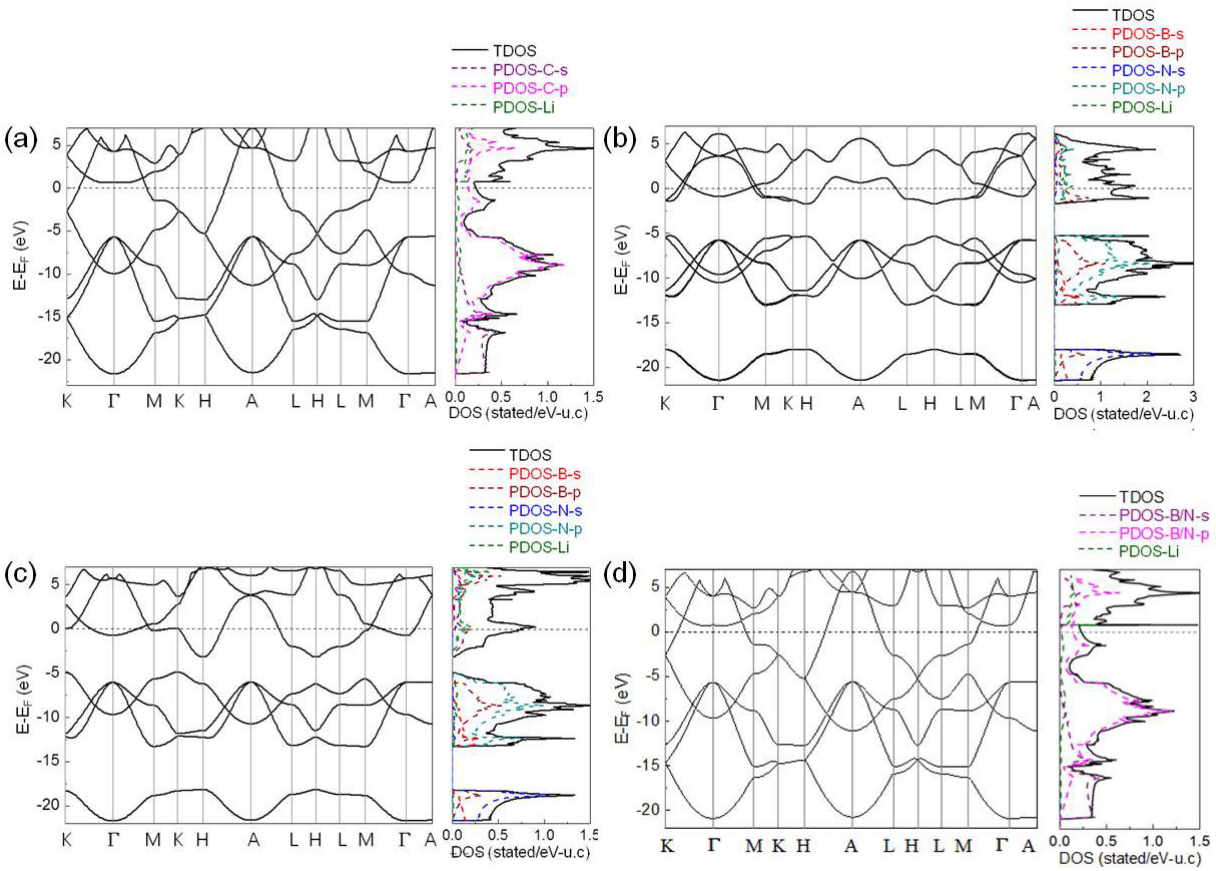

Fig. 6.7. Band structures and DOS for (a) LiC_2, (b) Li(BN), (c) 1L-model Li(BN) and (d) 1L-model Li(BN) with VCA calculation.

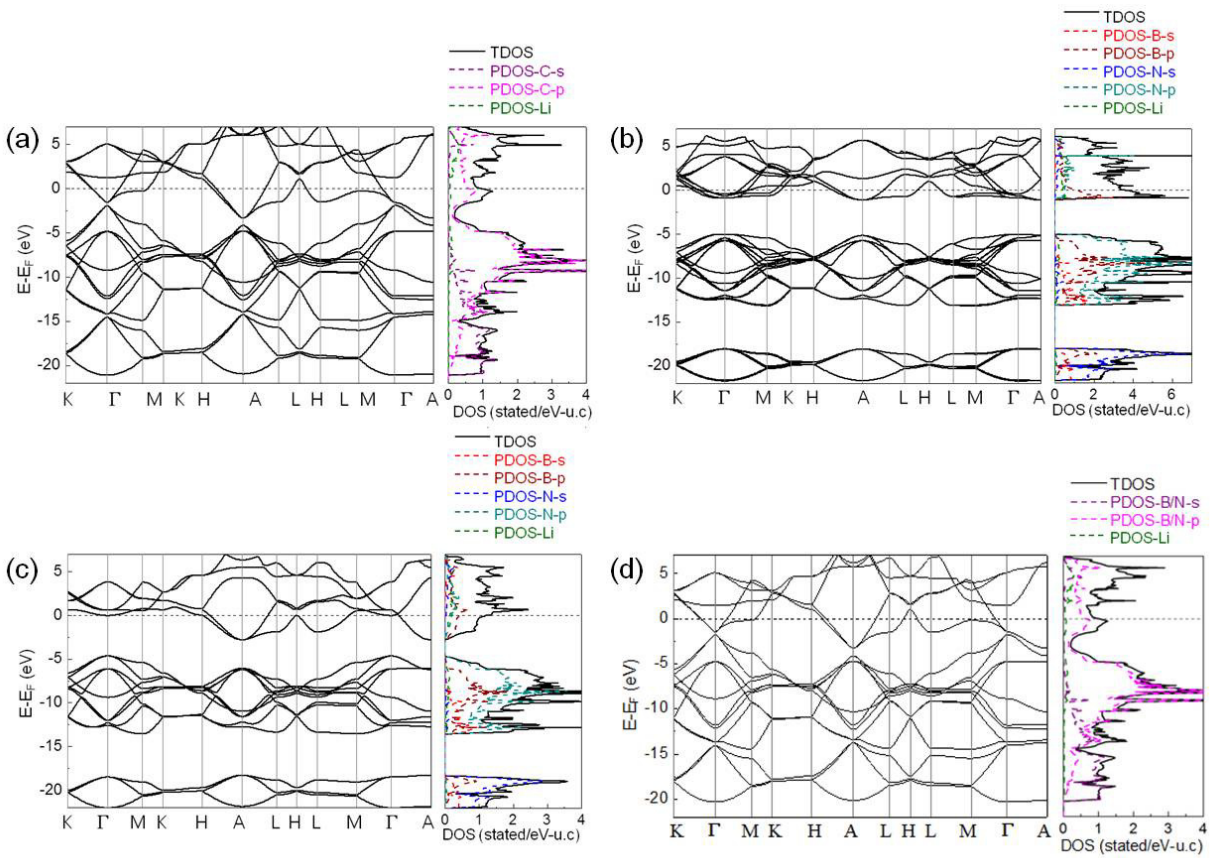

Fig. 6.8. Band structures and DOS for (a) LiC_3, (b) $Li_2(BN)_3$, (c) 1L-model $Li_2(BN)_3$ and (d) 1L-model $Li_2(BN)_3$ with VCA calculation.

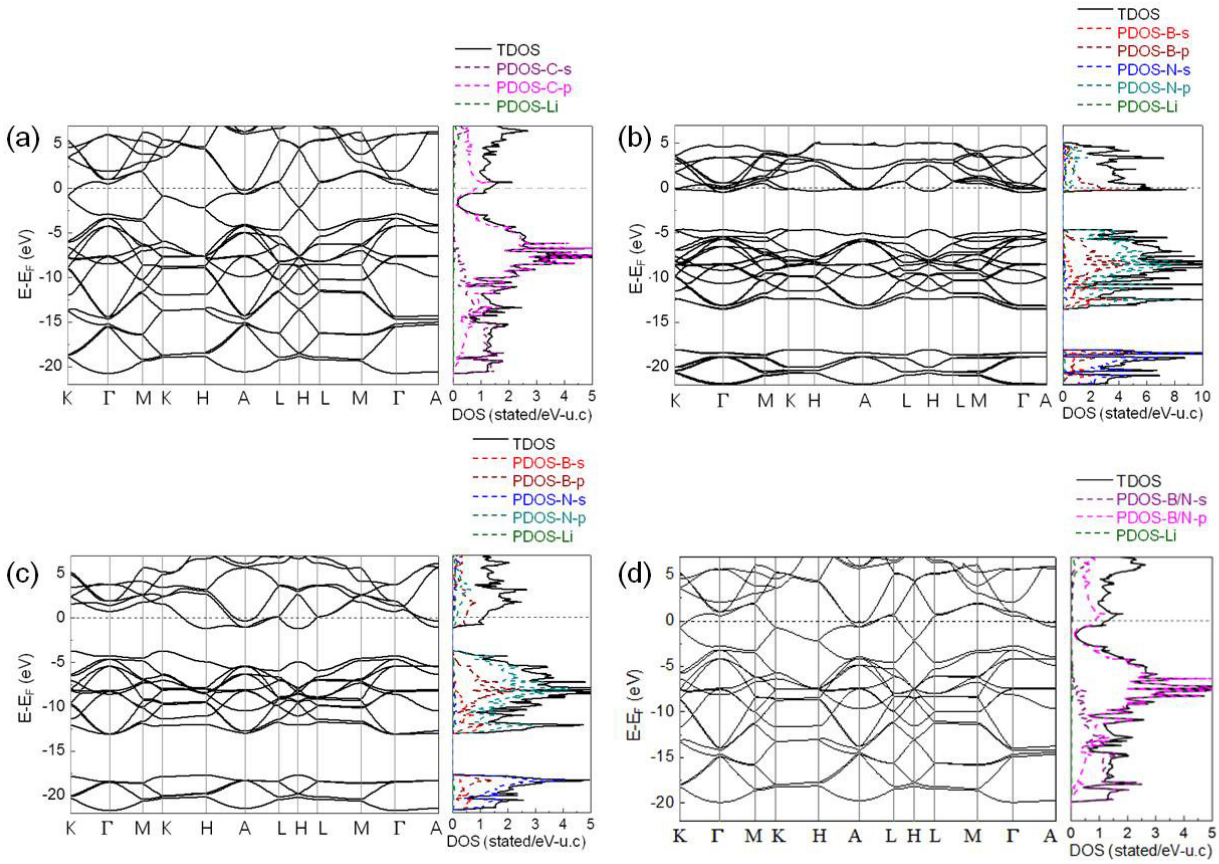

Fig. 6.9. Band structures and DOS for (a) LiC_8, (b) $Li(BN)_4$, (c) 1L-model $Li(BN)_4$ and (d) 1L-model $Li(BN)_4$ with VCA calculation.

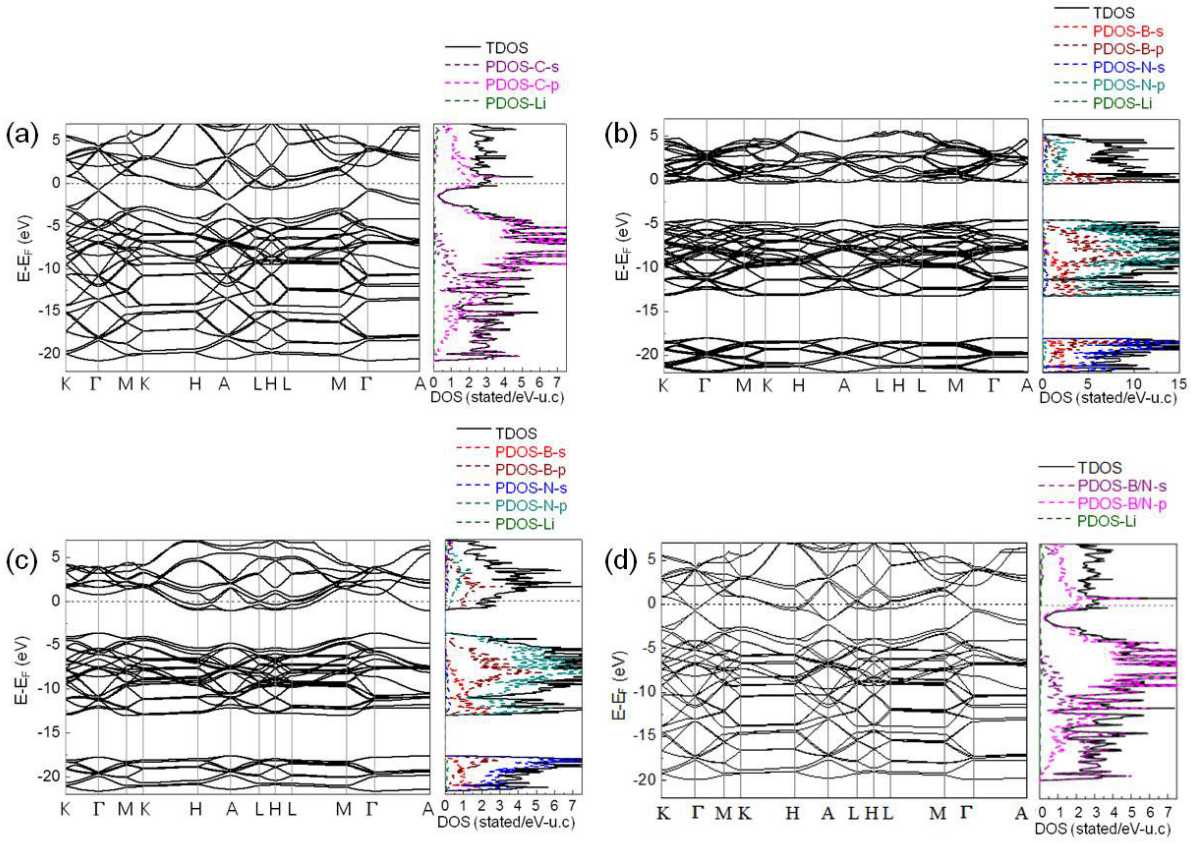

Fig. 6.10. Band structures and DOS for (a) LiC_9, (b) $Li_2(BN)_9$, (c) 1L-model $Li_2(BN)_9$ and (d) 1L-model $Li_2(BN)_9$ with VCA calculation.

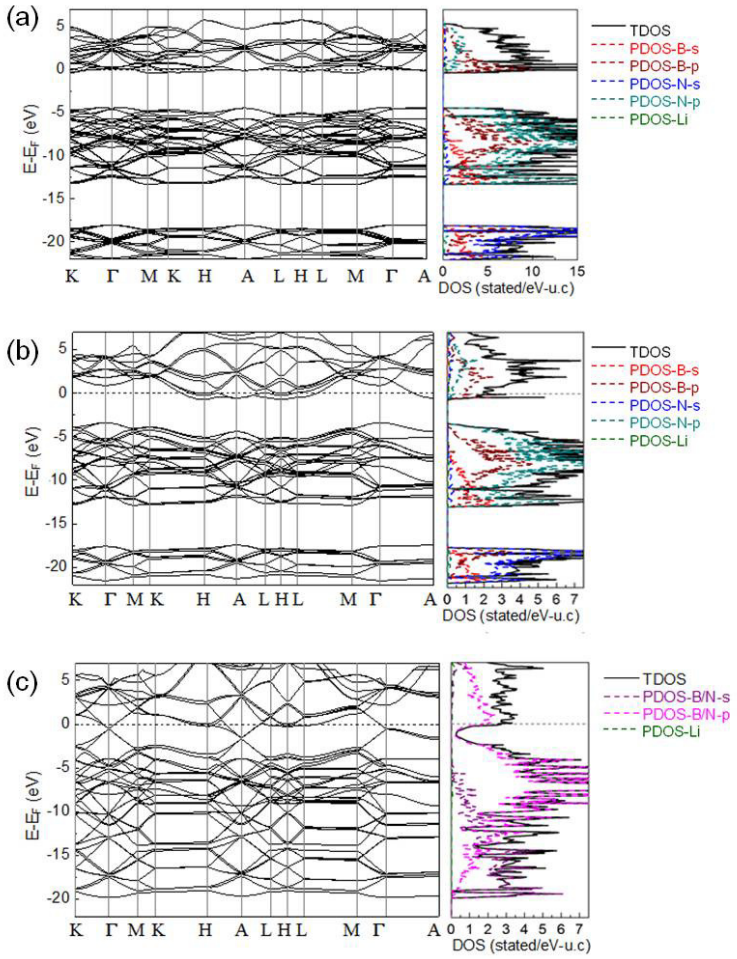

Fig. 6.11. Band structures and DOS for (a) $Li(BN)_9$, (b) 1L-model $Li(BN)_9$ and (c) 1L-model $Li(BN)_9$ with VCA calculation.

Table 6.7. Fermi energies, E_F (eV) and Fermi level (states/eV) of graphite, h-BN, Li-GICs and Li-BNICs calculated in this study.

Li concentration	Li-GICs		Li-BNICs			
	phase	E_F (eV) Fermi level (states/eV)	phase	E_F (eV) Fermi level (states/eV)		
				2L	1L	1L-VCA
0	graphite	5.7149	BN	3.5886	-	4.6398
		0.0005		0		0.0283
1/3	-	-	$Li(BN)_9$	7.4959	7.0363	6.0178
				15.9322	2.2849	2.7069
2/3	LiC_9	7.0668	$Li_2(BN)_9$	7.5260	7.5310	6.6578
		2.5259		13.2868	2.4655	2.5505
3/4	LiC_8	7.1699	$Li(BN)_4$	7.6546	7.0363	6.7917
		1.2750		5.7843	1.1131	1.2641
1	LiC_6	7.4815	$Li(BN)_3$	7.7827	8.0889	7.1106
		1.0269		3.7313	0.8802	1.0031
2	LiC_3	8.8603	$Li_2(BN)_3$	8.2744	8.9825	8.4799
		0.9755		3.6187	1.1834	1.0566
3	LiC_2	10.4280	Li(BN)	8.5353	8.9379	9.9996
		0.2255		1.3692	0.7553	0.2320

differential is about 1 eV.) The number of states at the Fermi level for LiC_6 is obtained as 1.03 states/eV compared with 1.31 and 1.26 states/eV by Altintas et al. [11] and Delhaes et al. [33]. Altintas et al. also have reported for $Li(BN)_3$: 6.90 states/eV, but in this study various Fermi levels are found to 3.73, 0.88, 1.00 states/eV for 3 kinds of $Li(BN)_3$; 2L model, 1L model and 1L model with VCA calculation, respectively. (In both cases, a sizable portion of DOS at E_F comes from localization in the interstitial region.) The band structure of $Li(BN)_3$ calculated by VCA with 1L model is very similar to LiC_6. The results of $Li(BN)_3$ without using VCA calculation show different conditions regarding band structure and DOS.

In case of other phases with 3, 2, 3/4, 2/3 and 1/3 Li concentration exhibited also similar tendency as seen in Fig. 6.7 $\sim$ 6.11. The band structures of Li-BNICs calculated by VCA with 1L model are very similar to those of Li-GICs, which correspond to Li concentration. The results of Li-BNICs without VCA calculation show different conditions for band structure and DOS. Li-BNICs exhibit metallic properties because their electronic band structure show the bands cross the Fermi energy and high DOS at the Fermi level are obtained as seen in Fig. 6.7 $\sim$ 6.11 and Table 6.7. Fermi energies increase with increasing Li concentration because the amount of electron is added more by lithium.

6.2.4 Rietveld analysis

The calculation results of lattice parameters, formation energies, reaction energies, reaction potentials, band structures and density of states for hypothetic Li-BNICs are discussed with comparing experimental reports, which are investigated in Chapter 3, 4 and 5 as follows:

1. Based on lattice parameters obtained from XRD results for Li-BNIC [3] in Chapter 3 comparing with Li-GICs, interlayer distance of the former (0.375 nm) is larger than the latter (0.370 nm). This tendency should be exhibited in the DFT results of this study. Meanwhile, experimental interplanar distance of Li-BNIC is not changed though various ratios of Li/BN when Li-BNIC was synthesized [3]. If this result is applied to DFT calculation, the calculated interplanar bonding lengths of Li-BNICs should be larger than that of LiC_6 (0.3523 nm) regardless of Li concentration for Li-GICs. The results included in this discussion are shown as follows: x = 2 and 3 for the 2L model, only x = 3 for 1L model and x = 1/3 and 1 for 1L model with VCA calculation as seen in Fig. 6.3 and Table 6.2 and 6.3.

2. For the 1L model Li-BNICs with VCA calculation, the calculated formation and reaction energies are negative and potentials are positive. Thus, all phase for VCA calculation can be possible.

3. Li-BNIC is thermodynamically more stable than Li-GICs although the activation energy of the former is higher than the latter as the results of Chapter 4. Also, from the electrochemical synthesis, Li intercalation occurred firstly into h-BN and then into graphite, i.e. the reaction potentials are 1.0 V vs. Li/Li^+ for h-BN and 0.3 vs. Li/Li^+ for graphite. Thereby, the calculated formation and reaction energies of Li-BNICs should be smaller than Li-GICs and potentials for the former are larger than the latter. Reaction potentials that are well agreement with this tendency, are the cases of 1L model with VCA calculation for $x \leq 1$ of Li concentration.

From this discussion, possible phases for Li-BNICs can be assumed as $x = 1/3$ and 1 ($Li(BN)_9$ and $Li(BN)_3$) for 1L model with VCA calculation.

The Rietveld analysis has been conducted using these two phases. In the case of the Rietveld method, virtual chemical species (VCS) can be induced for the disorder calculation in DFT. The XRD pattern used for the Rietveld analysis is the same one used in Chapter 3, which is obtained from the heat-treated samples at 700 °C for 2 h after milling for 2.5 h (X-ray radiation: Cu-K_α, 2θ range: $20 \sim 70.01$ ° with 0.03 ° step). Fig. 6.12 and Table 6.8 show the results of Rietveld analysis. Firstly, for $Li(BN)_3$ phase, the fitting result of VCS calculation (this Chapter) is better than without VCS calculation (Chapter 3). It means disordered Li-BNICs is possible to exist. Meanwhile, both phases ($Li(BN)_9$ and $Li(BN)_3$) show good-fitting results with small R_{wp} and S. It is suggested to exist two or various kinds of phases in the synthesized Li-BNICs. This suggestion can explain the broaden NMR spectra for Li–BN system (Chapter 3) and Li–BN–graphite system (Chapter 4).

6.3 Conclusion

The possible phases for Li-BNICs have been studied using DFT calculation and Rietveld analysis compared with experimental results. 6 kinds of phases, which are Li(BN), $Li_2(BN)_3$, $Li(BN)_3$, $Li(BN)_4$, $Li_2(BN)_9$ and $Li(BN)_9$ are referred from GICs. The in-plane B–N bonding distances increase with Li concentration for all conditions

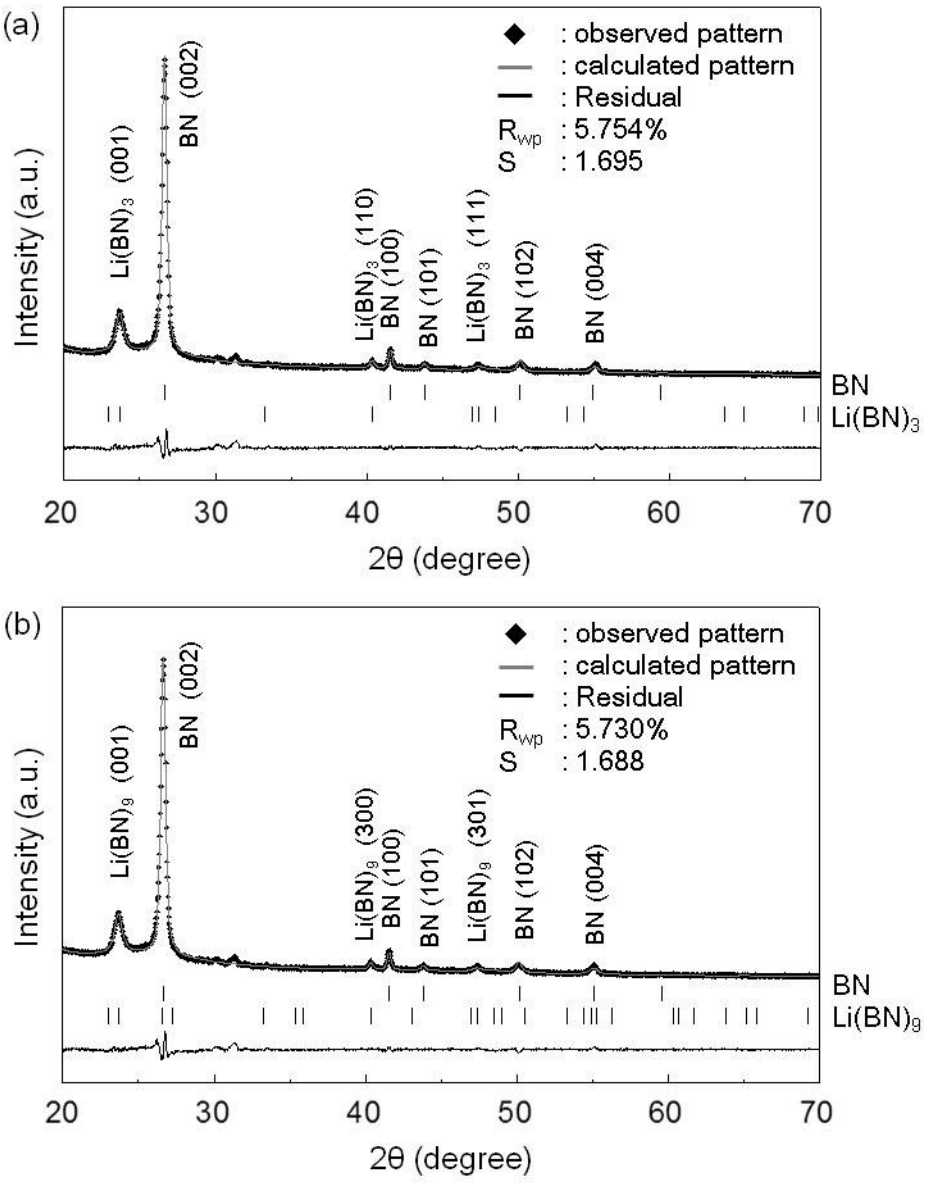

Fig. 6.12. Rietveld results of the heat-treated samples (after 2.5 h milling) for the 1L-model phases with VCS calculation of (a) $Li(BN)_3$, (b) $Li(BN)_9$.

Table 6.8. The results of Rietveld analysis.

Phase		$Li(BN)_3$	$Li(BN)_9$
R_{wp}		5.754	5.730
S		1.695	1.688
BN	R_B	0.653	0.820
	a (nm)	0.2506	0.2506
	c (nm)	0.6678	0.6678
Li-BNIC	R_B	1.403	1.586
	a (nm)	0.4465	0.7734
	c (nm)	0.3751	0.3752

of calculation, while the interplanar distances are not dependent on Li concentration. From the energy calculation, the possible reaction and phases are Li-GICs and 1L-model Li-BNICs with VCA calculation for x $\leq$ 1 of Li concentration in Li_xC_6 and $Li_x(BN)_3$ because they exhibited negative formation and reaction energy and positive potential. The band structures of 1L-model Li-BNICs with VCA calculation is very similar to those of Li-GICs. Li-BNICs exhibit metallic properties because their electronic band structure show the bands cross the Fermi energy and high DOS at the Fermi level. Comparing experimental results and DFT calculation, disordered $Li(BN)_9$ and $Li(BN)_3$ might be considered possible phases for Li-BNICs. As the Rietveld results using these two phases, it is supposed that various phases exist in the synthesized Li-BNICs.

Reference

[1] A. Sumiyoshi, H. Hyodo, and K. Kimura, "Li-intercalation into hexagonal boron nitride," *Journal of Physics and Chemistry of Solids*, vol. 71, no. 4, pp. 569–571, 2010.

[2] A. Sumiyoshi, H. Hyodo, Y. Sato, M. Terauchi, and K. Kimura, "Good reproductive preparation method of Li-intercalated hexagonal boron nitride and transmission electron microscopy–electron energy loss spectroscopy analysis," *Solid State Sciences*, vol. 47, pp. 68–72, 2015.

[3] J. Kim, E. Yamasue, H. Okumura, K. N. Ishihara, and C. Michioka, "Structures of boron nitride intercalation compound with lithium synthesized by mechanical milling and heat treatment," *Journal of Alloys and Compounds*, vol. 685, pp. 135–141, 2016.

[4] L. Bellaiche and D. Vanderbilt, "Virtual crystal approximation revisited: Application to dielectric and piezoelectric properties of perovskites," *Physical Review B*, vol. 61, no. 12, p. 7877, 2000.

[5] P. Soven, "Coherent-potential model of substitutional disordered alloys," *Physical Review*, vol. 156, no. 3, p. 809, 1967.

[6] B. Gyorffy, "Coherent-potential approximation for a nonoverlapping-muffin-tin-potential model of random substitutional alloys," *Physical Review B*, vol. 5, no. 6, p. 2382, 1972.

[7] A. Zunger, S.-H. Wei, L. Ferreira, and J. E. Bernard, "Special quasirandom structures," *Physical Review Letters*, vol. 65, no. 3, p. 353, 1990.

[8] S.-H. Wei, L. Ferreira, J. E. Bernard, and A. Zunger, "Electronic properties of random alloys: Special quasirandom structures," *Physical Review B*, vol. 42, no. 15, p. 9622, 1990.

[9] Y. Imai and A. Watanabe, "Energetic evaluation of possible stacking structures of Li-intercalation in graphite using a first-principle pseudopotential calculation," *Journal of alloys and compounds*, vol. 439, no. 1, pp. 258–267, 2007.

[10] Y. Qi, H. Guo, L. G. Hector, and A. Timmons, "Threefold increase in the Youngs modulus of graphite negative electrode during lithium intercalation," *Journal of The Electrochemical Society*, vol. 157, no. 5, pp. A558–A566, 2010.

[11] B. Altintas, C. Parlak, C. Bozkurt, and R. Eryiğit, "Intercalation of graphite and hexagonal boron nitride by lithium," *The European Physical Journal B*, vol. 79, no. 3, pp. 301–312, 2011.

[12] T. P. Kaloni and S. Mukherjee, "Comparative study of electronic properties of graphite and hexagonal boron nitride (h-BN) using pseudopotential plane wave method," *Modern Physics Letters B*, vol. 25, no. 22, pp. 1855–1866, 2011.

[13] M. Anderson and C. Swenson, "Experimental equations of state for cesium and lithium metals to 20 kbar and the high-pressure behavior of the alkali metals," *Physical Review B*, vol. 31, no. 2, p. 668, 1985.

[14] R. Nicklow, N. Wakabayashi, and H. Smith, "Lattice dynamics of pyrolytic graphite," *Physical Review B*, vol. 5, no. 12, p. 4951, 1972.

[15] A. Bosak, M. Krisch, M. Mohr, J. Maultzsch, and C. Thomsen, "Elasticity of single-crystalline graphite: Inelastic x-ray scattering study," *Physical Review B*, vol. 75, no. 15, p. 153408, 2007.

[16] V. Solozhenko and T. Peun, "Compression and thermal expansion of hexagonal graphite-like boron nitride up to 7GPa and 1800 K," *Journal of Physics and Chemistry of Solids*, vol. 58, no. 9, pp. 1321–1323, 1997.

[17] J. Duan, R. Xue, Y. Xu, and C. Sun, "Preparation of boron nitride flakes by a simple powder reaction," *Journal of the American Ceramic Society*, vol. 91, no. 7, pp. 2419–2421, 2008.

[18] R. Janot and D. Guerard, "Ball-milling in liquid media: Applications to the preparation of anodic materials for lithium-ion batteries," *Progress in Materials Science*, vol. 50, no. 1, pp. 1–92, 2005.

[19] T. Ohzuku, Y. Iwakoshi, and K. Sawai, "Formation of lithium-graphite intercalation compounds in nonaqueous electrolytes and their application as a negative electrode for a lithium ion (shuttlecock) cell," *Journal of The Electrochemical Society*, vol. 140, no. 9, pp. 2490–2498, 1993.

[20] D. Billaud, F. Henry, M. Lelaurain, and P. Willmann, "Revisited structures of dense and dilute stage II lithium-graphite intercalation compounds," *Journal of Physics and Chemistry of Solids*, vol. 57, no. 6, pp. 775–781, 1996.

[21] M. M. Dacorogna and M. L. Cohen, "First-principles study of the structural properties of alkali metals," *Physical Review B*, vol. 34, no. 8, p. 4996, 1986.

[22] J.-H. Cho, S.-H. Ihm, and M.-H. Kang, "Pseudopotential study of the structural properties of bulk Li," *Physical Review B*, vol. 47, no. 21, p. 14020, 1993.

[23] P. Staikov, A. Kara, and T. Rahman, "First-principles studies of the thermodynamic properties of bulk Li," *Journal of Physics: Condensed Matter*, vol. 9, no. 10, p. 2135, 1997.

[24] Y. Ma, "Simulation of interstitial diffusion in graphite," *Physical Review B*, vol. 76, no. 7, p. 075419, 2007.

[25] T. Tohei, A. Kuwabara, F. Oba, and I. Tanaka, "Debye temperature and stiffness of carbon and boron nitride polymorphs from first principles calculations," *Physical Review B*, vol. 73, no. 6, p. 064304, 2006.

[26] Y. Qi and L. G. Hector, "Planar stacking effect on elastic stability of hexagonal boron nitride," *Applied physics letters*, vol. 90, no. 8, p. 1922, 2007.

[27] C.-H. Doh, B. Han, B.-S. Jin, and H.-B. Gu, "Structures and formation energies of Li_xC_6 (x= 1-3) and its homologues for lithium rechargeable batteries," *Bull. Korean Chem. Soc*, vol. 32, no. 6, pp. 2045–2050, 2011.

[28] V. V. Avdeev, A. P. Savchenkova, L. A. Monyakina, I. V. Nikol'skaya, and A. V. Khvostov, "Intercalation reactions and carbide formation in graphite-lithium system," *Journal of Physics and Chemistry of Solids*, vol. 57, no. 6, pp. 947–949, 1996.

[29] Y. Reynier, R. Yazami, and B. Fultz, "The entropy and enthalpy of lithium intercalation into graphite," *Journal of power sources*, vol. 119, pp. 850–855, 2003.

[30] P. Djemia, M. Benhamida, K. Bouamama, L. Belliard, D. Faurie, and G. Abadias, "Structural and elastic properties of ternary metal nitrides $Ti_xTa_{1-x}N$

alloys: First-principles calculations versus experiments," *Surface and Coatings Technology*, vol. 215, pp. 199–208, 2013.

[31] B. Arnaud, S. Lebegue, P. Rabiller, and M. Alouani, "Huge excitonic effects in layered hexagonal boron nitride," *Physical review letters*, vol. 96, no. 2, p. 026402, 2006.

[32] G. Cappellini, G. Satta, M. Palummo, and G. Onida, "Optical properties of BN in cubic and layered hexagonal phases," *Physical Review B*, vol. 64, no. 3, p. 035104, 2001.

[33] P. Delhaes, J. Rouillon, J. Manceau, D. Guerard, and A. Herold, "Paramagnetism and specific heat of the graphite lamellar compound C_6Li," *Journal de Physique Lettres*, vol. 37, no. 5, pp. 127–129, 1976.

Chapter 7

Summary and recommendations

7.1 Summary

In this study, lithium intercalation boron nitride compounds (Li-BNICs) have been synthesized by two kinds of method; first is a sequential process of ball milling and heat treatment, and second is electrochemical synthesis. Their structures, behaviors of Li intercalation, thermal stability and electrochemical stabilities comparing with graphite, have been studied. The results and discussion about these studies in this thesis have been summarized below.

In Chapter 3, the pieces of lithium metal and h-BN powder with a 1/2.2 molar ratio, were ball-milled with various milling durations using a vibratory ball mill machine, and heat-treated at 700 °C for 2 h under argon atmosphere. Li-BNICs are synthesized and the samples contain both h-BN and Li-BNICs phases together. The exothermic DTA peaks observed between 200 $\sim$ 500 °C might be the synthesis temperatures of Li-BNIC. Same interplanar distance of synthesized Li-BNICs are obtained regardless variation of the ratios between Li and BN the results for XRD peak patterns. On the other hand, the various NMR spectra of Li-BNICs are exhibited when the ratio of Li to BN are changed. By Li intercalation, the BN lattice changes from 0.333 nm to 0.375 nm of the layer distance and from 0.145 nm to 0.149 nm of the B–N atomic bond length. The 1L-model Li-BNIC is well-fitted than 2L-model as the result of Rietveld refinement, The broadened XRD and NMR peaks of Li-BNICs indicate low symmetry Li-BNICs has been synthesized, for example the site of Li ion is irregular arrangement or multiple sites, not in each of the BN galleries, or BN become defective by intercalation with/without vacancies.

In Chapter 4, the pieces of lithium metal, h-BN and graphite powders with a 1/1.1/1.1 molar ratio, were ball-milled for 2.5 and 10 hours using a vibratory ball mill machine, and heat-treated at 700 °C for 2 h under argon atmosphere. Firstly, after milling, Li-GICs (LiC_6 and LiC_{12}) were mainly synthesized as well as small amount of Li_3N. Also, the unreacted and defective Li metal and h-BN are obtained. Then, after heat treatment of the milled samples, Li-BNICs were mainly synthesized, with a small amount of Li_2C_2, Li_3BN_2 and Al. Also, graphite is obtained from deintercalation of Li-GICs. This results suggested that during heat treatment, Li atoms are deintercalated from Li-GICs and then intercalated into BN. Namely, thermal stability of Li-BNIC is more stable than Li-GICs at an ambient condition. On the other hand, the activation energy for producing Li-BNICs obtained by Kissinger plot might be higher than Li-GICs. Meanwhile, the reaction between BN and graphite powders did not occur by a sequential process of ball milling and heat treatment. Also, more Li could be intercalated into h-BN with increasing milling duration, because the structure of h-BN become more defective.

In Chapter 5, Li intercalation into the pristine graphite, the pristine h-BN, and 2.5 h-milled various counterparts occurs by electrochemical method using a half cell with three electrodes. The CV experiments for those materials show the chemical potential of graphite is found 0.2 V vs. Li/Li^+, while of h-BN 1.0 V vs. Li/Li^+, regardless of pristine or milled. Thereby, Li-BNIC is more stable than Li-GICs in terms of thermodynamics under an ambient condition, and this is consistent with the results for thermal stabilities in Chapter 4. Also, the CV curves for Li intercalation into h-BN indicate two-phase reaction occurs, and this is consistent with the results that the XRD peaks patterns of both h-BN and Li-BNICs phases are exhibited in Chapter 3. The GCPL experiments for h-BN show the Li intercalation occurs on the surface of BN, and then Li atoms/ions are very slowly diffused inside BN particles. Accordingly, Li intercalation into BN is more difficult than into graphite through an electrochemical process although the milled h-BN become better than the pristine h-BN.

Finally, in Chapter 6, in order to understand phases for synthesized Li-BNICs, the atomic structures and phase stability for Li-BNICs are studied using DFT calculation and Rietveld analysis with/without disorder calculation (VCA (virtual chemical approximation) for DFT and VCS (virtual chemical species) for Rietveld method), compared with experimental results. 6 kinds of phases, which are $Li(BN)$, $Li_2(BN)_3$, $Li(BN)_3$, $Li(BN)_4$, $Li_2(BN)_9$ and $Li(BN)_9$ are referred from GICs. From the DFT cal-

culation, with increasing Li concentration calculated in-plane B–N bonding distances increase for all conditions of calculation. On the other hand, interlayer distances are not dependent on Li concentration. The calculation resulted in negative formation and reaction energy and positive potential indicate that possible reactions are VCA calculation of 1L-model Li-BNICs. The calculated band structures and density of states (DOS) for graphite, h-BN and LiC_6 are well agreed with other reports and for Li-BNICs exhibit metallic properties due to crossing the high DOS at the Fermi level. The band structures of Li-BNICs for 1L-model with VCA calculation and Li-GICs are very similar. The results without VCA calculation show different conditions for band structure and DOS. The disordered $Li(BN)_9$ and $Li(BN)_3$ phases suggested for possible atomic structures of Li-BNICs as discussed for comparing experimental results, DFT calculation and Rietveld results. It is supposed that the synthesized Li-BNICs include these two phases or more.

In this study, Li intercalation into h-BN occurred at lower temperatures and short time by inducing ball milling (a sequential process of ball milling and heat treatment) and Li atoms more easily intercalated into the milled h-BN electrochemically than the pristine h-BN. The results of disorder DFT calculation and Rietveld analysis also consistent with experimental results.

7.2 Recommendations

Some recommendations and directions for further investigations to fill in gaps for our understanding in this thesis are proposed as following:

1. Li-BNICs is thermally and electrochemically more stable than Li-GICs, while Li intercalation into h-BN is more difficult than graphite due to higher activation energy (Chapter 4). This implies that it is worth taking application for batteries used in a high temperature environment (> about 300 °C, which is the temperature that Li was deintercalated from Li-GICs.). If electrochemical Li intercalation into the milled h-BN occurs at higher temperature, it can be expected to obtain the better battery performance than this thesis.

2. By inducing ball milling, more Li atoms were intercalated into h-BN (Chapter 3 and 5). Also, the 1L-model atomic structures and disorder calculations for Li-BNICs shows consistent results with experimental analysis. In this thesis only dis-

order atomic sites for boron and nitrogen in Li-BNICs were considered. However, it is strongly suggested that the vacancies exist in real milled h-BN (and also Li-BNICs). Therefore, DFT calculation for Li-BNICs to include vacancies using supercell method is proposed for the future plan.

3. In Chapter 5, the milled graphite was mixed with the milled h-BN in order to increase electric conductivity of h-BN, which is an insulator. However, their electrochemical lithium intercalation occurred separately and graphite could not be a role of delivery for conductivity. It might be due to similar crystallite sizes between the 2.5 h-milled graphite and h-BN. Namely, the surface of the milled BN particles could not be surrounded by graphite particles. Therefore, the conductive additives with smaller particles than h-BN are recommended for well delivering electric conductivity.

Appendix A

Variations of sample weights before/after heat treatment in Li–BN system

In this appendix, the variations of weights for the milled samples before and after heat treatment in Li–BN system are organized in Table A.1 in order to refer DTA results of Chapter 3. The samples are milled Li and BN by a molar ratio of 1 : 2.2 for several milling durations ($0 \sim 60$ hours).

Table A.1. The variations of weights for the milled samples (a molar ratio of Li and BN is 1 : 2.2) before and after heat treatment in Li–BN system (Chapter 3).

Milling durations (hour)	Weight change (mg)	Variations of weights (%)
0	+20	5.9
1	+32	13.8
2.5	+38	14.1
5	+37	14.6
10	+30	11.6
35	+29	8.7
60	+29	11.2

List of publications

Papers related to this thesis

The thesis entitled "Synthesis, thermal stability and electrochemical behavior of lithium boron nitride intercalation compounds" is based on the following publications.

(1) Chapter 3
J. Kim, E.Yamasue, H. Okumura, K. N. Ishihara and C. Michioka,
"Structures of boron nitride intercalation compound with lithium synthesized by mechanical milling and heat treatment"
Journal of Alloys and Compounds, vol. 685, pp. 135–141 (2016)
DOI: http://dx.doi.org/10.1016/j.jallcom.2016.05.222

(2) Chapter 4
J. Kim, E. Yamasue, H. Okumura, C. Michioka and K. N. Ishihara,
"Intercalation of Hexagonal Boron Nitride and Graphite with Lithium by Sequential Process of Ball Milling and Heat Treatment"
Journal of Alloys and Compounds, accepted on 2017. 01, available online
DOI: http://dx.doi.org/10.1016/j.jallcom.2017.01.050

(3) Chapter 5
J. Kim, E. Yamasue, T. Ichitsubo, H. Okumura and K. N. Ishihara,
"Electrochemical lithium Intercalation behavior of pristine and milled hexagonal boron nitride"
Journal of Electroanalytical Chemistry, submitted on 2017.02, under review

(4) Chapter 6
J. Kim, E. Yamasue, H. Okumura and K. N. Ishihara,
"Atomic structures and phase stability of lithium boron nitride intercalation compounds"
Manuscript in preparation

Oral presentation in international / domestic conference

(1) **J. Kim**, E.Yamasue, H. Okumura and K. N. Ishihara
"Mechanical Milling of Boron Nitride and Lithium"
Spring Meeting 2014 of *The Journal of the Japan Society of Powder and Powder Metallurgy*, Osaka (Japan) 2014.10.31

(2) **J. Kim**, E.Yamasue, H. Okumura and K. N. Ishihara
"Lithium Intercalation into Hexagonal Boron Nitride and Graphite by Mechanical Milling and Heat Treatmen"
The 2015 International Symposium on Advanced Engineering, Busan (Korea) 2015.10.23

(3) **J. Kim**, E.Yamasue, H. Okumura and K. N. Ishihara
"Lithium Intercalation into Hexagonal Boron Nitride and Graphite by Mechanical Milling and Heat Treatmen"
3rd International Conference on Powder Metallurgy in Asia, Kyoto (Japan) 2015.11.10

(4) **J. Kim**, E.Yamasue, H. Okumura and K. N. Ishihara
"Lithium Intercalation into Hexagonal Boron Nitride and Graphite by Mechanical Milling and Heat Treatmen"
The 2016 Ajou-Kyoto Joint Symposium on Energy Science, Suwon (Korea) 2016.1.28

(5) **J. Kim**, E.Yamasue, H. Okumura, K. N. Ishihara and T. Ichitsubo
"Electrochemical Properties of Ball-milled Hexagonal Boron Nitride for Lithium Intercalation"
83rd Spring Meeting of *The Electrochemical Society of Japan*, Osaka (Japan) 2016.3.29